CHALMERS
UNIVERSITY OF TECHNOLOGY

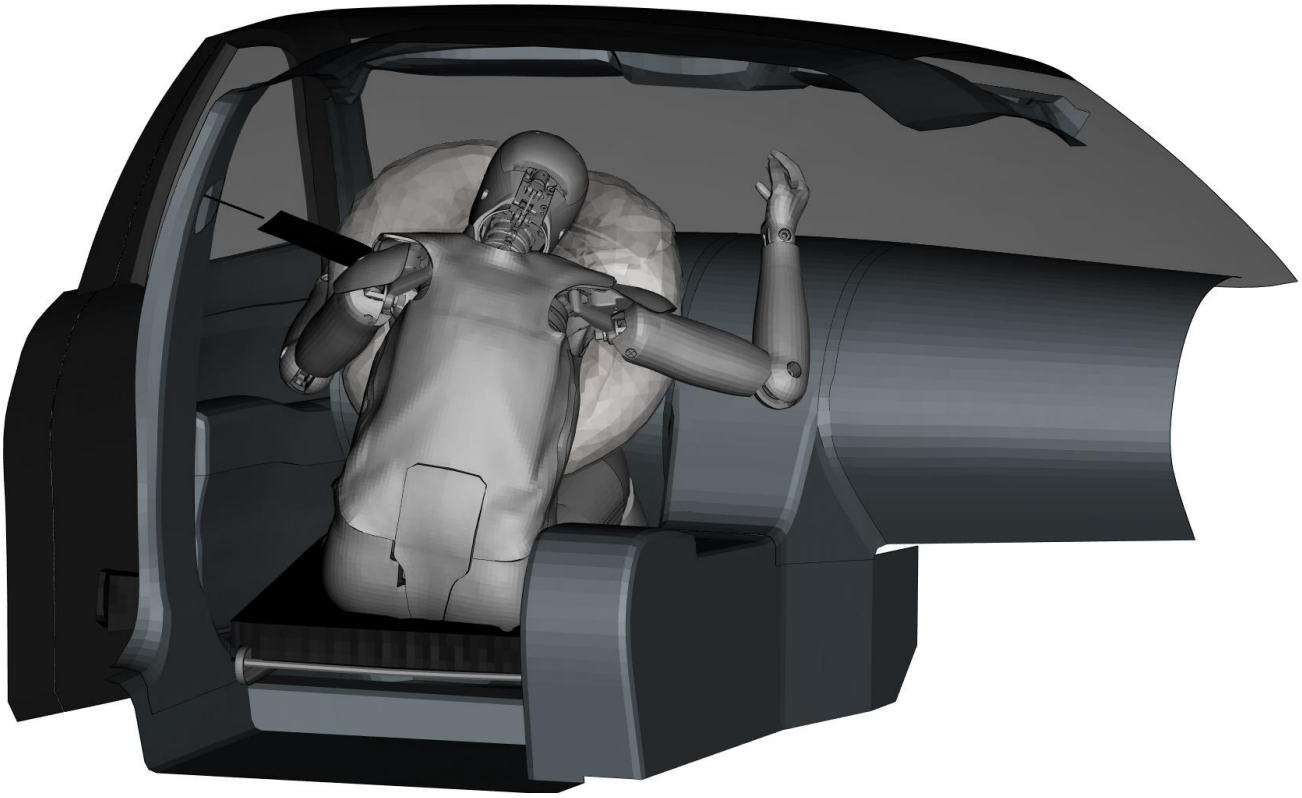

Rib fracture injury risk function assessment for the THOR-50M using population-based finite element crash reconstructions

Master's thesis in APPLIED MECHANICS AND AUTOMOTIVE ENGINEERING

Max Nylund
Nils Olofsson

DEPARTMENT OF MECHANICS AND MARITIME SCIENCES
CHALMERS UNIVERSITY OF TECHNOLOGY

Gothenburg, Sweden 2022
www.chalmers.se

MASTER'S THESIS IN APPLIED MECHANICS AND AUTOMOTIVE ENGINEERING

Rib fracture injury risk function assessment for the THOR-50M using population-based finite element crash reconstructions

MAX NYLUND
NILS OLOFSSON

Department of Mechanics and Maritime Sciences
Division of Vehicle Safety
CHALMERS UNIVERSITY OF TECHNOLOGY

Göteborg, Sweden 2022

Rib fracture injury risk function assessment for the THOR-50M using population-based finite element crash reconstructions
MAX NYLUND
NILS OLOFSSON

Master's thesis 2022:18
Department of Mechanics and Maritime Sciences
Division of Vehicle Safety
Chalmers University of Technology
SE-412 96 Göteborg
Sweden
Telephone: +46 (0)31-772 1000

Cover:
The THOR ATD positioned in the generic vehicle interior during a crash simulation event

Chalmers Reproservice
Göteborg, Sweden 2022

Rib fracture injury risk function assessment for the THOR-50M using population-based finite element crash reconstructions
Master's thesis in APPLIED MECHANICS AND AUTOMOTIVE ENGINEERING
MAX NYLUND
NILS OLOFSSON
Department of Mechanics and Maritime Sciences
Division of Vehicle Safety
Chalmers University of Technology

Abstract

Frontal crashes account for around 50% of all fatalities in passenger cars and thorax injuries are common in this type of crash. To evaluate car crash performance, mechanical representations of human occupants are used, which are called Anthropomorphic Test Devices. The most advanced for frontal crashes is the Test device for Human Occupant Restraint (THOR), which has multiple deflection measurement locations in the chest. This study used a generic Finite Element (FE) car interior model, that was based on several different cars, and was meant to represent the cars present in a selection of NASS/CDS accident cases. Several different injury criteria were used to evaluate the risk of sustaining a three or more severe injury on the Abbreviated Injury Scale (AIS3+), four or more Number of Fractured Ribs (NFR4+) or NFR3+ level of thorax injury. A population based stochastic simulation study was set up and 1000 simulations with parameterized and morphed car interior models were run in the explicit FE solver LS-DYNA, and parameters were sampled using the optimization software LS-OPT. Using logistic regression and a generalized linear model, risk curves were generated for several rib fracture risk criteria, based on the simulations results. These risk curves were then compared to the AIS3+ rib fracture risk from the NASS/CDS field data.

From the analysis of the results, it was apparent that the rib fracture risk criterion TIC NSFR fit the NASS/CDS risk curve the best. The rib fracture risk criteria based on R_{max} and D_{max} overpredicted the injury risk considerably, with a Winsmash Δv of 56 km/h and 49 km/h for 50% risk of AIS3+ rib fracture for R_{max} and D_{max}, respectively, while the NASS/CDS risk curve predicted a risk of 50% at 99 km/h. The rib fracture risk criterion TIC_{NSFR} had the 50% risk at a Winsmash Δv of 95 km/h, which was indeed closer to the NASS/CDS risk curve.
However, since TIC NSFR seemed to be too insensitive, with few risk predictions above 20%, it is not recommended as the best available rib fracture risk function to be used with the THOR ATD based on comparison to the risk of rib fracture in the selection of NASS/CDS data. The injury criteria TIC NFR and PCscore showed better sensitivity, while performing well compared to the selected NASS/CDS data. PCscore is slightly preferred, for it is defined for the same injury classification as used in NASS/CDS, AIS3+. PCscore is therefore recommended as the best risk function, among the ones considered, for evaluating the risk of rib fracture with the THOR-50M ATD.

Keywords: FE, FEM, Risk curves, Generic, Stochastic, THOR, ATD, Dummy, 50th, 50M, Biomechanics

Preface

This master thesis project was carried out at the Volvo Cars Safety Centre in Torslanda, Gothenburg, Sweden during the spring semester of 2022.

Acknowledgements

We wish to express our appreciation to all that have helped us throughout the master's thesis and during our studies on Chalmers University of Technology. We have met many helpful individuals throughout the years.

We would firstly like to express our deepest appreciation to **Volvo Car Corporation** for the opportunity with the master's thesis. We are extremely grateful for the supervisor **Jonas Östh** that helped and guided us throughout the whole project.

We would also like to extend our appreciation to **Johan Iraeus** which made the master's thesis possible with all the previous work that laid the foundations for the project, as well as being the examiner for our thesis.

We are also extremely grateful for the LS-DYNA course conducted by **Anders Bernhardsson** and **David Aspenberg** provided by DYNAmore Nordic. We would like to also thank for the LS-DYNA and LS-OPT support after the course was finished.

We also wish to thank **Peter Appelgren** for the ANSA and META support.

Many thanks to the whole **Injury Prevention Team**. Especially **Katarina Bohman** which provided knowledge about the field and **Isabelle Stockman** for the help with the presentation. We cannot forget the help from **Jacob Wass** regarding both META and LS-OPT.

Additional thanks to **Alexandros Leledakis** and **Ulf Westberg** regarding LS-DYNA and ANSA.

Thanks should also go to **Ulrich Sander** who helped us with the field data analysis and calculation of statistical metrics.

We would also like to acknowledge the helpful students during our time at Chalmers University of Technology. Among these are **Felix Hövik**, **Caspian Lago**, **Johan Nilsson**, **Filip Schwartz**, **Ranbir Singh** and **Jacob Sjöberg** which helped us during our studies in Mechanical Engineering.

Abbreviations

AIS	Abbreviated Injury Scale
ATD	Anthropomorphic Test Device
CFC	Channel Filter Class
CIREN	Crash Injury Research and Engineering Network
CPR	Cardiopulmonary resuscitation
Euro NCAP	Europe New Car Assesment Programme
EDR	Event Data Recorder
FE	Finite Element
GLM	Generalized Linear Model
GM	General Motors
HBM	Human Body Model
HIC	Head Injury Criterion
IIHS	Insurance Institute for Highway Safety
IR-TRACC	Infra-Red Telescoping Rod for the Assessment of Chest Compression
MAIS	Maximum Abbreviated Injury Scale
NASS/CDS	National Automotive Sampling System/Crashworthiness Data System
NCAP	New Car Assessment Programme
NHTSA	National Highway Traffic Safety Administration
NSFR	Number of Separated Fractured Ribs
NFR	Number of Fractured Ribs
ORM	Objective Rating Method
PCA	Principal Component Analysis
PCscore	Princial Components score
PDF	Probability Density Function
PDOF	Principal Direction of Force
PMHS	Post Mortem Human Subjects
TIC	Thoracic Injury Criterion
US	United States
USNCAP	United States New Car Assesment Programme
VPI	Vehicle Pulse Index
WHO	World Health Organization
World SID	Worldwide Harmonized Side Impact Dummy

Nomenclature

age	Age of the occupant
a_{res}	Resultant acceleration of the head
a_x	Acceleration of the head in X-direction
a_y	Acceleration of the head in Y-direction
a_z	Acceleration of the head in Z-direction
c_{age}	Coefficient of bias towards age
c_{LPINTR}	Coefficient of bias towards instrument panel intrusion
$c_{\Delta v}$	Coefficient of bias towards Δv
$DcTHOR$	Deflection of the thorax according to DcTHOR
D_m	Mean deflection for the 4 IR-TRACC sensors in the thorax
D_{max}	Maximum X-directional deflection
dD_{lw}	Upper deflection difference for DcTHOR
dD_{up}	Lower deflection difference for DcTHOR
D_x	X-axis deflection
e	Natural exponential function
erf	Gauss error function
$error$	Optimizing error
$F(t)$	Force acting on the car
FN	False negatives
FP	False positives
FPR	False positive rate
Fracture risk	Fracture risk of a rib
$Height$	Height of the ATD
HIC_{15}	Head injury criteria for 15ms range
int	Intercept
k	Spring stiffness
l_i	Principal component loading weight factors for PCscore
ln	Natural logarithm
LL	Lower left deflection
LL_x	Lower left deflection on x-axis
$logscale$	Logarithmic scale factor for D_{max} and DcTHOR
LOW_{dif}	Difference in lower deflection
LOW_{tot}	Sum of lower deflection
$LPINTR$	Instrument panel intrusion
LR	Lower right deflection
LR_x	Lower right deflection on x-axis
m	Mass of driver
M	Mass of vehicle
n	Number of data points
N	Random samples from a normal distribution
$NASS/CDS70$	70% underprediction rate curve of the NASS/CDS data
$NASS/CDS50$	50% underprediction rate curve of the NASS/CDS data
$Occupants_{changed}$	Number of occupants changed from uninjured to injured

$Occupants_{injured}$	Real life injured occupants
$Occupants_{new}$	Injured occupants regarding underprediction correction
P	Probability of injury
$PCScore$	Principal Component Score
$P(t)$	Force acting on driver
R	Resultant deflection
R_{max}	Maximum resultant deflection
$R_{max,Adjusted}$	Maximum resultant deflection for the adjusted function for R_{max}
$R_{max,decreased30\%}$	Resultant max deflection decreased by 30%
$R_{max,decreased50\%}$	Resultant max deflection decreased by 50%
R^2	R-squared
s	Slack
SS_R	Sum of squared resuduals
SS_T	Sum of squares
$strain$	Rib strain
s_i	Standard deviations for input deflection metrics for PCscore
t_i	Time
TIC_{NFR}	Deflection according to TIC for Number of Fractured Ribs
TIC_{NSFR}	Deflection according to TIC for Number of Separated Fractured Ribs
TN	True negatives
TP	True positives
TPR	True positive rate
UL	Upper left deflection
UL_x	Upper left deflection on x-axis
UP_{dif}	Difference of upper deflection
UP_{tot}	Sum of upper deflection
UR	Upper right deflection
UR_x	Upper right deflection on x-axis
U_{rate}	Underprediction rate
x	X-coordinate
$\ddot{x}$	Acceleration on the car
y	Y-coordinate
Y	Age correction
y_{glm}	Logistic regression value
y_i	Actual risk probabilities from the simulations
$\ddot{y}$	Acceleration percieved by the occupant
$\bar{y}$	Mean risk probability from simulations
α	Shape parameter for Weibull risk function
α_{strain}	??
β	Scaling factor for TIC
β_0	Intercept for Weibull risk function
β_1	Age coefficient for Weibull risk function
δ	Offset distance for IR-TRACC chest sensor
Δv	Velocity change
$\Delta v_{Winsmash}$	Velocity change calculated with Winsmash

μ	Mean regarding the samling distribution
σ	Scatter standard deviation
φ_y	Deflection angle around y-axis of the rib
φ_z	Deflection angle around z-axis of the rib

Contents

Abstract i

Preface iii

Acknowledgements iii

Abbreviations v

Nomenclature vi

Contents ix

List of Figures xiii

List of Tables xvi

1 Introduction 1
1.1 Aim . . . 2
1.2 Limitations . . . 2

2 Background 3
2.1 Finite Element Method . . . 3
2.2 Impact Biomechanics . . . 3
2.3 Crash Testing of Cars . . . 4
2.4 Anthropomorphic Test Devices . . . 4
2.5 Chest Injuries . . . 6
2.6 Rib Fracture Injury Criteria . . . 8
2.6.1 Resultant Deflection, R_{max} . . . 8
2.6.2 X-axis Deflection, D_{max} . . . 9
2.6.3 DcTHOR . . . 9
2.6.4 Thoracic Injury Criterion . . . 9
2.6.5 Principal Component score . . . 10
2.7 Injury Risk . . . 10

3 Method 11
3.1 FE model of generic vehicle interior . . . 11
3.2 Simulation Post Processing . . . 12
3.3 Injury Criteria Calculation . . . 13
3.3.1 Rmax . . . 13
3.3.2 Dmax . . . 14
3.3.3 DcTHOR . . . 15
3.3.4 Thoracic Injury Criterion (TIC) . . . 16
3.3.5 PCscore . . . 18
3.3.6 Additional Injury Criteria . . . 19
3.4 Parameter Sampling in LS-OPT . . . 20

3.5 THOR positioning . . . 23
3.6 Pilot Study . . . 24
3.7 Statistical Analysis . . . 25
3.7.1 Processing of NASS/CDS Data . . . 25
3.7.2 Risk Curve Generation for Simulation Data . . . 27
3.7.3 Logistic Regression using Vehicle Pulse Index as a Predictor . . . 28
3.7.4 Goodness of Fit . . . 29
3.8 Comparison to Human Body Model . . . 30
3.9 Underprediction of Rib Fractures in NASS/CDS . . . 31
3.10 Sampling of Crashes of Higher Severity . . . 32
3.11 Adjusted R_{max} . . . 32
3.12 EDR Δv NASS/CDS . . . 33
3.13 THOR Accuracy . . . 34

4 Results **35**
4.1 Pilot Study . . . 35
4.2 Simulation Study . . . 37
4.2.1 Results From Sampling of Parameters . . . 37
4.2.2 Winsmash Δv Distribution . . . 39
4.2.3 LS-DYNA Simulations . . . 40
4.2.4 Troubleshooting and Rectifying Errors . . . 40
4.3 Analysis of Simulations . . . 40
4.3.1 Results from Simulations . . . 41
4.3.2 Goodness of Fit . . . 46
4.4 Additional Results . . . 46
4.4.1 Additional Injury Criteria Evaluation . . . 46
4.4.2 Simulation Analysis with Vehicle Pulse Index . . . 47
4.4.3 HBM comparison . . . 49
4.4.4 Effects of Underpredicting Rib Fractures in NASS/CDS . . . 50
4.4.5 Effects of Adding More Severe Crashes . . . 51
4.4.6 $R_{max,Adjusted}$ . . . 52
4.4.7 THOR Accuracy . . . 54
4.5 EDR Δv NASS/CDS . . . 55

5 Discussion **56**
5.1 Overpredicting vs Underpredicting Injury Risk . . . 56
5.2 Injury Risk Probabilities . . . 56
5.3 Processing of NASS/CDS Data . . . 60
5.4 Effects of Under Prediction in NASS/CDS Data . . . 60
5.5 Comparison to Human Body Model . . . 61
5.6 Vehicle Pulse Index . . . 61
5.7 Validation of the Generic Sled . . . 63
5.8 THOR Validation . . . 64
5.8.1 Crash Angles Valid for THOR . . . 64
5.8.2 Correlation Between FE-THOR and Physical THOR . . . 64
5.9 Winsmash Δv Effects on Risk Prediction . . . 65
5.10 THOR Accuracy . . . 67

5.11 Adjusted R_{max} 68
5.12 EDR Δv NASS/CDS 69
5.13 Post Mortem Human Subjects and Real Life Crashes 70
5.14 Limitations 71
5.15 Future Work 71

6 Conclusion **72**

List of Figures

2.1 The THOR ATD and the locations of the IR-TRACC sensors, the top four sensors are the measuring chest deflection, while the two at the bottom correspond to the abdomen. The coordinate system is marked in yellow and the angles in red. 5
2.2 Ribcage surrounding the lungs and pleural cavity. Adapted from *Gray's Anatomy of the Human Body* Lewis(ed.) (1924). 7
3.1 Visualization of the workflow to carry out population-based accident reconstructions using the method by Iraeus and Lindquist (2016). 11
3.2 The FE model of a generic vehicle interior based on an average of 14 cars. . 12
3.3 R_{max} AIS3+ risk curve for a 40 year old occupant. 14
3.4 D_{max} NFR5+ risk curve for a 40 year old occupant. 15
3.5 $DcTHOR$ NFR5+ risk curve for a 40 year old occupant. 16
3.6 The fitting of the Weibull distribution to obtain coefficients for TIC NFR and NSFR. 18
3.7 Risk curve for a set of values for $PCscore$. 19
3.8 LS-OPT stages marked in grey in the workflow. 20
3.9 Latin hypercube example distribution of the airbag size. One dot represents a random sample within the range, where the higher distribution measure within the bins means more samples. 21
3.10 Trig time distribution curve, the dotted line represents the original distribution while the grey curve is the modified distribution for the sampling range. 23
3.11 THOR position in the generic vehicle interior. Pelvis angle shown in green, lumbar spine pitch adjustment in red, neck pitch in yellow and leg position in orange. 24
3.12 Pilot study iteration loop. 25
3.13 The NASS/CDS risk curve derived from Iraeus and Lindquist (2016) for a 40 year-old occupant. 27
3.14 A schematic figure of the interaction between car and driver, accoring to Newton's second law of motion. To the left, a simplified crash is modelled with springs, and the resulting forces to the right. 28
3.15 A schematic figure of the slack present in the restraint system in the car, modelled with a spring and slack distance s. 29
3.16 The generic car sled model with fitted with the SAFER Human Body model. 31
3.17 MAIS3+ Thoracic NASS/CDS EDR Δv Comparison with the recalculated MAIS3+ Thoracic curve 33
4.1 The chest bushing locations in THOR 36
4.2 R_{max} comparison of the same simulation with and without the 0.6mm thick null shells for the bushings in the thorax 37
4.3 The distribution of the sampled Δv from LS-OPT, compared to the theoretical log-normal distribution 38
4.4 The distribution of the sampled crash time duration from LS-OPT, compared to the theoretical normal distribution 38
4.5 Distrubution of Δv after winsmash correction 39

4.6 Scatter plot and curve fitment for simulation results for R_{max}, as well as the NASS/CDS data risk curve. The silver coloured points are the simulation results, i.e., one point corresponds to a risk and a value for the average Winsmash Δv. The 95% confidence interval is marked in grey, around the black NASS/CDS curve. 41
4.7 Scatter plot and curve fitment for simulation results for D_{max}, as well as the NASS/CDS data. The silver coloured points are the simulation results, i.e., one point corresponds to a risk and a value for the average Winsmash Δv. The 95% confidence interval is marked in grey, around the black NASS/CDS curve. 42
4.8 Scatter plot and curve fitment for simulation results for $DcTHOR$, as well as the NASS/CDS data, The silver coloured points are the simulation results, i.e., one point corresponds to a risk and a value for the average Winsmash Δv. The 95% confidence interval is marked in grey, around the black NASS/CDS curve. 43
4.9 Scatter plot and curve fitment for simulation results for $PCscore$, as well as the NASS/CDS data. The silver coloured points are the simulation results, i.e., one point corresponds to a risk and a value for the average Winsmash Δv. The 95% confidence interval is marked in grey, around the black NASS/CDS curve. 43
4.10 Scatter plot and curve fitment for simulation results for TIC_{NFR}, as well as the NASS/CDS data. The silver coloured points are the simulation results, i.e., one point corresponds to a risk and a value for the average Winsmash Δv. The 95% confidence interval is marked in grey, around the black NASS/CDS curve. 44
4.11 Scatter plot and curve fitment for simulation results for TIC_{NSFR}, as well as the NASS/CDS data. The silver coloured points are the simulation results, i.e., one point corresponds to a risk and a value for the average Winsmash Δv. The 95% confidence interval is marked in grey, around the black NASS/CDS curve. 45
4.12 All fitted risk curves, as well as the NASS/CDS data 45
4.13 Distribution of the peak abdomen displcement for all simulations. 47
4.14 Distribution of the peak HIC values from all simulations. 47
4.15 Distribution of the Vehicle Pulse Index. 48
4.16 Injury risk curves using VPI as the predictor. 48
4.17 Risk curve for the SAFER HBM compared to the calculated injury risks for THOR. 49
4.18 Influence of underprediction rib fractures in the NASS/CDS data. 50
4.19 The new distribution of Δv after the addition of more severe crashes. . . . 51
4.20 The risk curves for the newly added cases, a shift to the right can be seen for all cases. 52
4.21 Rmax AIS3+ comparison for a 40-year-old between the adjusted and original R_{max} curve. The individual simulations plotted as grey dots for the $R_{max,Adjusted}$. 53
4.22 Rmax AIS3+ deflection comparison for a 40 year old between the adjusted and original R_{max} curve. 53

4.23 Rmax AIS3+ comparison for a 30 year old between the adjusted and original R_{max} curve. The individual simulations plotted as grey dots for the $R_{max,Adjusted}$. 54
4.24 R_{max} plotted together with two special cases, the dotted line indicates the cases where the R_{max} value was decreased by 30 %, and the dashed line where the R_{max} value was decreased by 50 %. 54
4.25 All injury criteria for true Δv plotted against Brumbelow (2019) thoracic MAIS3+ curve for 40-59 years old. 55
5.1 Distribution of simulation risk prediction by TIC_{NSFR}. 57
5.2 Distribution of simulation risk prediction by $PCscore$ and TIC_{NFR}. . . . 58
5.3 Distribution of simulation risk prediction by TIC_{NSFR}. 58
5.4 Risk curve for R_{max} in log-odds space. 59
5.5 The NASS/CDS risk curve, along with the re-scaled markings for injured/uninjured. 60
5.6 The Vehicle Pulse Index as a function of Δv, with the linear regression line in black. 62
5.7 The risk curves for all injury criteria and compared to the VPI risk curve from Tsoi and Gabler (2015). Note that this risk was computed using the MAIS3+ injury scale. 63
5.8 The risk curve for R_{max}, with the special case marked with a green circle. . 65
5.9 The effect of changing Δv according to the Winsmash estimation. The dashed line represents the risk curve for the Δv used in the simulations, while the solid line was the Winsmash Δv 66
5.10 The risk curves computed and plotted for true Δv. 67
5.11 Rmax AIS3+ comparison for a 70-year-old between the adjusted and original R_{max} curve. The individual simulations plotted as grey dots for the Adjusted R_{max} and plotted in light blue for the original R_{max}. 68
5.12 The risk curves computed and plotted for true Δv, and compared to the risk curve derived using EDR Δv from Tsoi and Gabler (2015). 70

List of Tables

2.1 AIS injury scales, adapted from Schmitt et al. (2019). 6
3.1 Car models used by Iraeus and Lindquist (2016) to generate the generic model used in this study. 12
3.2 CFC filter values. 13
3.3 All parameters and their respective distributions, that were used. 22
3.4 The underpredition rates and increase in injured occupants for each leve.l . 32
4.1 All the error that occured during the pilot study, and the corresponding fix implemented to solve the problem 35
4.2 All injury criteria and their respective R^2 scores, as well as the Δv at the 50% risk. The curve fit parameters are also included. 46

1 Introduction

Every year lives are lost in the traffic and according to the World Health Organization (WHO 2018), the number of fatalities each year is 1.35 million. This means that traffic deaths is the 8^{th} leading cause of death for people in all ages. Car occupants contribute to 29% of the total fatalities on the road. Furthermore, as reported by the Insurance Institute for Highway Safety (IIHS 2019) frontal crashes make up for most of the total car related deaths in the United States (US) with over 50%.

The distribution of injuries in frontal crashes has been investigated previously. For instance, Sherwood et al. (2019) used data from the National Automotive Sampling System/Crashworthiness Data System (NASS/CDS) and analyzed the injury mechanisms for occupants in small overlap crashes. Sherwood concluded that 75% of the drivers studied had an AIS2+, according to the Abbreviated Injury Scale (AIS), injury on the thorax, and 70% had an AIS3+ injury to the thorax. Another study, by Hallman et al. (2011), made a similar conclusion as Sherwood. Hallman used data from two different sources in the study. The data sources were Crash Injury Research (CIREN) and NASS/ CDS for cases with a Principal Direction of Force (PDOF) between -20° to 20° for large overlap impacts. Injuries of type AIS3+ to the thorax were the second most common injury type after injuries to the lower extremities. Thorax injuries are closely associated with rib fractures, which was previously studied by Crandall et al. (2000) on Post Mortem Human Subjects (PMHS). Thus, rib fractures are one of the main driving mechanisms behind injuries to the thorax.

During the development of cars and their restraint systems, Anthropomorphic Test Devices (ATDs) are commonly used for development and verification testing. The ATDs are mechanical representations of the human body, equipped with sensors to gather data. Historically, there has been several different ATDs in use, but the most frequently used ATD is the Hybrid III which was developed by General Motors (GM) in the US (Foster et al. 1977) during the 1970s. Hybrid III was created with the objective of obtaining better biomechanical response (Foster et al. 1977), compared to its predecessors Hybrid I and II. In addition, Hybrid III displayed better reproducibility, documentation and improved possibilities to measure additional parameters. A more recent design is the Test device for Human Occupant Restraint 50^{th} male (THOR-50M, hereby referred to as THOR), which is a more advanced ATD than Hybrid III, in particular it was designed with improved biofidelity and better chest deflection measurement capabilities (Parent et al. 2017). Four chest mounted sensors, compared to one in Hybrid III, was mounted on THOR, to better reflect the thorax loading in a crash event. Parent et al. (2017) made a biofidelity evaluation of THOR and Hybrid III. The assessment was made using the National Highway Traffic Safety Administration's (NHTSA) Biofidelity Ranking System in a total of 21 test conditions. THOR scored better than Hybrid III in 5 of 7 internal body regions, while THOR was better in 6 of 7 external biofidelity conditions. The scores were based on comparisons with PMHS. In addition to the physical ATDs, there are also finite element (FE) models of the ATDs, that can be used in a simulation environment before any real life crash testing might be made during car development programmes.

This study used the THOR, for its improved evaluation of the chest deflection, by using four three-dimensional displacement gauges. An FE-model of the THOR ATD was positioned inside a generic FE vehicle compartment model, consisting of a driver's seat and included safety systems such as and airbag and seatbelt, and surrounding structure for the vehicle. The FE vehicle compartment model was previously developed by Iraeus and Lindquist (2016). A population based stochastic simulation study was setup up, using the generic FE vehicle compartment model equipped with THOR, to enable a comparison with a selection of NASS/CDS data based risk curve derived by Iraeus and Lindquist (2016). The simulated population of crashes were derived from real life distributions (Iraeus and Lindquist 2016).

1.1 Aim

The aim of this study was to compare rib fracture risk functions for the THOR ATD with respect to the risk of injury in real life crashes sampled from NASS/CDS using the method and generic FE vehicle compartment model developed by Iraeus and Lindquist (2016), using multiple injury criteria.

1.2 Limitations

The current study was limited in that it only assesses oblique near side frontal collisions, with a Principal Direction of Force (PDOF) of -45° to 10°. Additionally, since the work is carried out using the THOR ATD, which is an average sized male occupant model, it might be difficult to generalize the findings to occupants of other sizes. The car environment and THOR ATD will be part of a simulation environment, and no real-life testing was made.

2 Background

An ATD is a mechanical representation of a human, for the purpose of using them in place of humans when crash testing. When evaluating injuries sustained in crashes, an injury scale classification is used, where the different severity levels correspond to a number, depending on the level of injury endured. To bridge the gap between crash testing with ATDs and real-life injury probability, risk functions computing the risk of sustaining an injury are used, these risk functions use the sensor outputs retrieved from the ATD. An introduction to impact biomechanics and the Finite Element method (FE-method) is also given.

2.1 Finite Element Method

The FE-method is a way of numerically solving differential equations relating to e.g. mechanical or thermal problems. In particular, nonlinear FE-analysis is an essential part of computer aided design. The testing of prototypes are more often replaced by simulating with nonlinear FE-method, since it is a faster and less expensive method to evaluate design concepts (Belytschko et al. 2014). For instance, in the automotive industry, simulations of crashes are replacing full scale crash tests, both for evaluating design concepts as well as more detailed parts, such as crash structures and safety system interaction. This method can be used to determine if a car meets the crashworthiness criteria. The FE-method can also be used in fields of manufacturing, for simulating the effects of manufacturing processes. In addition, electronics industries are replacing traditional methods with simulation (Belytschko et al. 2014). It is important that analysts and developers understand fundamental concepts, to fully grasp the implications of the method and to make better decisions.

There are different types of problems, that require different solvers. Explicit or implicit analyses are the most common. Implicit FE is known as solving for the unknowns through matrix inversion. Explicit FE-problems are characterized by solving the equations in time, i.e. explicit FE-method is used to compute the state of the system at a different time from the current (Belytschko et al. 2014). Car crashes depend heavily on the different time steps, and thus LS-DYNA (ANSYS/LST, Livermore, CA, USA) was used in this study, since it is the preferred explicit FE-solver for crash simulation events.

2.2 Impact Biomechanics

Mechanical loads are something that the human body is exposed to throughout its life. Apart from the forces generated by gravity or electromagnetic fields, there is great variety of forces that might affect the human body. The science of biomechanics is dedicated to the analysis, measurement and modeling of the effects during different mechanical loading situations (Schmitt et al. 2019), first and foremost on humans, but also on animals and plants. Internal forces can span a great range of cases, while the same applies for external load cases. Magnitudes of forces that lay of interest range between pN to MN, and can vary greatly in time (Schmitt et al. 2019).

Injury to the human body may occur because of applied forces, and such cases are often connected to actions which include excessive external forces being applied during an accident for example. In fact, accidents of all kinds are a leading cause of death, especially among young people (Schmitt et al. 2019). Self-inflicted injuries, i.e. injuries caused by the body itself, can also happen, e.g. a broken rib due to intense coughing (Schmitt et al. 2019).

There are many different types of injuries, injury mechanisms and injury causing activities, biomechanics must consider a large variety of human activities where injuries may take place. Thus, it is apparent that biomechanics is an interdisciplinary science. Moreover, clinical medicine is of importance, with respect to classifying injury severity, for example. The knowledge within the field, gathered for hundreds of years in different disciplines, have greatly contributed to impact biomechanics, for giving a detailed understanding of injuries and their causes (Schmitt et al. 2019).

2.3 Crash Testing of Cars

Safety is an important aspect of a car's properties, in fact a survey conducted by McCartt, A.T. and Wells J.K., (2010), says that safety ranks second among the participants, as the most important factor to consider when buying a car. Accordingly, this means that car manufactures must produce safe cars. During the development, an automotive company may set up a list of requirements that a car must meet. In many cases the developments within the industry lead to higher safety standards across the whole markets.

In addition to the set of requirements a car producer sets on its own cars, independent ratings are made, to objectively quantify how well a car can protects its occupants in a set of standardized tests. This system is called New Car Assessment Programme (NCAP), either in the US (USNCAP) or in Europe (Euro NCAP). Other actors may also test the cars, such as the IIHS in the US. These tests then let the customer have access to and compare the different test results. In addition, there are governing bodies that regulate what standards must be met for a car to be legally sold, in the US this body is called the National Highway Traffic Safety Administration (NHTSA). It is the role of NHTSA to set legal requirements for car manufacturers, to improve overall safety levels.

2.4 Anthropomorphic Test Devices

An ATD simulates the human response in a car crash scenario, and are designed to imitate the shape and form of the human body (Schmitt et al. 2019), and even more importantly the kinematic and kinetic responses during a crash. There are many different types of ATDs today, where Hybrid III (Foster et al. 1977) and THOR (Parent et al. 2017) are commonly used in frontal crashes. Hybrid III has been used as the standard ATD during the latter part of the 20^{th} century and the beginning of the 21^{th} century, and is the most widely used ATD currently (Foster et al. 1977). Hybrid III was developed as a successor for Hybrid I and Hybrid II, by General Motors during the 1970s, Foster et al. (1977). The objective during development was to create an ATD with a more

biomechanical response, in particular structures around the neck, thorax and knees. The Hybrid III was a significant improvement to its predecessor, though it is by no means the "ultimate" test device (Foster et al. 1977). The authors argued that further improvements must however await with better understanding of car crash injury mechanisms. A limitation of the Hybrid III ATD is that it only has one centrally mounted chest deflection sensor.

An improved ATD, and the proposed successor of Hybrid III, was developed starting in 1995, Humanetics (2022). The new device was called Test device for Human Occupant Restraint, or THOR for short. The main purpose of the development was to create a device with improved biofidelity, dynamic response, instrumentation, repeatability, durability and user-friendliness. The development of THOR was supported actively by the NHTSA. Among the improvements, lay particularly the increased number of chest measurement locations, with four locations instead of one location. The sensors were not mounted in the center, as for the Hybrid III, but rather off center, corresponding to the actual location of the fourth and eight ribs, on each side, Figure 2.1. THOR is equipped with 6 Infra-Red Telescoping Rod for the Assessment of Chest Compression (IR-TRACC) sensors, 4 of which measures the ribcage deflection in mm. The 2 other, located at the bottom, correspond to deflection for the abdomen.

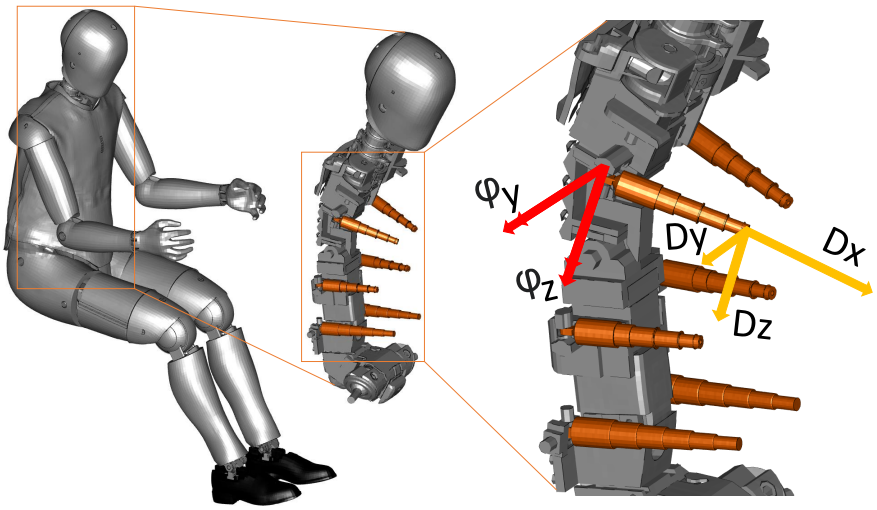

Figure 2.1: The THOR ATD and the locations of the IR-TRACC sensors, the top four sensors are the measuring chest deflection, while the two at the bottom correspond to the abdomen. The coordinate system is marked in yellow and the angles in red.

According to Craig et al. (2020) NHTSA traditionally uses the 50^{th} male ATDs in frontal collision tests. 50^{th} male refers to a male in the 50^{th} percentile among a normal distribution of the population, i.e. a 50^{th} male would be the size and weight of an average North American man. NHTSA reported that the THOR 50^{th} male ATD will replace Hybrid III, and will be used in the future for frontal crash test scenarios.

There are several requirements for an ATD. Firstly, it must be reproducible, meaning that the manufacturing of the ATD can be done over and over, and get equally accurate test devices. In addition, it must be repeatable, which means that an ATD must be able to

produce similar results if a crash test setup is repeated. The THOR ATD is also modelled for FE-simulations, which is a more controlled environment, where it is important that the model correlates well with the real life model.

In this study an FE model of the Humanetics USNCAP THOR 1.7 50^{th} male was used. The ATD itself does not have any age, and one may therefore use the risk function to correct for age depency. The THOR ATD has numerous sensors and accelerometers mounted within, but for this project, the output from the sensors mounted in the chest were the main focus.

2.5 Chest Injuries

Traumatic injuries can be classified according to the AIS, which is classifying injuries according to the threat to life for the injured person. In the AIS classification method, 1 is a minor injury, 2 moderate, 3 serious, 4 severe, 5 critical and 6 maximal/currently untreatable (Genrelli and Wodzin, 2005). The AIS levels of thorax injuries were summarized by Schmitt et al. (2019), Table 2.1.

Table 2.1: AIS injury scales, adapted from Schmitt et al. (2019).

AIS Skeletal injury	
1	One rib fracture
2	Two rib fractures; sternum fracture; pneunothorax
3	Three or more rib fractures on one side; hemothorax; fractures with flail
4	Four or more rib fractures on each of the two sides; four or more rib fractures with hemo- or pneumothorax
5	Bilateral flail chest

There are many other injuries that can be sustained to the thorax than a closed rib fracture (Schmitt et al. 2019). Pneumothorax is a collapse of the lung due to the negative pressure in the pleural cavity cannot be maintained and is therefore filled with air. The pleural cavity can be seen in Figure 2.2, together with the lungs and ribcage. Similarly, for AIS3 which includes hemothorax, where the cavity is instead of air, filled with blood (Schmitt et al. 2019). AIS3 also includes fractures with flail which happens when there is a fracture in 2 or more places in the same rib. Flail means that the stability of the thorax is lost, and that parts of it may move when breathing. Bilateral flail means instablity on both sides, which means breathing is no longer possible (Schmitt et al. 2019). Finally, AIS5 is the risk of a bilateral flail chest, which is synonymous with rib fractures leading to flail chest on both sides.

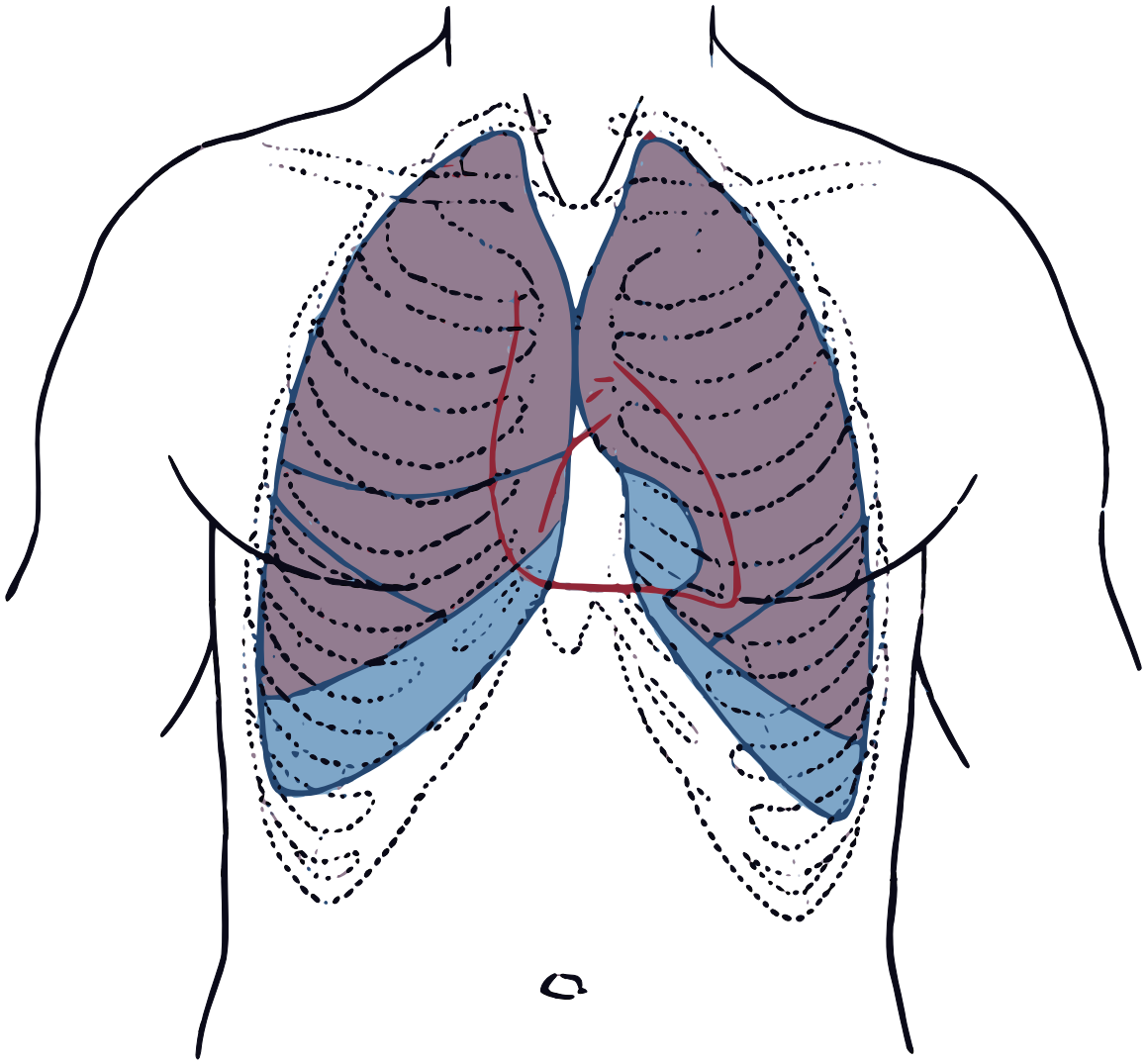

Figure 2.2: Ribcage surrounding the lungs and pleural cavity. Adapted from *Gray's Anatomy of the Human Body* Lewis(ed.) (1924).

In tests with PMHS, as well as for accidents in the field, rib fractures are sometimes quantified using Number of Fractured Ribs (NFR) or Number of Separated Fractured Ribs (NSFR) (Troseille et al. 2019). The first is simply the number of fractured ribs, while the latter is the number of fractured ribs for which the ends are separated from each other so that they can be seen on X-ray. Hence, NSFR is a correction for the cases in which the rib fractures are visible on an X-ray. This means, that, on average NSFR count fewer rib fractures than NFR does. There might, for example, be cases in which the injured occupant has a rib fracture but might not be diagnosed as such if it is not seen on an X-ray (Troseille et al. 2019). Similarly, to AIS, both NFR and NSFR have magnitudes of the injury scales starting from 1, which means 1 fractured- or separated fractured rib. Another way of denoting injury severity is to classify it as e.g., AIS3+ or NFR3+, which means all injuries worse than and including AIS3 or NFR3, respectively. Furthermore, one could also consider the Maximum Abbreviated Injury Scale (MAIS), for an injured

occupant. MAIS states the highest AIS code sustained by one person on any part of the body studied, e.g., if an occupant suffers AIS2 level of injuries to the thorax but no more than AIS1 on any other body part, the MAIS would be MAIS2 for this example (Schmitt et al. 2019).

2.6 Rib Fracture Injury Criteria

An injury criterion is a way to relate a certain loading of the thorax with a corresponding risk of e.g., AIS3+ injury (Schmitt et al. 2019). According to Schmitt et al. (2019) the driving mechanism for rib fracture is the deflection of the ribs. Hence, a rib fracture criterion should consider the rib deformation of the test object. The introduction of THOR and its multiple measurement points facilitates the possibility to improve the prediction of injury risk, with new injury criteria. All injury criteria used in this study were developed from tests with PMHS.

Previously developed injury risk functions, for Hybrid III (Eppinger 1999 and Laituri et al. 2005), required corrections or assumptions to account for the center mounted single-point measurement capability of the Hybrid III (Craig et al. 2020). Previously, NHTSA has identified that increasing the number of measurement points, can improve the thoracic loading assessment in vehicles with more advanced restraint technology, such as airbags and pretensioners (Yoganandan et al. 2009). Morgan et al. (1994) discovered that thoracic trauma might not always occur at the same ribcage location for occupants in frontal crashes. If using multiple measurement locations on the chest, the injury prediction could be improved (Kuppa and Eppinger 1998). The authors studied a dataset of 71 PMHS test, with different levels of crash severity and restraint systems, and found an improved injury prediction when using multiple deflection measurement points (Kuppa and Eppinger 1998).

Real world data suggest that a multiple point deflection measurement is required to better reflect actual injury patterns. Shimamura et al. (2003) found that rib fractures occur more often in the lower than the upper ribs. In addition, the rib fracture pattern might often be asymmetric (Craig et al. 2020). As such, the peak deflection does not normally occur centrally, and are thus unlikely to correspond to the mid-mounted sensor location of the Hybrid III.

2.6.1 Resultant Deflection, R_{max}

Craig et al. (2020) developed a measure for peak chest deflection, R_{max}, which considers the peak resultant deflection in any of the four chest mounted sensors of the THOR ATD. During the development of this thoracic injury criterion several datasets were considered. A recent matrix of PMHS tests collected by the University of Virginia was considered, with a total of 42 PMHS observations. Additionally, a total of 14 matched pair tests with PMHS and THOR were also included. Tests from Eppinger et al. (1999) that were similar to the already extracted ones, a total of five, were also considered.

Several different predictor variables were considered, and Craig et al. (2020) briefly argues that including measurements from all four sensors was likely to cause overfitting of the injury risk curve. The final proposal, R_{max}, was chosen for its relative simplicity, since there is no need to recompute the sensor outputs, in addition to the fact that none of the other considered criteria could predict injuries significantly better. This measure is proposed by NHTSA as the injury criterion to be used for evaluating thorax injuries when crash testing with THOR.

2.6.2 X-axis Deflection, D_{max}

D_{max} was developed by Davidsson et al. (2014) and considers the peak x-axis deflection in any of the IR-TRACC four locations. Principal component analyses were carried out, and in one instance it showed that a significant portion of the variance could be explained by considering the peak x-axis deflections in the upper left, upper right, lower right and the peak of the upper points. Further, it was found that, for some datasets, D_{max} offered a better prediction than R_{max}. The x-axis deflection was computed using the resultant deflection R_{max} and the inward angles of the IR-TRACC sensors, Figure 2.1.

2.6.3 DcTHOR

Another criterion was developed in the same paper, DcTHOR (Davidsson et al. 2014), which is a differential measure, taking all four sensors into account. This criterion uses the general thoracic compression level and the ribcage twisting level at both the upper and lower locations. The method of developing this injury criterion did not differ substantially from the other already mentioned. A set of 153 PMHS test were analyzed, with different loading conditions and restraint types. The PMHS tests were reproduced with the THORAX demonstrator, and Cox regression was used to ensure there were differences between the responses. NFR was chosen as the injury scale for both DcTHOR and D_{max} since the AIS coding has changed over time, thus the AIS classification might not be consistent for PMHS test done in previous times (Davidsson et al. 2014).

2.6.4 Thoracic Injury Criterion

The Thoracic Injury Criterion (TIC) was developed by Trosseille et al. (2019) as a linear combination of R_{max} and upper differential deflection (UPdif), which is the difference in deflection of the upper IR-TRACC sensors on the THOR ATD. TIC is hence a linear combination of the maximum value of the four chest resultant deflections and the absolute value of the difference of the upper right and left deflections. TIC was defined for the NFR and NSFR injury classifications.

2.6.5 Principal Component score

Principal Component score (PCscore) is an injury criterion developed by Poplin et al. (2017), where the objective was to create a function to predict the probability of thoracic rib injuries, using multiple chest deflection measurements. The approach was to match the injury outcome of PMHS tests, to chest deflection measured on the THOR ATD. This measure was only defined for the maximum value in time, i.e., there was only one value when analyzing one crash as opposed to the other which can be plotted over the crash time. However, for this study the maximum value was the only value of interest anyhow, meaning the variation over time of the injury criterion in one crash does not come in to play.

To summarize, six different injury criteria were used in the study, two of which, R_{max} and D_{max}, consider the maximum value across the four sensors, i.e. only one sensor. The other four were differential measures, taking more than one sensor into account when computing the final injury criterion value.

2.7 Injury Risk

The injury criteria each have a corresponding risk function, that calculates the risk of sustaining an injury to a specified severity level, e.g., AIS3+, where the value computed for the injury criteria were inserted in the formula for computing the risk. The injury criteria follow different distributions, either a Weibull or log-normal distribution, in accordance with the function it was developed for. The risk functions have separate parameter values for the individual criteria.

For the injury criteria considered in this study, the injury risk functions for the criteria R_{max}, TIC and $PCScore$ all follow a Weibull distribution, while D_{max} and $DcTHOR$ follow log-normal distributions. In addition, R_{max} and $PCScore$ were computed with respect to the AIS3+, while D_{max} and $DcTHOR$ were in relation to NFR5+ and TIC was computed for both NFR3+ and NSFR3+. These definitions were not exactly the same, however, in this study, a comparison between the different metrics were made since they were of similar injury levels, Table 2.1.

3 Method

The work conducted in this study was based on a generic FE model of generic vehicle interior developed by Iraeus and Lindquist (2016). The basic workflow was to first replace the existing Human Body Model (HBM) in the generic vehicle interior, with the THOR FE-model. Then, sample the parameters for the generic vehicle interior and re-morph the model in the pre-processor ANSA version 21.0.1 (Beta CAE Systems, Luzern, Switzerland). After the model had been pre-processed, the simulations in LS-DYNA version 7 were run. Results were then extracted and post-processed in META (Beta CAE Systems, Luzern, Switzerland), where several different injury criteria were considered. Finally, the field crash data from NASS/CDS was processed, and the injury risks could be compared. Figure 3.1 shows a flow chart of the work stages.

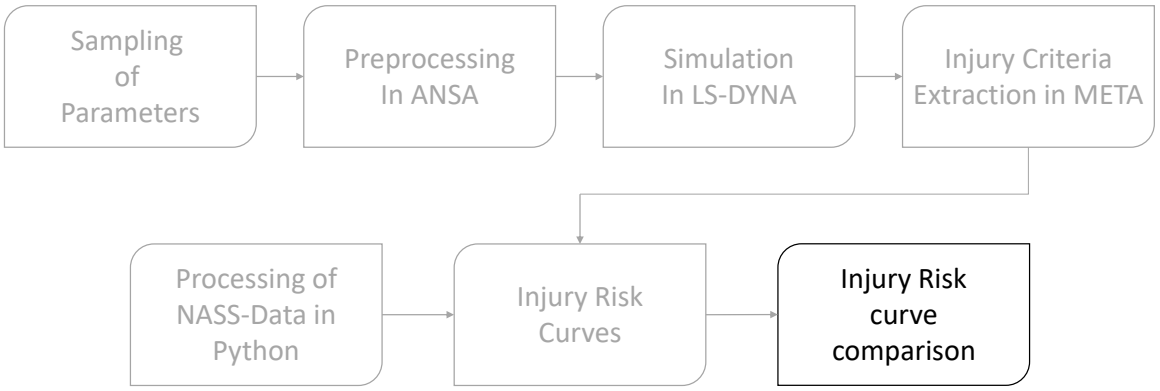

Figure 3.1: Visualization of the workflow to carry out population-based accident reconstructions using the method by Iraeus and Lindquist (2016).

3.1 FE model of generic vehicle interior

The FE model of a generic vehicle interior was developed by Iraeus and Lindquist (2016), and the method of producing it is described here. The most important parts of the vehicle interior for this study were the structures that the occupant comes into contact with during a crash. Properties of importance include the geometry, stiffness of impact surfaces as well as properties for the belt and airbag systems.

The chosen cars had to fulfill 3 criteria: be available in the A2MAC1 (A2MAC1, Boulogne Billancourt, France) database, physically accessible (in Sweden) for measurements and tested in the NCAP program. The cars in Table 3.1 met these criteria. A2MAC1 is a database containing detailed information about cars, such as the geometry and other specifications. The cars represented were of different sizes as well as different vehicle classes. The range of model years, between 2003 and 2017, means different generations of safety systems were equipped. The average car interior was then modeled, Figure 3.2, and consists of the floor, b-pillar- door trim, roof liner, instrument panel, center console, steering wheel, pedals and a seat. For visualization purposes, a roof, door with glass and

a windscreen were included. The selected car models represent the car included in the analyzed NASS/CDS data, Iraeus and Lindquist (2016).

Table 3.1: Car models used by Iraeus and Lindquist (2016) to generate the generic model used in this study.

Model	Model Year	Curb weight [kg]	Vehicle class	NCAP test no
Audi A4	2006-2008	1673	Compact executive	7027
Audi Q5	2008-2017	1941	Compact SUV	6732
BMW 318	2005-2012	1525	Compact executive	5590
BMW 523	2003-2010	1793	Compact executive	7024
Honda CRV	2006-2011	1581	Compact crossover SUV	5875
Honda Insight	2009-2014	1239	Compact	6729
Hyundai Santa Fe	2007-2012	1812	Mid-size crossover SUV	5838
Lexus RX350	2009-2015	1986	Mid-size SUV	6643
Mazda 6	2008-2013	1501	Mid-size	6513
Mercedes E	2010-2016	1826	Executive	6822
Mini Cooper	2006-2014	1130	Subcompact	6291
Toyota Prius	2003-2009	1340	Mid-size	5587
Toyota Rav 4	2006-2012	1597	Crossover SUV	5611
Toyota Yaris	2005-2010	1078	Subcompact	5677

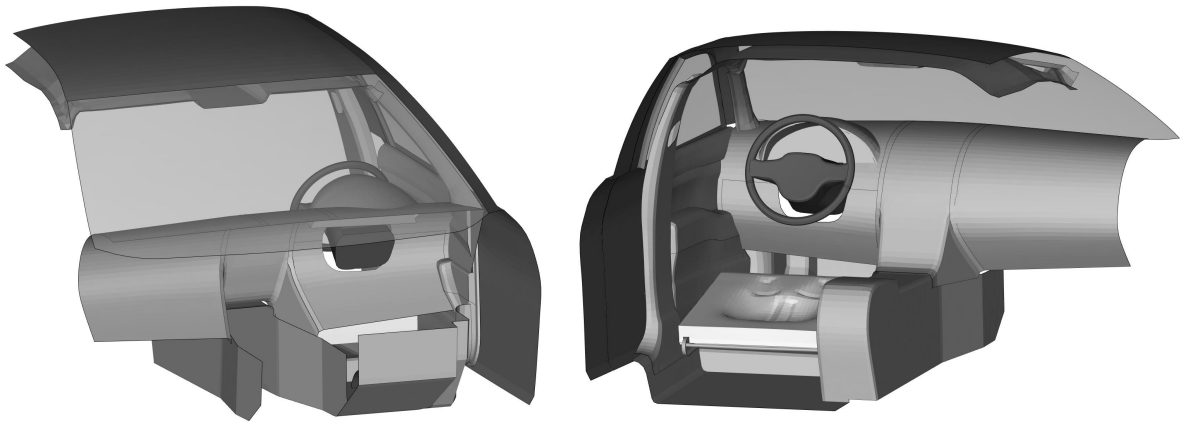

Figure 3.2: The FE model of a generic vehicle interior based on an average of 14 cars.

3.2 Simulation Post Processing

Simulation post-processing was carried out using Meta v 22.0.1 that were run via a Python 3 (Python Software Foundation, https://www.python.org/) script. Signals analyzed were the thoracic and abdominal IR-TRACC displacements, neck forces and IR-TRACC rotations. All signals were filtered using SAE J211-1 (2003) Channel Filter Class (CFC) filters according to Craig et al. (2020), Table 3.2. After extracting the ATD signals, injury criteria calculation was conducted.

Table 3.2: CFC filter values.

Signal	CFC
Head CG Accelerometer, X, Y and Z-axis (g)	1000
Upper and Lower Neck Force, X, Y and Z-axis (N)	1000
Left and Right abdomen Y and Z-axis rotational pot. (deg)	180
Upper Left and right Y and Z-axis rotational pot. (deg)	180
Lower Left and right Y and Z-axis rotational pot. (deg)	180

Following the post-process calculations in META, the data was plotted, and the peak injury criteria and risks were stored in a text.csv-file. Furthermore, another csv-file containing all data was also made, to allow for plotting in another software, e.g., Python, where the user can have more control when plotting.

3.3 Injury Criteria Calculation

Several different chest injury criteria were considered and computed for each simulation. This, in order to evaluate the risk of injury from different perspectives, e.g., using peak deflection or using a linear combination of all sensors. The sensors used for the calculations were the IR-TRACC sensors located in the THOR ATD, seen in Figure 2.1 together with the coordinate system used.

3.3.1 Rmax

The chest injury criteria R_{max} (Craig et al. 2020) is the max resultant chest deflection of any of the Upper Left UL, Upper Right UR, Lower Left LL, and Lower Right LR IR-TRACC gauges of the THOR ATD, Equation (3.1).

$$R_{max} = \max\left(|UL, UR, LL, LR|\right) \tag{3.1}$$

Based on the R_{max} deflection calculated for each simulation, a probability for sustaining an AIS3+ level of injury was computed using the function described in Craig et al. (2020), which follows a Weibull distribution, Equation (3.2)

$$P(AIS3+) = 1 - e^{-\left(R_{max}/e^{\beta_0+\beta_1 age}\right)^{\alpha}} \tag{3.2}$$

For which *age* is the age of the occupant, and in the case studied in this report, a 40-year-old. β_0, β_1 and α are coefficients from the regression model. For this case they take the values 4.7276, 0.0166 and 2.977, respectively. The R_{max} risk function for a 40 year old occupant has a risk of 50%, for sustaining an AIS3+ chest injury, for 51.5 mm R_{max} chest deflection, Figure 3.3.

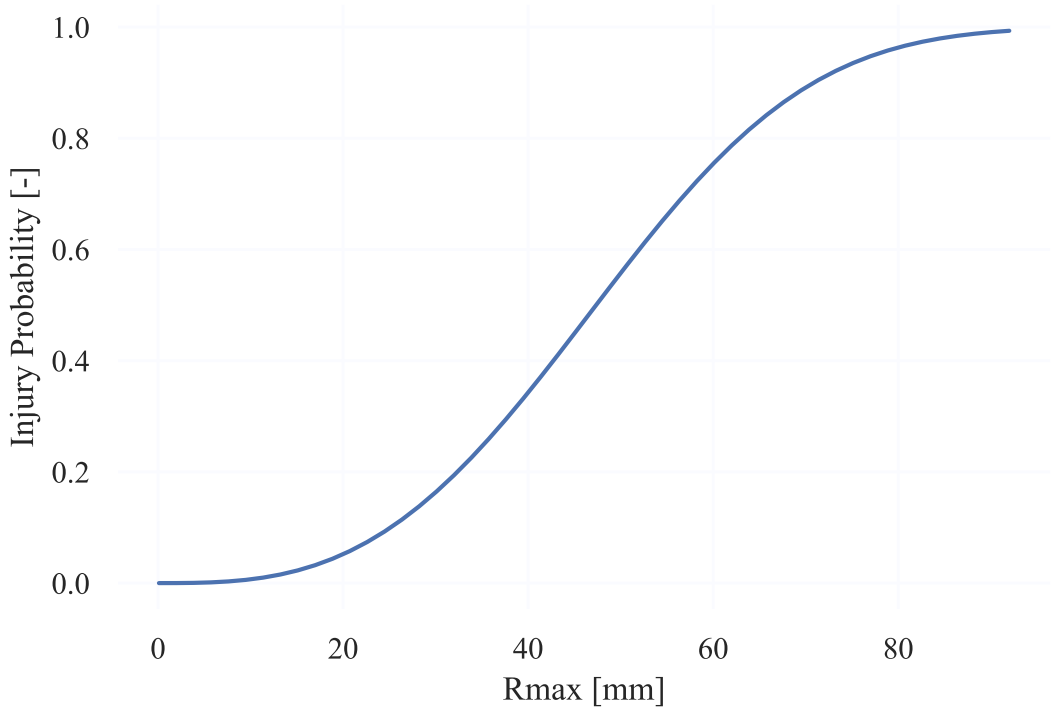

Figure 3.3: R_{max} AIS3+ risk curve for a 40 year old occupant.

3.3.2 Dmax

This injury criterion is similar to R_{max}, however instead of resultant deflection, D_{max} only considers the deflection along the x-axis, Davidsson et al. (2014). For the deflection to be computed along the x-direction, the angles of each deflected rib must be extracted. Each rib IR-TRACC sensor has two angular sensor measures, one for y-axis rotation and one for z-axis rotation, as shown in Figure 2.1. Then, the recalculation of the deflection was done according to Humanetics (2016), for every sensor, Equation (3.3).

$$D_x = \delta \sin \varphi_y + R \cos \varphi_y \cos \varphi_z \tag{3.3}$$

φ is the angle of a rib, y and z means which axis the angles are measured around. R is the resultant deflection for an IR-TRACC sensor. δ is the offset distance for the sensors. D_{max} is then computed as the maximum x-deflection for any of the four ribs.

$$D_{max} = \max\Big(|UL_x, UR_x, LL_x, LR_x|\Big) \tag{3.4}$$

The injury risk function follows a log-normal distribution, Davidsson et al. (2014).

$$P(NFR5+) = \frac{1}{2} + \frac{1}{2} erf \frac{ln(D_{max}) - (int + age \cdot c_{age})}{\sqrt{2(e^{logscale})^2}} \tag{3.5}$$

Where erf is the error function, int,c_{age} and $logscale$ are parameters from Davidsson et al. (2014), and they take the values 3.99, -0.003 and -1.18, respectively. age is the age of

the occupant. The D_{max} risk function for a 40 year old occupant has a risk of 50%, for sustaining an NFR5+ chest injury, for 47.54 mm D_{max} chest deflection, Figure 3.4.

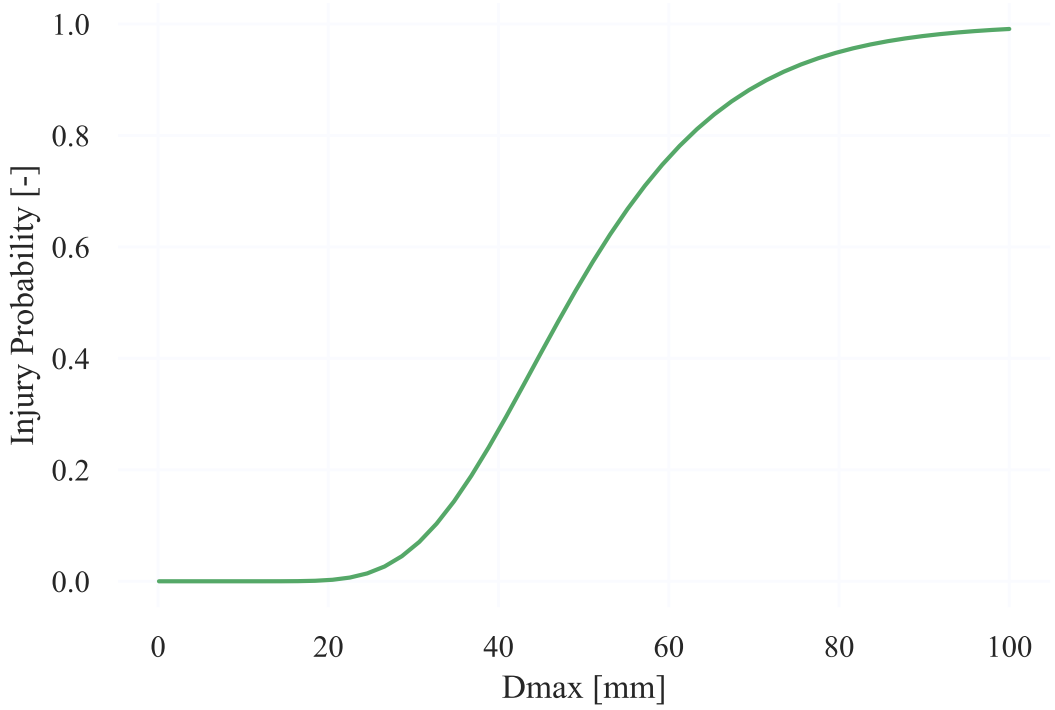

Figure 3.4: D_{max} NFR5+ risk curve for a 40 year old occupant.

3.3.3 DcTHOR

The $DcTHOR$ criterion, developed by Davidsson et al. (2014), uses all four chest-displacement sensors to compute overall and differential deflections. The criterion was defined as shown in Equation (3.6).

$$DcTHOR = D_m + dD_{up} + dD_{lw} \tag{3.6}$$

For which

$$D_m = \frac{\left(|UL_x| + |UR_x| + |LL_x| + |LR_x|\right)}{4} \tag{3.7}$$

$$dD_{up} = |UL_x - UR_x| - 20 = 0;\ \text{if } |UL_x - UR_x| \leq 20 \text{ or } \min\left(|UL_x|, |UR_x|\right) \leq 5 \tag{3.8}$$

$$dD_{lw} = |LL_x - LR_x| - 20 = 0;\ \text{if } |LL_x - LR_x| \leq 20 \text{ or } \min\left(|LL_x|, |LR_x|\right) \leq 5 \tag{3.9}$$

UL_x, UR_x, LL_x, LR_x are the x-components computed according to Equations 3.3. Dm is the general thoracic compression level, dD_{up} and dD_{lw} are the ribcage twisting level at the upper and lower positions, respectively. A log-normal risk function is used for DcTHOR, Davidsson et al. (2014).

$$P(NFR5+) = \frac{1}{2} + \frac{1}{2} erf \frac{ln(DcTHOR) - (int + age \cdot c_a)}{\sqrt{2(e^{logscale})^2}} \tag{3.10}$$

For DcTHOR the coefficients int, c_a and logscale take different values from before, 4.11, -0.008 and -0.89, respectively. The $DcTHOR$ risk function for a 40 year old occupant has a risk of 50%, for sustaining an NFR5+ chest injury, for 41.52 mm $DcTHOR$ chest deflection, Figure 3.5.

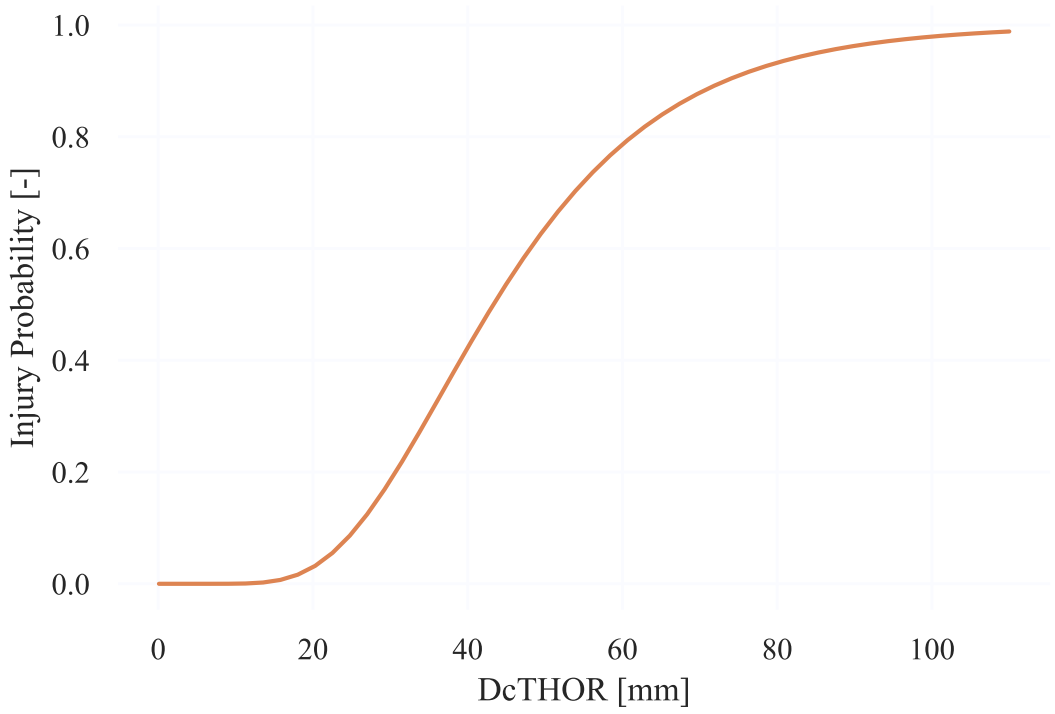

Figure 3.5: $DcTHOR$ NFR5+ risk curve for a 40 year old occupant.

3.3.4 Thoracic Injury Criterion (TIC)

TIC, Trosseille et al. (2019), is defined for two rib injury classifications, NFR and NSFR. $TIC_{NFR}(subject)$ is defined in Equation (3.11).

$$TIC_{NFR}(subject) = R_{max} + 1.66UP_{dif} \tag{3.11}$$

and $TIC_{NSFR}(subject)$ is defined in Equation (3.12).

$$TIC_{NSFR}(subject) = R_{max} + 3UP_{dif} \tag{3.12}$$

The criteria were developed for each subject, and then corrected for a given size ($Height$) and age (Y) for TIC_{NFR}

$$TIC_{NFR} = TIC_{NFR}(subject)\text{–}1.25(Height\text{–}175) + 1.18(age - Y) \tag{3.13}$$

and for TIC_{NSFR} as

$$TIC_{NSFR} = TIC_{NSFR}(subject) + 2.86(age - Y) \tag{3.14}$$

The correction factor for the occupant's age is -5 in this case, since this study considers a 40-year-old occupant, and a 45 year old was used in the study by Troseille et al. (2019), i.e., $age - Y = 40 - 45 = -5$. The height correction is zero, for each case, since THOR is 175 cm tall. These values are then used to construct a risk curve according to the Weibull distribution

$$P(NFR3+ \text{ or } NSFR3+) = 1 - e^{-(TIC/\beta)^{\alpha}} \tag{3.15}$$

Where TIC is the injury criterion, either for NFR or NSFR, β is the scaling factor for the injury criterion, while α is the form factor. The NFR and NSFR risk functions for a 40 year old occupant has a risk of 50%, for sustaining and NFR3+ and NSFR3+ chest injury, for 94.2 mm and 168.1 mm, TIC chest deflection, respectively, Figure 3.6.

The parameter values α and β were not published by Troseille et al. (2019). Instead, they were obtained by digitization of the published risk curves, in Troseille et al. (2019), and a Weibull distribution was fitted to match the 10, 50, and 90% digitized risks. This resulted in values of $\beta = 105.67$ and 181.44 for TIC NFR and TIC NSFR, respectively, and $\alpha = 3.25$ and 4.79 for TIC NFR and TIC NSFR, respectively. Finally, a check was made to make sure that the computed parameters did indeed fit the original data, Figure 3.6.

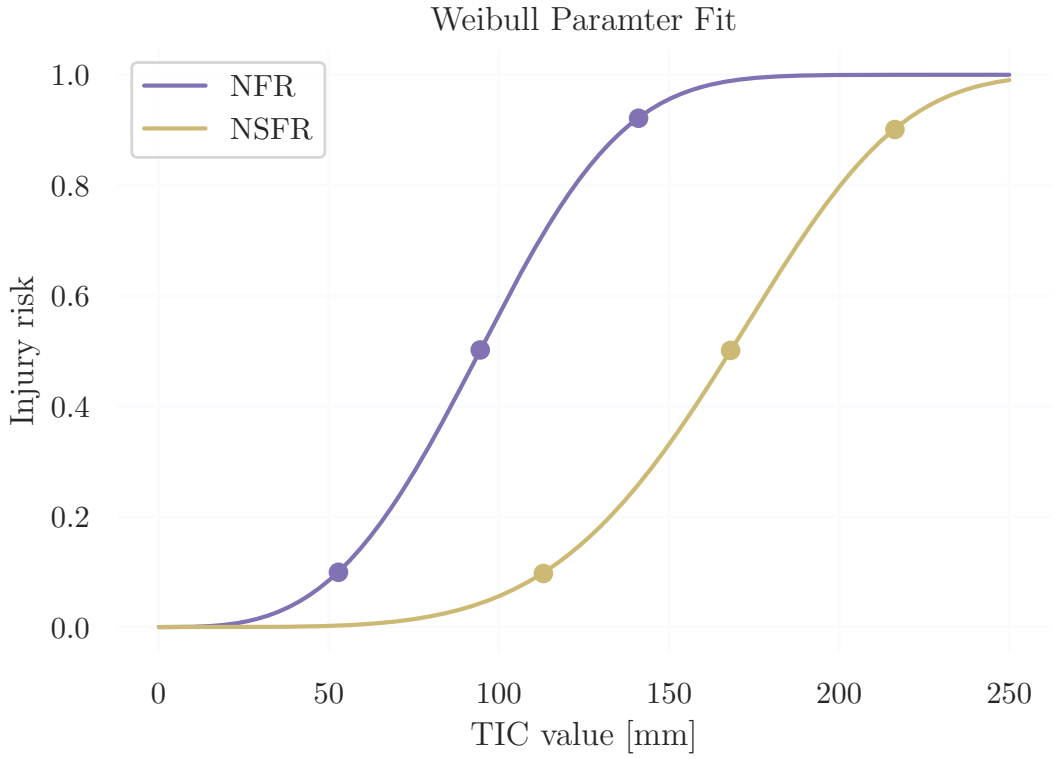

Figure 3.6: The fitting of the Weibull distribution to obtain coefficients for TIC NFR and NSFR.

3.3.5 PCscore

PCscore was generated through a Principal Component Analysis (PCA) (Poplin et al. 2017) and is defined as in Equation (3.16).

$$PCscore = l_1\left(\frac{UP_{tot}}{s_1}\right) + l_2\left(\frac{LOW_{tot}}{s_2}\right) + l_3\left(\frac{UP_{dif}}{s_3}\right) + l_4\left(\frac{LOW_{dif}}{s_4}\right) \tag{3.16}$$

UP_{tot} is the sum of the deflections on the upper chest sensors, while LOW_{tot} is the equivalent for the lower sensors. The same idea is applied UP_{dif} and LOW_{dif}, though for the difference rather than the sum. l_1 - l_4 are weight factors, s_1 - s_4 are standard deviations of the the input deflection metrics in mm, hence PCscore is dimensionless. The risk function is computed as the equation provided in Poplin et al. (2017).

$$P(AIS3+) = 1 - e^{(-PCscore/(\beta_0 - \beta_1 age))^{\alpha}} \tag{3.17}$$

For which *age* is the age of the occupant. The risk function follows a Weibull distribution, and the coefficents β_0, β_1 and α take the values 2.868, 0.018 and 3.31, respectively. The risk function is computed for AIS3+, thus being directly comparable to R_{max}. The $PCScore$ risk function for a 40 year old occupant has a risk of 50%, for sustaining and AIS3+ chest injury, for a $PCScore$ of 7.01, Figure 3.7.

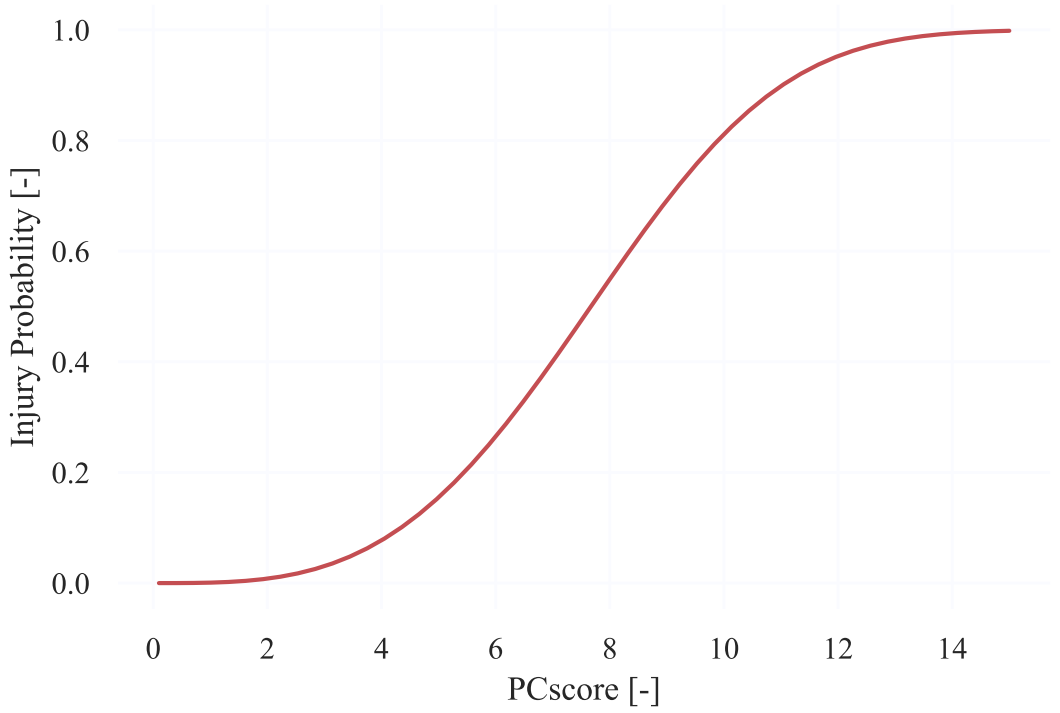

Figure 3.7: Risk curve for a set of values for $PCscore$.

3.3.6 Additional Injury Criteria

In order to monitor that the loading of the thorax was not influenced by head impacts or submarining, head, neck and abdomen sensors were monitored and the Head Injury Criterion (HIC) (Craig et al. 2020), which is used for evaluating the risk of skull fractures, was extracted from the simulation data. HIC was calculated with the resultant acceleration in the center of gravity of the head. The resultant acceleration was calculated from the CFC1000 filtered acceleration in x, y and z as:

$$a_{res} = \sqrt{a_x^2 + a_y^2 + a_z^2} \tag{3.18}$$

The HIC value was then calculated with Equation (3.19). Though, this was calculated with a 15 ms time span using the inbuilt routine in Meta,

$$HIC_{15} = \max\left(\frac{1}{t_2 - t_1}\int_{t_1}^{t_2}\left(a_{res}(t)dt\right)^{\frac{5}{2}} \cdot (t_2 - t_1)\right) \tag{3.19}$$

For the monitoring of submarining, which is when the belt slides over the pelvis and loads the soft tissues in the abdomen, the maximum deflection as well as the angle of the IR-TRACC load sensors were extracted. The deflection was used as a flag to warn of any indication for submarining, a limit was set to 60 mm. This since, according to Craig et al. (2020) a deflection of 60 mm on THOR predicts less than 10% risk of sustaining an AIS3+

injury to the abdomen.

THOR is equipped with neck data sensors as well, both for the upper and lower positions of the neck, and these were monitored in both x- and y-directions to make sure the belt did not load the neck in an excessive manner. The x-direction force corresponds to shear force, which makes particularly interesting since a big difference between 2 similar simulations could mean the belt got caught in the neck of the ATD.

3.4 Parameter Sampling in LS-OPT

The generic vehicle interior described in Section 3.1 was parametrized with respect to the geometry, safety systems as well as crash severity. The optimization software LS-OPT (ANSYS/LST, Livermore, CA, USA) was used for the sampling, since it was well suited for integration of the pre-processing in ANSA and LS-DYNA. Parameter sampling was part of the initial stages in the workflow, filled in grey in Figure 3.8. These two steps were done entirely by LS-OPT, i.e. no extra steps were required between sampling and pre-processing, changing the model geometry, in ANSA. There was also an option to start the simulations directly from LS-OPT, though this step was done via a script instead, for more user control.

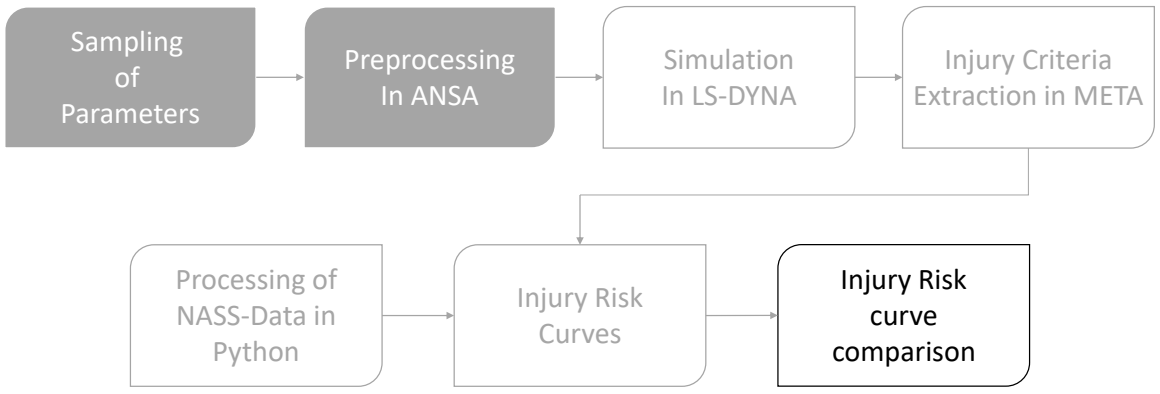

Figure 3.8: LS-OPT stages marked in grey in the workflow.

The sampling of the parameters was based on a Monte Carlo randomization, with a Latin Hypercube alogrithm, which was based on the method from Iraeus and Lindquist (2016). Hence, all the individual parameters sampled in this study were the same as used by Iraeus and Lindquist (2016), Table 3.3. The parameters were sampled independently of each other and, in total, there were 27 different parameters that LS-OPT sampled. The Latin Hypercube algorithm, in essence, meant that the sampled values would still follow the specified distribution, Figure 3.9, but the total distribution curve gets sliced into smaller bins to make sure all extremes are covered. The y-axis of the sample curve represents a measure of the probability of the sampled value, while the x-axis represents the parameter input to ANSA.

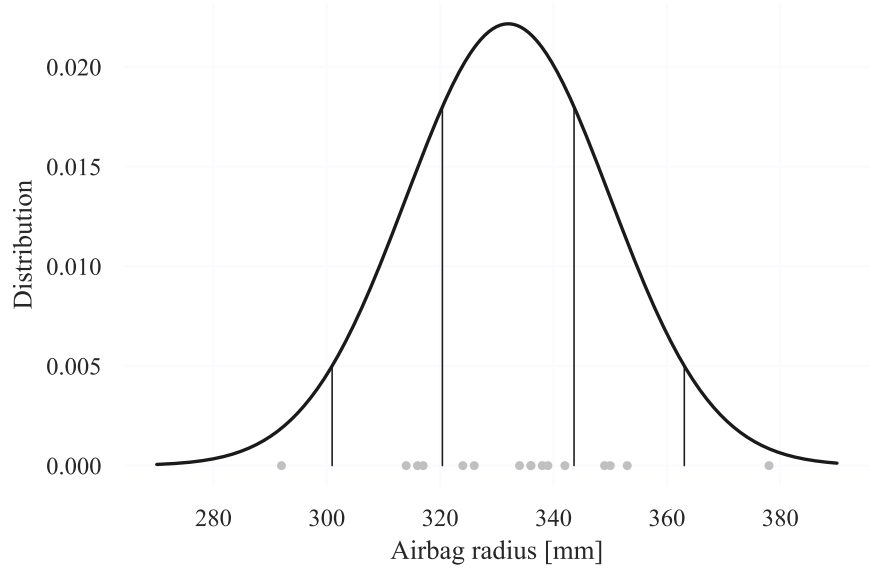

Figure 3.9: Latin hypercube example distribution of the airbag size. One dot represents a random sample within the range, where the higher distribution measure within the bins means more samples.

The airbag size is simply the radius of the fully deployed airbag, while the steering slide is the stroke length of the collapsible steering wheel column. Side structure distance and instrument panel distance are the distances to the door on the side and to the instrument panel, respectively. Delta velocity (Δv) is the speed change of a crash. PDOF is the angle at which the sled crashed. Duration, measured in milliseconds, is the time for which the crash endured. This relates to the length of the crash pulse, i.e., the time from which the crash starts until it ends. Thus, the duration affects the acceleration. EV1-EV3 are eigen vectors for the crash pulse, determined by Iraeus and Lindquist (2015). EV1-EV3 changes the shape of the crash pulse.

Table 3.3: All parameters and their respective distributions, that were used.

Parameter	Unit	Distribution	Distribution parameters
Airbag size (radius)	[mm]	Normal	μ = 332, σ = 18
Steering slide	[mm]	Uniform	min = -30, max = +30
Steering rot	[deg]	Uniform	min = -2.7, max = +2.7
Side structure distance	[mm]	Normal (trunk.)	μ = 0, σ = 33 [min = -60, max = 20]
Instrument panel distance	[mm]	Normal (trunk.)	μ = 0, σ = 33 [min = -60, max = 60]
Delta velocity	[km/h]	LOG-normal	μ = 3.30, σ = 0.40
PDOF	[deg]	Normal (trunk.)	μ = -2.2, σ = 21.2 [min = -45, max = 10]
Duration	[ms]	Normal	μ = 109.6, σ = 16.2
EV1	[-]	Normal	μ = -0.48 + 0.015 ΔV, σ = 1.64
EV2	[-]	Normal	μ = 0.97 + 0.030 ΔV, σ = 1.05
EV3	[-]	Normal	μ = -0.33 + 0.010 ΔV, σ = 0.74
Yaw scale factor	[-]	Normal	μ = -0.068, σ = 0.0019
Intrusion instrument panel	[mm]	Exponential	Step one: Bernoulli(p = invlogit(-5.47 + 0.074 dv)) Step two: Exponential rate = 0.079
Intrusion floor panel	[mm]	Exponential	Step one: Bernoulli(p = invlogit(-5.15 + 0.076 dv)) Step two: Exponential rate = 0.071
Airbag pressure s.f.	[-]	Normal	μ = 1.31, σ = 0.10
Airbag trig time	[ms]	LOG-normal	μ = 3.04, σ = 0.64 [min = 5, max = 40]
Steering column force	[kN]	Normal	μ = 4.80, σ = 0.90
Steering rim force	[kN]	Normal	μ = 2.80, σ = 0.80
Belt pretensioner force	[kN]	Normal	μ = 1.93, σ = 0.47
Belt force limiter	[kN]	Normal	μ = 3.94, σ = 0.69
Knee force stiffness	[kN/100 mm]	Normal (trunk.)	μ = 9.45, σ = 3.86 [min = 3, max = 20]
Belt friction	[-]	Uniform	min = 0.2, max = 0.4
Seat friction	[-]	Uniform	min = 0.2, max = 0.4
IP friction	[-]	Uniform	min = 0.2, max = 0.4
Airbag friction	[-]	Uniform	min = 0.2, max = 0.4
Door friction	[-]	Uniform	min = 0.2, max = 0.4
Buckle slipring friction	[-]	Normal (trunk.)	μ = 0.18, σ = 0.08 [min = 0, max = 0.5]

Yaw scale factor is the yaw rotational velocity. Intrusion instrument panel and intrusion floor panel is simply the intrusion, in the respective area. Airbag pressure is the deployment pressure of the airbag, while the trig time is the reaction time or the time it takes before the safety systems are activated. Steering column force is the force the steering column can withstand before collapsing, while steering rim force is the same, although for the rim. The belt pretensioner force is the initial force generated by the pyrotechnical pretensioner upon activation at the start of the crash, and belt force limiter is the constant load generated by the belt during the later crash phase. The last six parameters relate to frictions in different parts of the vehicle, and serve as important factors for the ATDs interaction with the interior.

One of the parameter sampling ranges was changed from the original sampling by Iraeus and Lindquist (2016). The restraint activation trig time was found to have a log-normal distribution with a mean of 3.04 ms and standard deviation of 0.64 ms, which resulted in restraint activation times of over 100 ms. In the present study, the distribution was truncated at 40 ms to avoid restraint activation after the ATD would interact with the steering wheel, to increase the robustness of the simulations, Figure 3.10.

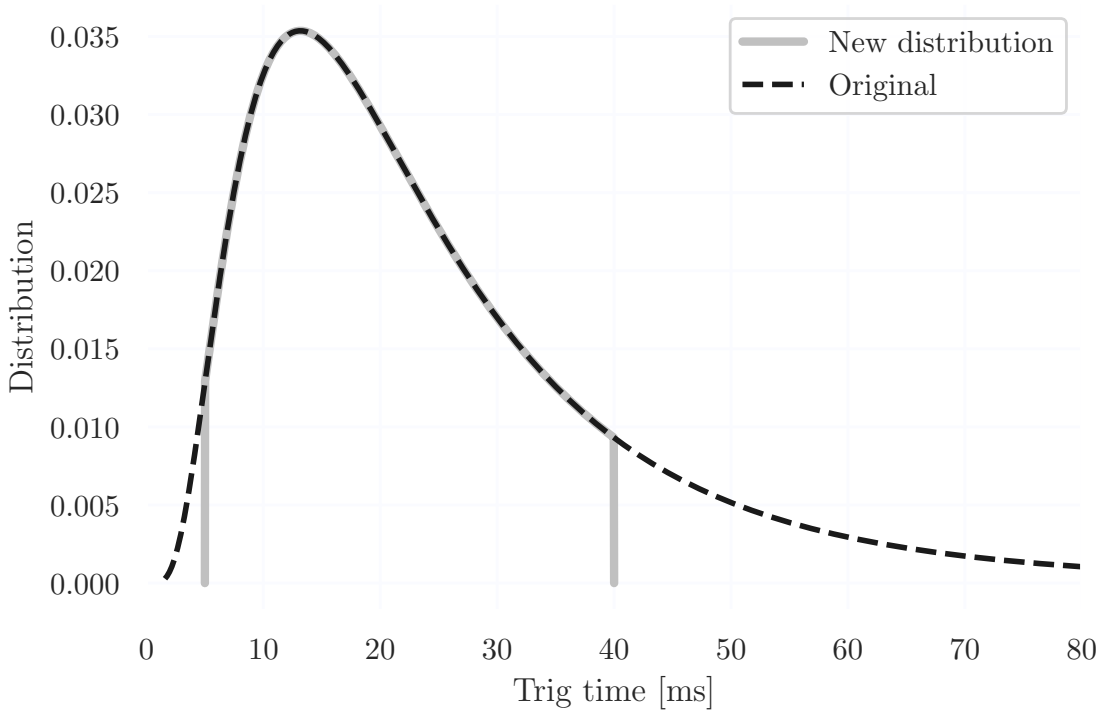

Figure 3.10: Trig time distribution curve, the dotted line represents the original distribution while the grey curve is the modified distribution for the sampling range.

This change makes sure that the airbag triggers before the ATD hits the steering wheel, and that the sled does provide adequate levels of safety system activation, in addition to making sure that the simulations reached normal termination.

To make sure that the sampling of the parameters was done correctly an analysis of the parameter distribution was made, to make sure LS-OPT had indeed produced a distribution that was satisfactory, i.e. a manual check to verify whether LS-OPT sampled in the expected manner. This was done by comparing the sampling from LS-OPT to the theorethical sampling curves.

3.5 THOR positioning

Since the original generic vehicle interior was fitted with an HBM, THOR had to be placed in the model before any further steps could be made, Figure 3.11. The THOR ATD was positioned in the seat model 20 mm upward from the H-point location used for the HBM, with the legs positioned symmetrically with 270 mm width from the outer surfaces of the knee joint clevises. The feet were positioned on the floorboard, the arms close to the torso with the hands close to the steering wheel at 2 and 10 o'clock. The pelvis angle of the ATD was 33°, the lumbar spine pitch adjustment 9° (slouched position), the neck pitch change adjustment 0° (neutral position) and the resulting head angle around the X and Y

axes were 0°.

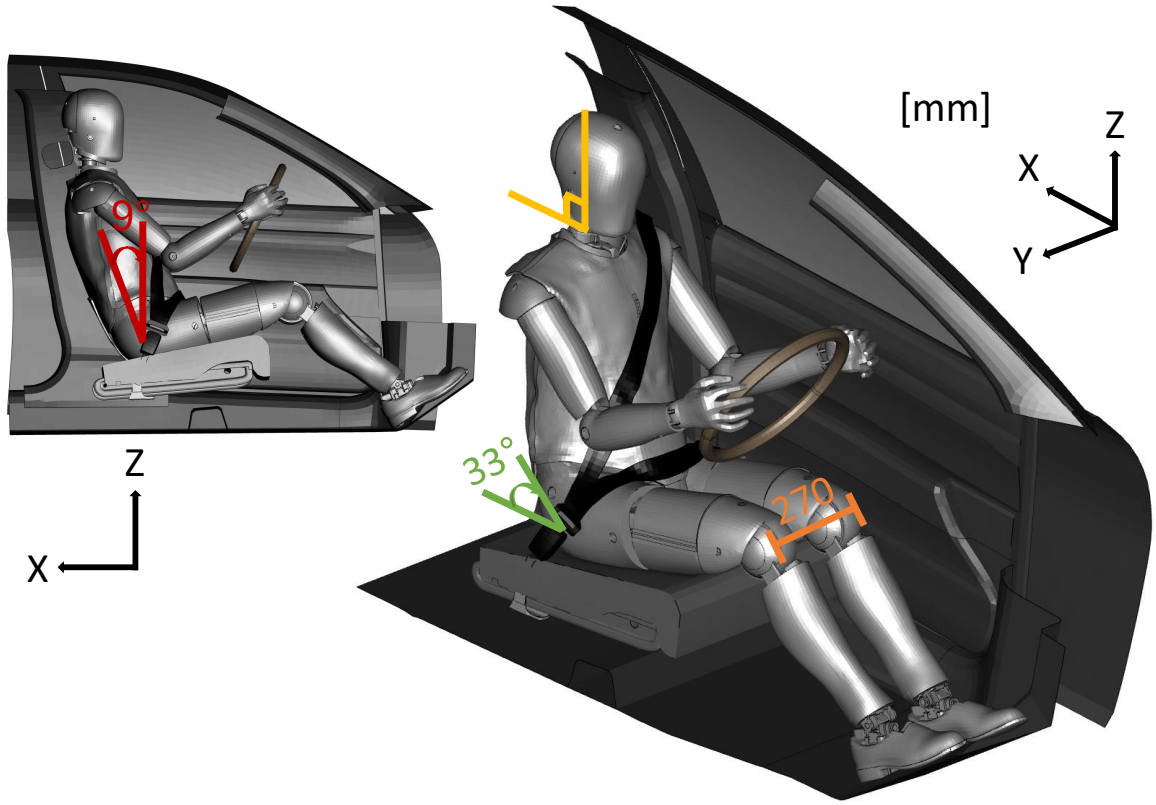

Figure 3.11: THOR position in the generic vehicle interior. Pelvis angle shown in green, lumbar spine pitch adjustment in red, neck pitch in yellow and leg position in orange.

3.6 Pilot Study

In order to make sure that the generic car model with the THOR ATD behaved as expected, a pilot study was conducted, and was done as shown in the flow chart in Figure 3.12. This enabled a way to rectify any errors or other malfunctions before the larger study was begun. The pilot study was done by generating a set of input files in LS-OPT, ten files were chosen as it was a manageable amount to begin with. The pilot study was re-run a number of times, since new errors popped up for each new batch of inputs, causing the simulations to crash, yielding none or unreliable results. This prompted for changes in the model, to sort out the identified problems.

To make sure the most possible potential error situations were encountered, extreme values were set, such as high Δv or short duration pulses, which caused high accelerations for a given Δv. These selections were made manually, instead of relying on the sampling, to make sure these cases were included. Of course, all different scenarios could not be replicated since there would be an infinite number of setups to try, though by catching some of the extremes, the chances of sampling worse cases were lowered.

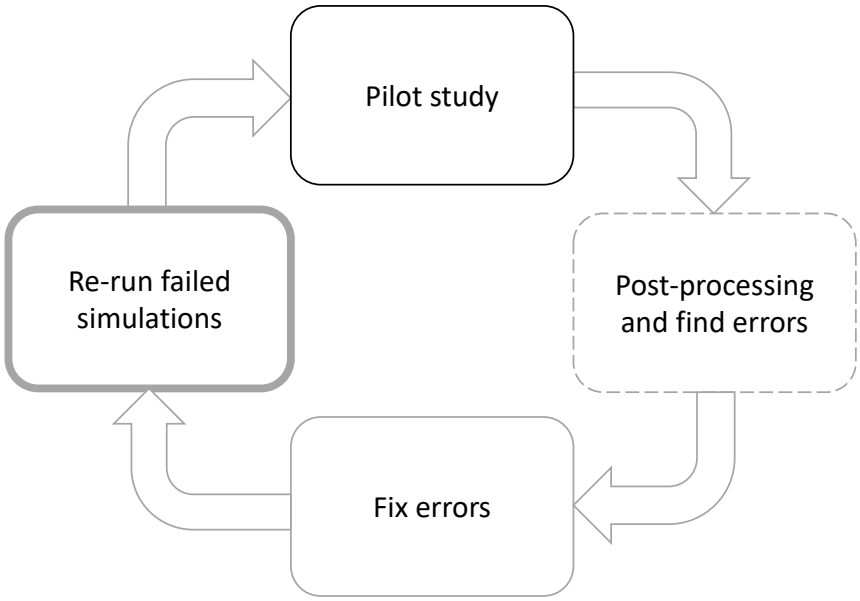

Figure 3.12: Pilot study iteration loop.

When the pilot study was finalized, the model was more robust and accurate than before. The amount of simulations that crashed cannot be guaranteed to be zero, but at least minimized to get the best results possible.

3.7 Statistical Analysis

The statistical analysis consisted of two parts, firstly the generation of the field crash risk curve from the NASS/CDS database and secondly the calculation of risk curves for the simulations. The method for creating the two different risk curves were similar, however with different input data. In addition, a regression was also made using Vehicle Pulse Index (VPI) as the risk predictor. To further evaluate the regression models R^2 values for each criteria were computed.

3.7.1 Processing of NASS/CDS Data

Herein the creation of the field crash risk curve was done according to the methods used by Iraeus and Lindquist (2016). The dataset from NASS/CDS consisted of several different injury parameters among a lot of other information. This database consists of information from real crashes collected in the USA. The data used in this study was sampled by Iraeus and Lindquist (2016) with a number of inclusion criteria to get the same representation of crashes as in the simulation data. The selection of NASS/CDS data was limited to driver occupants in frontal crashes with a PDOF of -45° to 10 °, for vehicles produced between 2000 to 2012 to only include vehicles with restraint systems comparable to the generic car model. The driver was the only occupant accounted for, so injuries to other passengers were sorted out from the data.

Furthermore, the steering wheel airbag should have been deployed and no rollover of the vehicle should be present in the crash scenario. All data sourcing had previously been done by Iraeus and Lindquist (2016) and the NASS/CDS risk curve was derived from the authors published paper. Cases where age, sex and curb weight of the car were unknown, were excluded. After this filtering, 4980 cases were left to be studied.

Of interest for this study, was the THORAX502 parameter, which determined the injury severity level sustained to the skeletal parts of the thorax, according to the AIS injury scale. All cases where the value was 3 or more were set to injured, i.e. all occupants that were injured to AIS3+ levels. This yielded either a 0 for uninjured or a 1 for injured, for all cases in the NASS/CDS data.

The generation of the risk curve was computed by Iraeus and Lindquist (2016) with the usage of a Generalized Linear Model (GLM) in the statistical software R (R Foundation for Statistical Computing, Vienna, Austria). Iraeus and Lindquist (2016) used Δv, age and instrument panel intrusion as the independent variables to predict the injury risk, since it was found these parameters showed empirical support of influencing risk of rib fracture, at the 5% significance level, Iraeus and Lindquist (2016). The GLM yielded coefficients for the intercept, Δv, age and instrument panel intrusion, LPINTR, bias. The coefficients were used to compute the linear curve fit, equation (3.20).

$$y_{glm} = int + c_{\Delta v}\Delta v + c_{age}age + c_{LPINTR}LPINTR \tag{3.20}$$

int is the intercept, i.e the value for which the curve intersects the y-axis, $c_{\Delta v}$ is the coefficient for the bias towards Δv and likewise for c_{age} and c_{LPintr}, though for the age and the instrument panel intrusion, respectively. Instrument panel intrusion was the measure for how much the instrument panel has been moved towards the occupant. This linear curve was then transferred to a probability between 0 and 1 by applying a logistic function, by using the function for converting to the log-odds space, equation (3.21).

$$P(injury) = \frac{e^{y_{glm}}}{1 + e^{y_{glm}}} \tag{3.21}$$

y_{glm} is the y-values from the linear curve fit. The equation thus yielded the risk curve for the NASS/CDS data. From this conversion the risk curve for a 40 year old occupant, as well as the 95% confidence interval, in light grey, was plotted, Figure 3.13. Note the green markings along the x-axis, these were the cases in the NASS/CDS data where the occupant was injured (1) or uninjured (0). Figure 3.13 is the risk curve generated by Iraeus and Lindquist (2016), but plotted using Python instead.

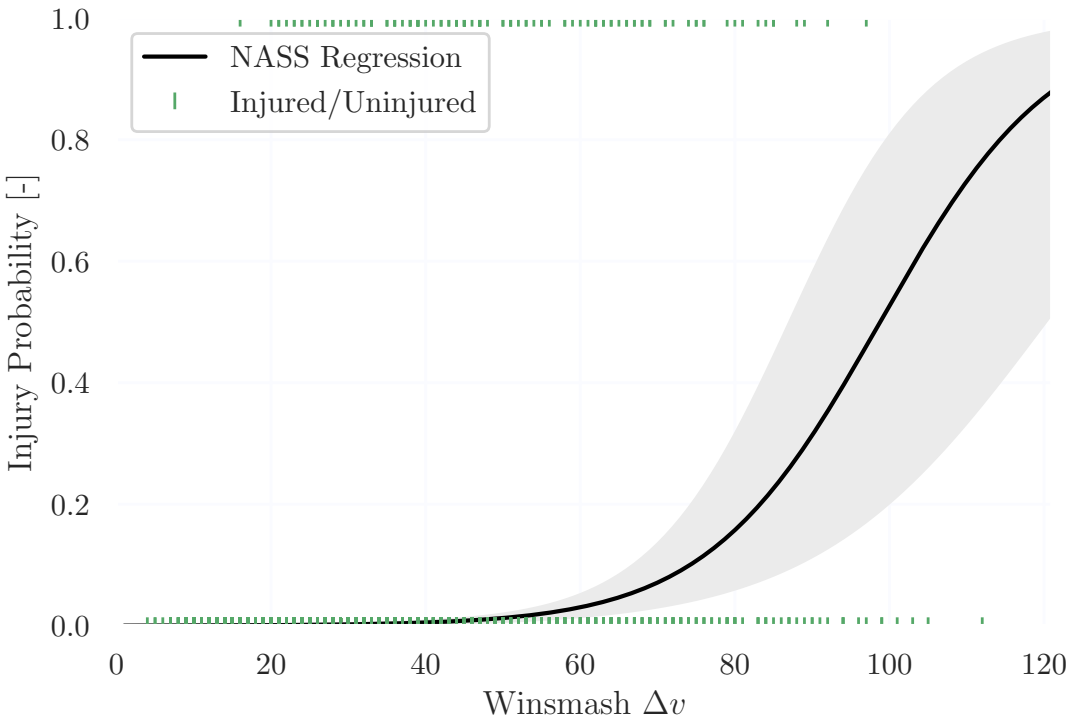

Figure 3.13: The NASS/CDS risk curve derived from Iraeus and Lindquist (2016) for a 40 year-old occupant.

3.7.2 Risk Curve Generation for Simulation Data

The method of computing risk curves for the simulation data was more or less entirely the same as described previously for generating the NASS/CDS risk curve. However, according to Iraeus and Lindquist (2016) the NASS/CDS database Δv was biased since it consists of estimations according to the Winsmash calculation of Δv. The Winsmash Δv calculation includes a scatter error, and therefore the simulation data generated must be biased in the same way to be comparable the real crash outcome. The calculation of Winsmash Δv for the simulations can be seen in equation 3.22 (Funk et al. 2008). The Δv used as input can thus not be used when generating the risk curves, since the comparison with the NASS/CDS curve cannot be made in such a case. Since the Winsmash estimation consists of a randomized term, the results can change each time when re-running the algorithm. To combat this, 100 iterations were run, and a mean value of the calculated curve fit coefficients were used for the final curve fit.

$$\Delta v_{Winsmash} = 0.81 \cdot \Delta v + N(0, \sigma) \tag{3.22}$$

For which $N(0, \sigma)$ is the normally distributed scatter according to Funk et al. (2008), with standard deviation σ. The scatter error can lead to that small Δv get randomized to a negative value. Iraeus and Lindquist (2016) minimized this effect by decreasing the scatter error linearly down to zero for Δv below 22km/h, while keeping the original scatter

error. Winsmash Δv was hereby used as the speed predictor. The curve fitment of the datapoints was done with using a GLM. This model was computed using age and Δv as predictors for the rib injury risk. The same covariates were used for this prediction. This linear model would then provide coefficients for the intercept as well as the age and Δv bias, to be applied to the linear curve equation (3.20). The risk curve generation in this study based on the simulation data was entirely done in Python, using the same method Iraeus and Lindquist had implemented in R.

3.7.3 Logistic Regression using Vehicle Pulse Index as a Predictor

Vehicle Pulse Index (VPI) ISO TR12353 (2016) is the crash pulse affecting the car occupant as a result of slack in the system, caused by the time it takes for the seatbelt to restrain the occupant. A simplified sketch in Figure 3.14 shows the principle of relative motion between occupant and car.

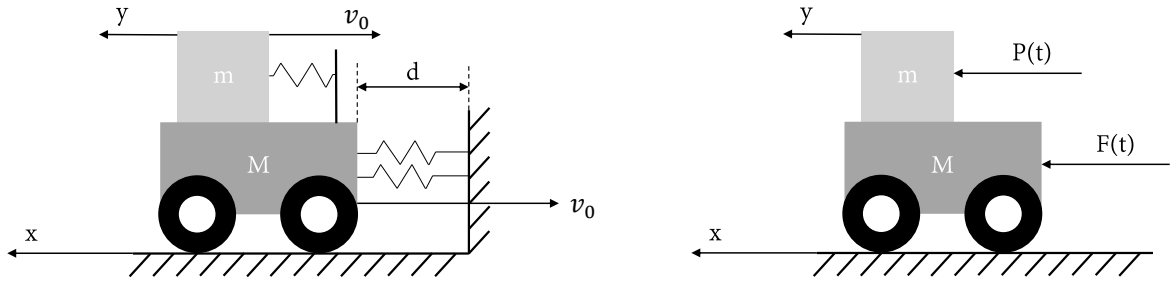

Figure 3.14: A schematic figure of the interaction between car and driver, accoring to Newton's second law of motion. To the left, a simplified crash is modelled with springs, and the resulting forces to the right.

VPI is different from the vehicle acceleration and represents the approximate acceleration an occupant in the vehicle would experience in the crash. The equations used to compute this index were derived from Newton's second law of motion.

$$M\ddot{x} = F(t) \longleftrightarrow \ddot{x}(t) = \frac{F(t)}{M} \tag{3.23}$$

Here, $F(t)$ is the force generated by the front structure and M is the effective mass of the vehicle. Typically, the vehicle acceleration $\ddot{x}(t)$ is recorded and is the input for the VPI calculation. The movement of the occupant with mass m inside a vehicle would then be:

$$m\ddot{y} = P(t) \longleftrightarrow \ddot{y}(t) = \frac{P(t)}{m} \tag{3.24}$$

$P(t)$ is the restraint system force, a combination of seatbelt and airbag loading to a front row occupant. $\ddot{y}$ is the acceleration as felt by the occupant, and VPI is the maximum acceleration ($\ddot{y}$) value. VPI is based on the relative movement between occupant and vehicle. Hence, the initial velocities of both vehicle and occupant, v_0, can be neglected, but if desired they can be used to compute stopping distance and Δv of the vehicle motion.

For the VPI, the restraint force $P(t)$ was calculated with a spring stiffness k and a slack distance s as:

$$P(t) = \begin{cases} 0 \ , \ x - y < s \\ k((x - y) - s) \ , \ x - y \geq s \end{cases} \tag{3.25}$$

The restraint model with slack s and spring stiffness k, is modelled in Figure 3.15

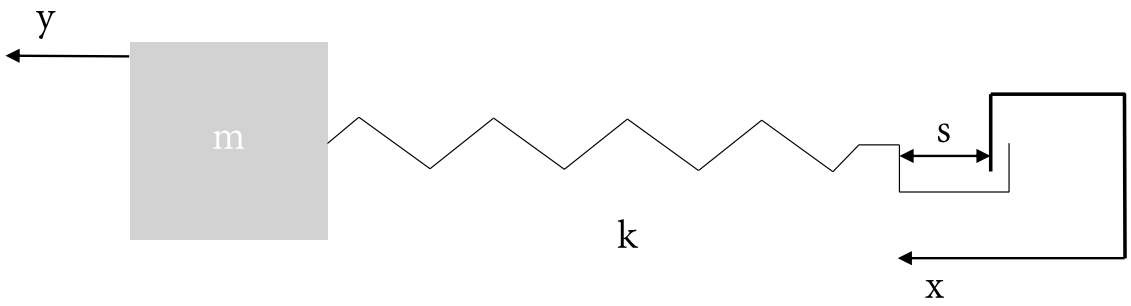

Figure 3.15: A schematic figure of the slack present in the restraint system in the car, modelled with a spring and slack distance s.

The standardized values used for the calculation of VPI according to ISO TR12353 (2016) were

$$m = 1 \text{ kg} \tag{3.26}$$

$$k = 1 \text{ N/m} \tag{3.27}$$

$$s = 0.03 \text{ m} \tag{3.28}$$

VPI was calculated for each simulation, and was used to compute the risk of injury in the same way as done before, but replacing Winsmash Δv with VPI.

3.7.4 Goodness of Fit

To be able to quantitatively measure how well the linear regression model used fits the underlying data, one may use R^2 as a metric to determine this correlation. R^2 is the proportion of the variation in the dependent variable that can be explained by the independent variable (Glantz et al. 2017) *Applied Regression & Analysis of Variance*. R^2 was computed as shown in Equation (3.29)

$$R^2 = 1 - \frac{SS_R}{SS_T} \tag{3.29}$$

SS_R is defined as the sum of the squared residuals as:

$$SS_R = \sum_i^n (y_i - y_{glm,i})^2 \tag{3.30}$$

y_i are the actual values from the simulations while $y_{glm,i}$ are the predicted value from the regression model. SS_T is the total sum of the squares as

$$SS_T = \sum_i^n (y_i - \bar{y})^2 \tag{3.31}$$

$\bar{y}$ is the mean value of the actual data. In the best case scenario one would obtain $R^2 = 1$ which means that the model always predicts the actual values, while a baseline model $R^2 = 0$ would always predict $\bar{y}$ (Glantz et al. 2017).

3.8 Comparison to Human Body Model

An HBM is a mathematical model which directly models the human anatomy and tissues, rather than modelling the steel and rubber parts of an ATD which is a mechanical model of a human. The aim with the study of Iraeus and Lindquist (2016) was to compare the risk assessed with an FE HBM to the risk of rib fracture with field data. In this study, a comparison with an updated version of the HBM analysis (Larsson et al. 2021) will be conducted. An HBM has several features not present on an ATD, such as human bone and human organs. All these are modelled to the best precision possible. An HBM can be used to evaluate the human response in a crash, however since no crash testing can be made with live humans there might difficulties in comparing the HBM simulations to real crash testing using ATDs.

The results from the simulation study were compared to a similar study made by Larsson et al. (2021) but using a SAFER HBM version 9 instead of THOR. No new simulations were run in Larssons's study. The basis of the stochastic simulation data comes from a previous study by Pipkorn et al. (2019) and was run with the same generic car model, as used in this study. The data was re-calculated by Larsson et al. (2021) as the "newly developed risk function". Moreover, the authors used the same method as previously presented in the Iraeus and Lindquist (2016) to extract the NASS/CDS data. Since the HBM is a model of a physical human, the rib strain can be extracted from all the ribs and a risk of fracture can be calculated for each one and hence the tissue loading can be predicted. This was done for Log-normal distributions according to equation 3.32

$$\text{Fracture risk}(strain, age) = \frac{1}{2} + \frac{1}{2} erf\left[\frac{\ln(\text{strain}) - (\beta_0 + \beta_1 age)}{\sqrt{2}\alpha_{strain}}\right] \tag{3.32}$$

erf() is the Gauss error function and ln() is the natural logarithm. The distribution parameters for the Log-normal function are $\beta_0 = -2.9866$, $\beta_1 = -0.0130$ and $\alpha_{strain} = 0.3026$.

The risk curves were generated by digitizing the figures from the Larsson et al. (2021) paper, and creating a curve fit in the same fashion as done previously for TIC NFR and TIC NSFR. Larsson et al. (2021) used Winsmash Δv as the predictor on the x-axis, which makes for reasonable comparison to the results in this study. However, the study by Larsson et al. (2021) was made for 30- and 70-year-old occupants, while this study considers a 40-year-old. However, risk curves for different ages could conveniently be extracted for this study as well. Larsson also used the probability of a fracture for NFR2+.

In order to compare the curves, all risk curves in this study were re-calculated for the ages 30 and 70. The SAFER (SAFER, Göteborg, Sweden)HBM in the generic car model can be seen in Figure 3.16

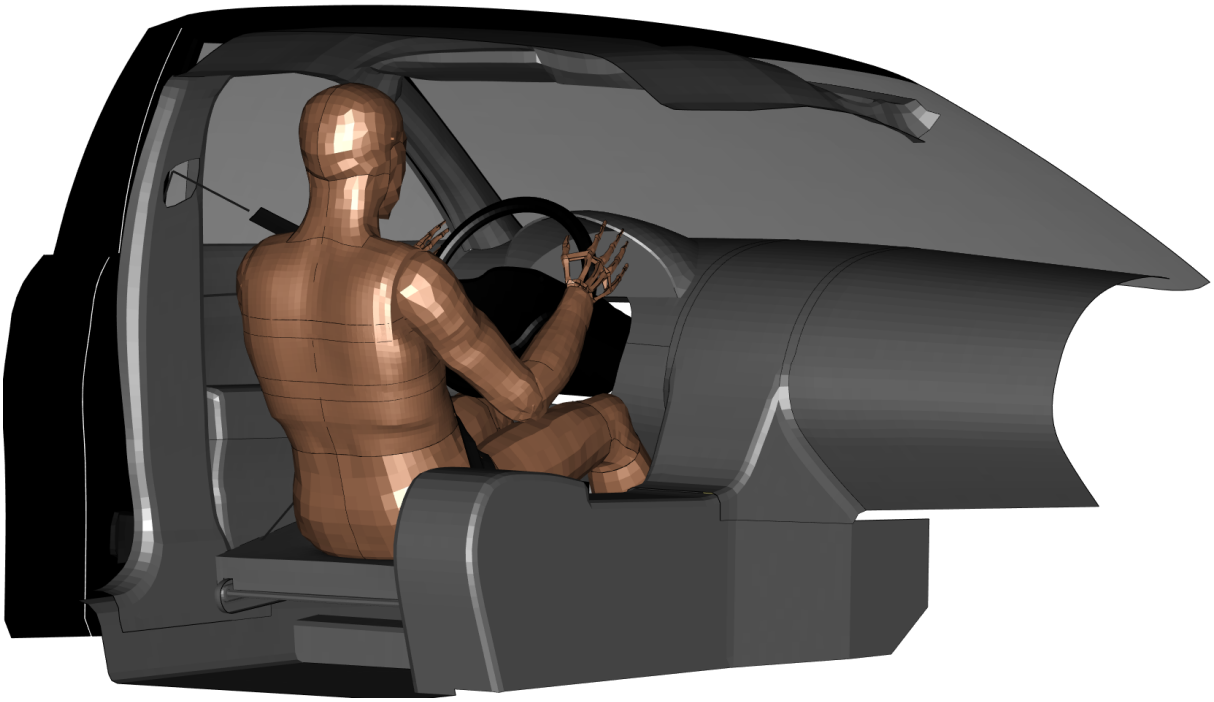

Figure 3.16: The generic car sled model with fitted with the SAFER Human Body model.

3.9 Underprediction of Rib Fractures in NASS/CDS

In order to examine the possible underprediction of rib fractures in the NASS/CDS data some statistical simulations were run according to Iraeus and Lindquist (2016). The method behind this was to change a fraction of the uninjured occupants to injured. This was done by partially deriving the NASS/CDS risk curve and using this as a probability density function. The approach will lead to the assumption that the underprediction is the largest where the inclination of the curve is the highest. A 50% and 70% underestimation rate was used, according to Equation 3.33.

$$Occupants_{changed} = round\left(\left(\frac{1}{U_{rate}} - 1\right) \cdot 120 \cdot 0.8\right) \tag{3.33}$$

The number of injured occupants in the original data set was 120 for AIS3+. The new total of injured in the data set will be the number of changed occupants added with the number of injured occupants in the original data set, as demonstrated in Equation 3.34

$$Occupants_{new} = Occupants_{changed} + Occupants_{injured} \tag{3.34}$$

The new number of injured occupants for a 50% and 70% underprediction can be seen in the Table 3.4.

Table 3.4: The underpredition rates and increase in injured occupants for each leve.l

Underprediction rate	U_{rate}	$Occupants_{changed}$	$Occupants_{new}$
50%	0.5	96	216
70%	0.3	224	344

3.10 Sampling of Crashes of Higher Severity

Since the Δv sampling is LOG-normal, most of the crashes will be at a low Δv. In order to study what happens when a larger number of crashes with high Δv is added to the data, 50 new simulations was sampled. As previously the sampling method is the same, the only difference will be that the newly sampled crashes will have a Δv ranging between 60 and 120 km/h. This was done by changing the distribution of Δv to a uniform distribution. A comparison was then be made with a new fitment of the risk against the newly sampled crashes added together with the batch of 1000 that were run.

3.11 Adjusted R_{max}

In order to investigate R_{max} further, an adjusted R_{max} curve was developed, $R_{max,Adjusted}$. Firstly, the 70 and 50% underpredict curves were chosen to aid the new curve path. This was done by checking the sum of distances from the R_{max} curve to the 2 underpredict curves according to equation 3.35.

$$error = math.dist(R_{max}, NASS/CDS70) + math.dist(R_{max}, NASS/CDS50) \quad (3.35)$$

Where *math.dist* is a Euclidean distance function in Python. The error was minimized by computing values in a nested loop for the collected term $e^{(\beta_0 - \beta_1 age)}$, in the Weibull distribution function for R_{max} Equation 3.2, and the exponent α as seen in the calculation of P(AIS 3+) Equation 3.36.

$$P(R_{max,Adjusted}) = 1\text{–}e^{-\left(R_{max}/e^{\beta_0 - \beta_1 age}\right)^{\alpha}} \quad (3.36)$$

The parameter value for which the function had the smallest error were recorded for the 40-year-old. The exponent α was then transferred to running the same setup for the 30-year-old. From here according to equation 3.37 the parameters β_0 and β_1 were calculated, since there were now two equations and two unknowns.

$$\begin{cases} e^{\beta_0 - \beta_1 \cdot 40} = 65.545 \\ e^{\beta_0 - \beta_1 \cdot 30} = 70.216 \end{cases} \quad (3.37)$$

One assumption was made when initially calculating the variables for the 40-year-old occupant. The assumption was that when, the sensors in the ATD bottomed out, the risk should be above 95%, but not as big as 1. This was made to make sure that the risk firstly did not reach 1 well before the ATD bottoms out, and that the risk predicted

when bottoming would not be too low. The complete $R_{max,Adjusted}$ function can be seen in Equation 3.38, for which $\beta_0 = 4.45809$, $\beta_1 = 0.0069$ and $\alpha = 6.793$.

$$P(R_{max,Adjusted}) = 1 - e^{-\left(R_{max}/e^{4.45809-0.0069age}\right)^{6.793}} \tag{3.38}$$

3.12 EDR Δv NASS/CDS

To get an additional comparison between real life data and the simulations, EDR equivalent Δv curves were extracted from Brumbelow (2019). Brumbelow used crashes from the NASS/CDS database with EDR data and some crashes with pure Winsmash data to predict the EDR Δv for cases when the EDR module was not present. Several inclusion criteria such as that the driver should be restrained by a belt and the airbag should have been deployed were used (Brumbelow 2019). Cases with rollover or multiple severe impacts were not included in the data. Much like Iraeus and Lindquist (2016), which used an equivalent approach in the data sourcing.

The risk curves were calculated by Brumbelow (2019) for MAIS3+ thoracic injury, and were recreated by digitizing the plots. The NASS/CDS curve was also recalculated from the data set used by Iraeus and Lindquist (2016) with respect to Thoracic MAIS3+. The comparison between the recalculated curve from Iraeus and Lindquist (2016) and Brumbelow (2019) can be seen in Figure 3.17.

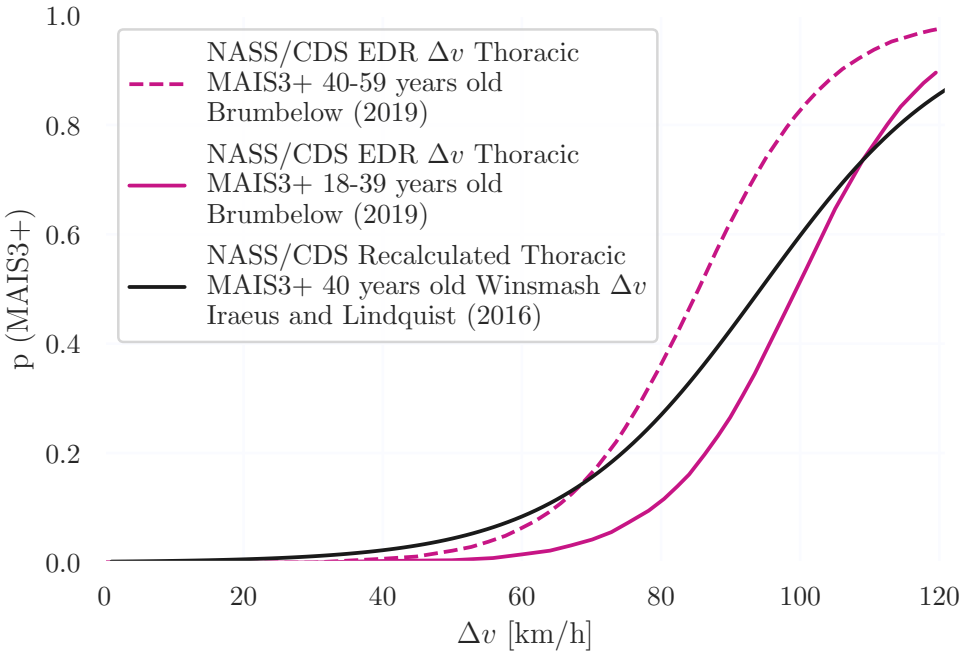

Figure 3.17: MAIS3+ Thoracic NASS/CDS EDR Δv Comparison with the recalculated MAIS3+ Thoracic curve

3.13 THOR Accuracy

In order to investigate R_{max} even further, the theory that the THOR ATD may overestimate the deflection compared to a real human (Parent et al. 2017), new calculations for the injury risk predicted for R_{max} was made. Here the direct deflection of THOR was scaled down with the assumption that THOR has a 30-50% higher deflection than when testing PMHS. Parent et al. (2017) tested the biofidelity of the THOR ATD compared to PMHS and Hybrid III. Although THOR got a good biofidelity score for the thorax in that study, there was some evidence that there may be an excessive deflection in the oblique load case. Parent et al. (2017) showed data where the peak-to-peak difference in deflection between THOR and PMHS was as much as 30% more for THOR. For tests using the same time span, a difference of 50% more deflection in THOR was observed, compared to PMHS. The sternal force and deflection measurements had better correlation and was within the confidence bands. Thus, a test was made in this study, by scaling down the resultant deflection measure R_{max} outputted by THOR. These "new" values were then used as input to the risk function, and the difference in response could be observed. Equations 3.39 and 3.40 show the downscaled values for R_{max}.

$$R_{max,decreased30\%} = \frac{R_{max}}{1.3} \tag{3.39}$$

$$R_{max,decreased50\%} = \frac{R_{max}}{1.5} \tag{3.40}$$

4 Results

This chapter presents all the results obtained from the simulations, as well as some errors encountered during the pilot study. In addition, the measures taken to correct these errors are described.

4.1 Pilot Study

While conducting the pilot study, several issues arose that needed to be addressed, Table 4.1. The airbag trig time was capped at 40ms, to make sure that the occupant did not hit the steering wheel due to a late trig time for the airbag. This was indeed an altercation from the original method from Iraeus and Lindquist (2016), though this change was required to make sure the simulations finished.

This study uses an FE-model of THOR, which also comes as a physical ATD with details such as bushings, screws etc, which can fail when sustaining large loads, thus causing the simulation to terminate, which was of course unwanted. Iraeus and Lindquist (2016) used an HBM, which is an FE-model of the human body, meaning it has no such features, but are generally more complex.

Table 4.1: All the error that occured during the pilot study, and the corresponding fix implemented to solve the problem

Error type	Termination	Cause	Fix
Airbag trigg time	Error	Airbag not triggering before driver hit the steering wheel	Limiting the trigg time to maximum 40ms
Belt oscillating	Error/Normal	1D belt oscillating and disturbing the routing	Elongate the elements in the 1D belt
Belt penetration	Normal	Belt penetrating either abdomen or the neck	Scaling of the thickness in the contact between belt and dummy
Belt roll up	Normal	Lap- and shoulder belt folding up to a thin line	Compressive stress elimination decided automatically by LS-Dyna
Belt segment free end	Error	Discrete element or nodal rigid body going through the sliprings or retractor	Moving the retractor and the discrete element in the 1D belt downward
Bushings in chest	Error	Negative volume in the bushings	0.6mm thick null-shells without stiffness around the bushings
Head rubber cover	Error	Negative volume in the head rubber cover	No fix needed
Head clash to inner liner	Normal	Head hit the inner liner and changed the ATD behaviour	Contact between THOR and liner removed
Shoulder belt sliding	Normal	Shoulder belt sliding over the shoulder and loading the abdomen	Elongated the 2d belt

The errors did not all occur at the same time, they were merely discovered after one problem had been fixed, i.e. one fix could lead to creating its own issues. However, after the pilot study loop, Figure 3.12, was iterated a number of times, so all encountered issues

could be addressed and remedied. The pilot study yielded approximately 80 simulation runs, in batches of 10, where inputs were generated according to the latin hypercube sampling in LS-OPT, but were in some cases manually changed to capture the extreme cases of the simulations.

The 0.6mm thick null-shells with a self-contact added in the thorax of the THOR ATD can be seen in Figure 4.1. The null-shells made sure that the bushings maintained a positive volume and the simulation could achieve normal termination.

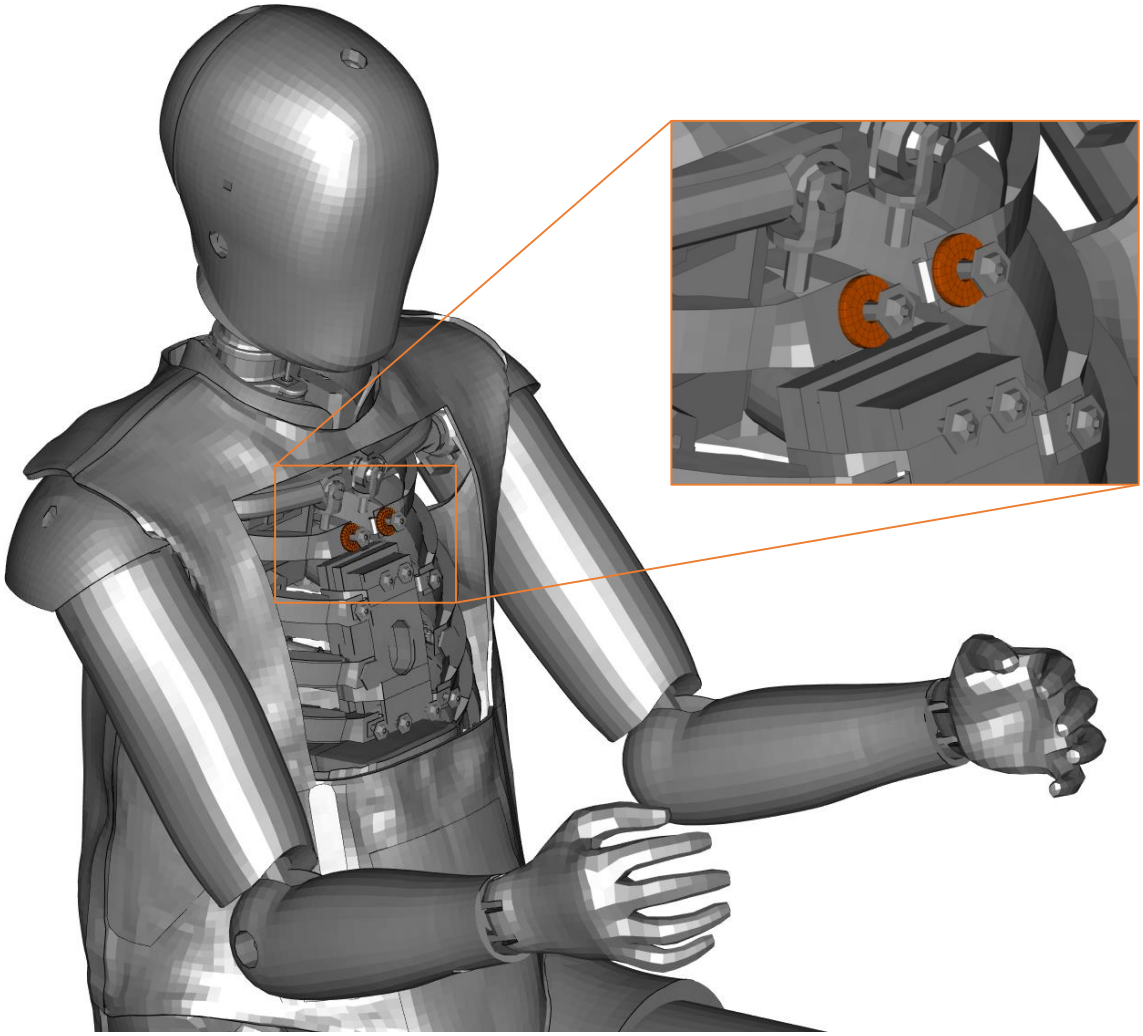

Figure 4.1: The chest bushing locations in THOR

To compare how much the shell bushings in the thorax of the THOR ATD influenced the results, a comparison between both setups with and without the shells was made. The same simulation was run for both cases for a randomly selected simulation. The results from this can be seen in Figure 4.2. R_{max} is the total deflection in mm of the IR-TRACC sensors mounted in THOR and the shells led to that the deflection was slightly smaller for the ATD mounted without shells.

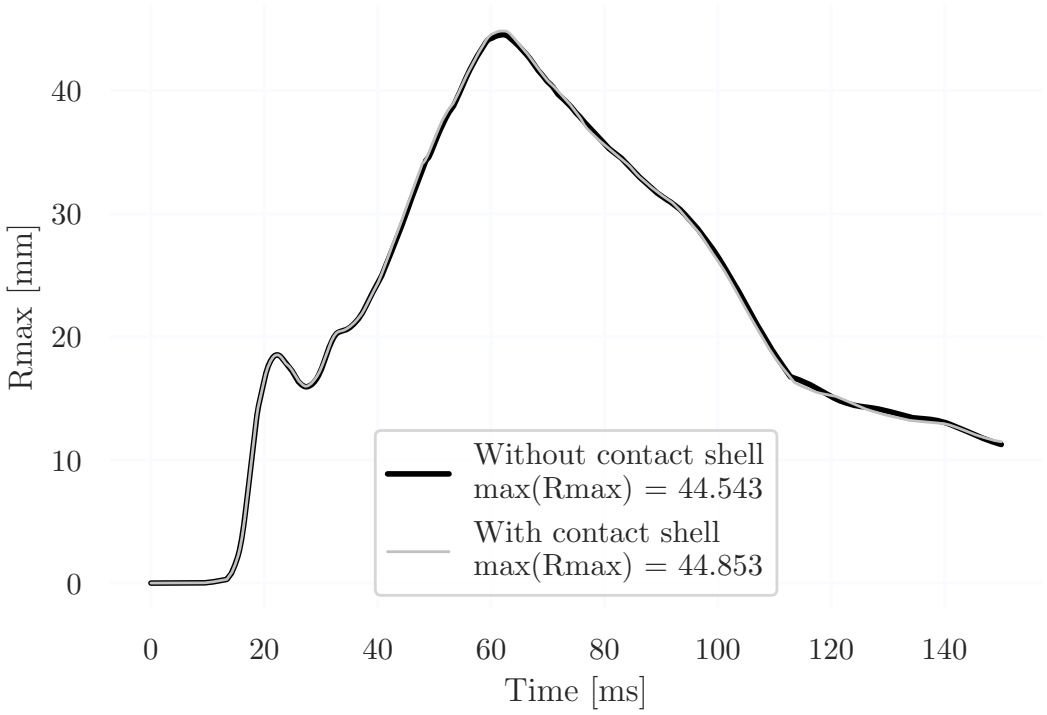

Figure 4.2: R_{max} comparison of the same simulation with and without the 0.6mm thick null shells for the bushings in the thorax

All changes to the model were intended not to change the behavior of the model, but merely to make sure that the simulations finished with normal termination, and that reliable results could be extracted.

4.2 Simulation Study

In this section, the results of the simulation study are presented, with the sampled parameters and the output from the simulations.

4.2.1 Results From Sampling of Parameters

The distribution of airbag trig time was not affected when changing the curve, and spikes around the endpoints were eliminated, Figure 3.10. Approximately 17% of the values lay above 40 ms, thus meaning these values were "lost". The variable sampling from the simulations generated and the theoretical sampling curve can be seen below in Figure 4.3. The distribution for Δv was log-normal. The theoretical distribution was computed by sampling datapoints with the same means and standard deviations as used in LS-OPT. These datapoints were then used to compute the associated Probability Density Function (PDF). From Figure 4.3 it was apparent that the distribution does follow the expected distribution quite well.

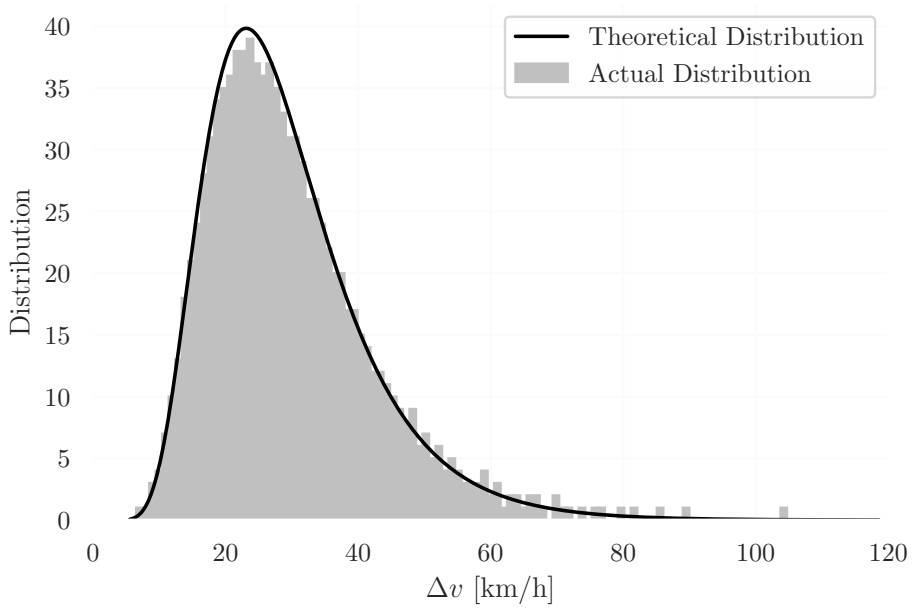

Figure 4.3: The distribution of the sampled Δv from LS-OPT, compared to the theoretical log-normal distribution

A further example of the distribution can be seen in Figure 4.4, where the crash pulse duration was plotted. In Figure 4.4, it is clear that the distribution does correlate well with the expected outcome.

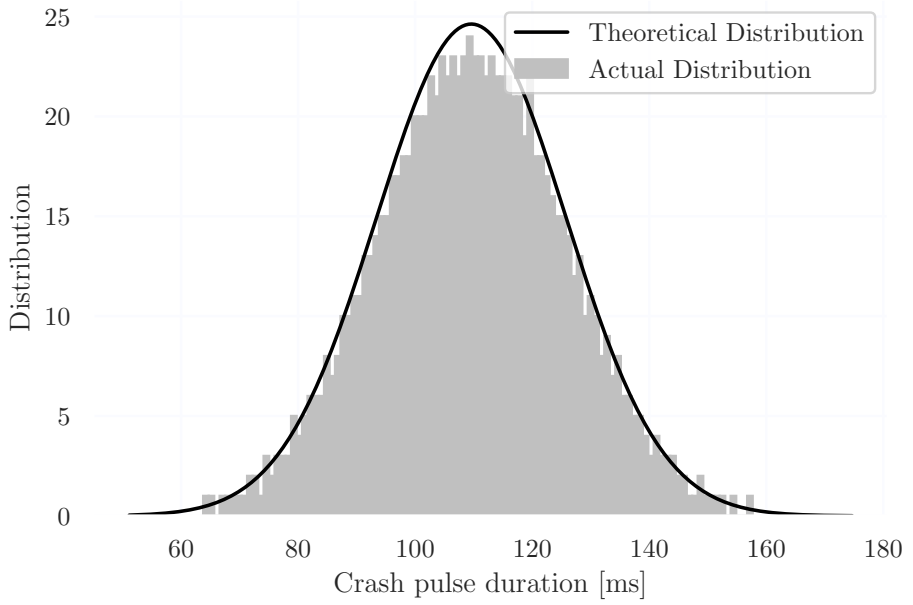

Figure 4.4: The distribution of the sampled crash time duration from LS-OPT, compared to the theoretical normal distribution

From Figure 4.3 and 4.4 it can be seen that the outputted parameter generation followed the distribution that was expected for each of the different parameters. The sampled distribution would be expected to follow the theoretical distribution. If the input to LS-OPT was desired to follow a normal distribution, then the output should be of a normal distribution. Thus, after the sampling was done in LS-OPT, it could be deemed as a satisfactory sampling, and the generated input files were ready to be simulated in LS-DYNA. For the purpose of the report, only a smaller sample of distribution plot were presented here, however all parameters were plotted and checked individually, to make sure no unexpected outputs were generated.

4.2.2 Winsmash Δv Distribution

The distribution for Winsmash Δv was plotted in a histogram, Figure 4.5. It was compared to the original Δv, to see whether or not the distribution was changed or merely shifted in one or the other direction. The theoretical distribution from Figure 4.3 was kept and in the Winsmash distribution seen in Figure 4.5, the velocities were weighted more to the left, meaning smaller Δv overall. That Winsmash Δv underestimated the speed change was not unexpected, since the systematic error in this method does cause exactly that, Iraeus and Lindquist (2016).

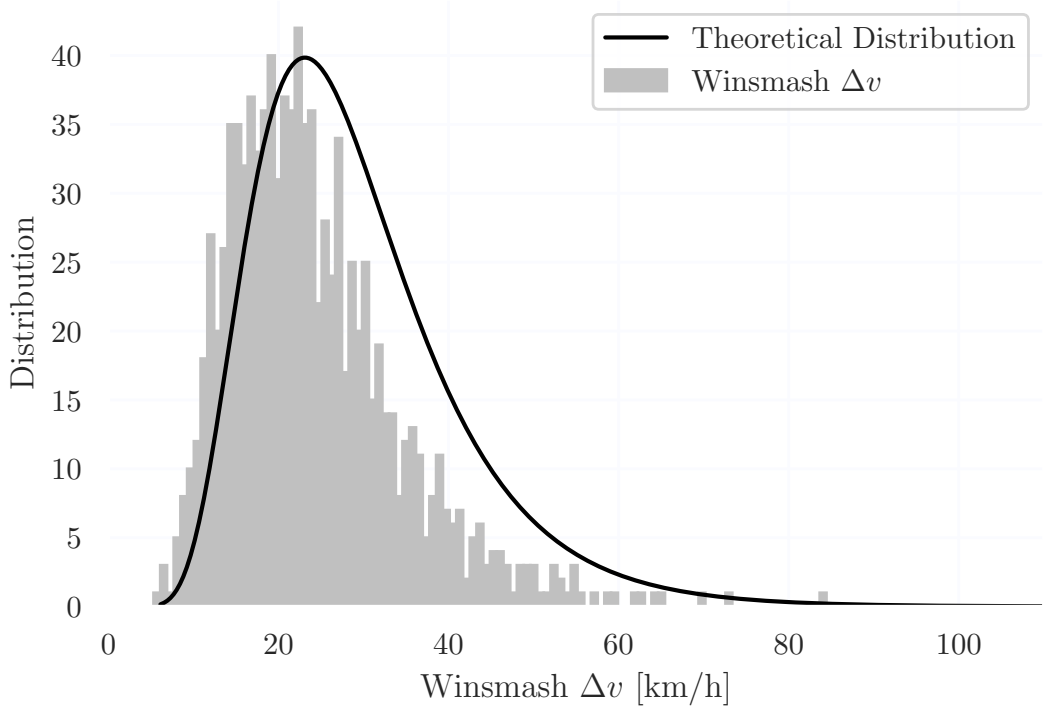

Figure 4.5: Distrubution of Δv after winsmash correction

4.2.3 LS-DYNA Simulations

When the sampling of the parameters had been done and checked the batch of inputs were ready to be simulated in LS-DYNA. When all simulations had been completed, it was found that 32 of the 1000 simulation had ended with error termination, i.e. 3.2% failed.

4.2.4 Troubleshooting and Rectifying Errors

Of the 32 failed simulations, one failed due to a bushing in the chest attaining negative volume and one failed due to the same reason, though for the head rubber cover. The cause of this, for the first case, was that the impact was very tough, meaning the forces on the chest induced by the belt were too large for the bushings in the ATD to handle. The reason behind the second case was similar, however only this time the head impacted the dashboard, causing abnormally high deflections to the ATD's face.

For the chest bushing, an extra insert was made to the model, namely an extra set of 0.6mm thick null elements around the affected bushing. Since this problem was encountered during the pilot study, this fix was already set-up and easy to implement on the failed simulation. The simulation with the failed head bushing was not re-run, since the simulation failed at such a late stage, the peak values for the chest sensors had already been reached.

The other 30 simulations that failed, did so because a belt segment had a free end. This issue was fixed by reverting back to the original length of the 2D part of the belt, which previously fixed the problem with the shoulder belt sliding, Table 4.1. The model was otherwise unchanged and the rerunned simulations did not have any problem with the belt sliding. A quick analysis was done to see if there was a common cause for this problem, by plotting all the input parameter values for the failed simulation versus the total distribution. From this, it was concluded that there was no clear correlation between the values of the input parameters and a failed simulation due to a free belt end.

In total, 31 of the 32 failed simulations were re-run with updated input files. All of the 31 simulations ended with normal termination, thus all simulations were now completed and results from all 1000 simulations were extracted.

4.3 Analysis of Simulations

When the simulations that ended due to error termination had been corrected, the complete analysis of the results was started. To summarize, all of the 1000 generated simulation yielded results, thus all of the simulation results were considered for the analysis and presentation of results.

4.3.1 Results from Simulations

The first part of the analysis was to compute a curve that fit the data from the simulations, for all different injury criteria. Firstly, the results for the injury criterion R_{max} are presented, Figure 4.6, where it can be seen that the spread between risk and Δv was quite large, i.e., one specific value for Δv does not inherently always correspond to the same risk. From Figure 4.6, one can observe that the risk function for R_{max} does not correspond to the NASS/CDS curve. The fitted curve has an R^2 of 0.580, thus indicating that the curve fits the datapoints from the simulations quite well. A Winsmash Δv of 55.5 km/h gives a 50% risk for the R_{max} measure. D_{max} does also show a risk that is quite high, Figure 4.7, compared to the NASS/CDS data. Compared to R_{max}, D_{max} seems to display a greater risk as well as a steeper increase in risk for higher Winsmash Δv. A Winsmash Δv of 48.8 km/h gives a 50% risk for the D_{max} measure. The fitted D_{max} curve has an R^2 of 0.378, which indicates a worse goodness of fit between the curve and datapoints compared to R_{max}. It should be considered when observing the results that D_{max} was computed for NFR5+, rather than AIS3+.

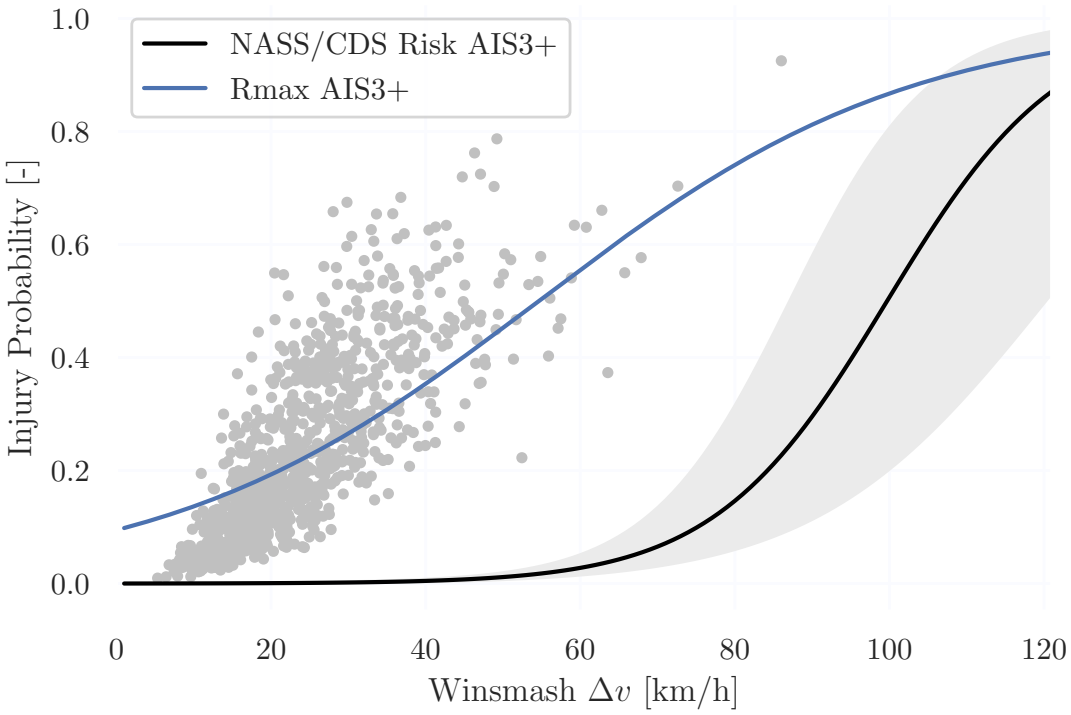

Figure 4.6: Scatter plot and curve fitment for simulation results for R_{max}, as well as the NASS/CDS data risk curve. The silver coloured points are the simulation results, i.e., one point corresponds to a risk and a value for the average Winsmash Δv. The 95% confidence interval is marked in grey, around the black NASS/CDS curve.

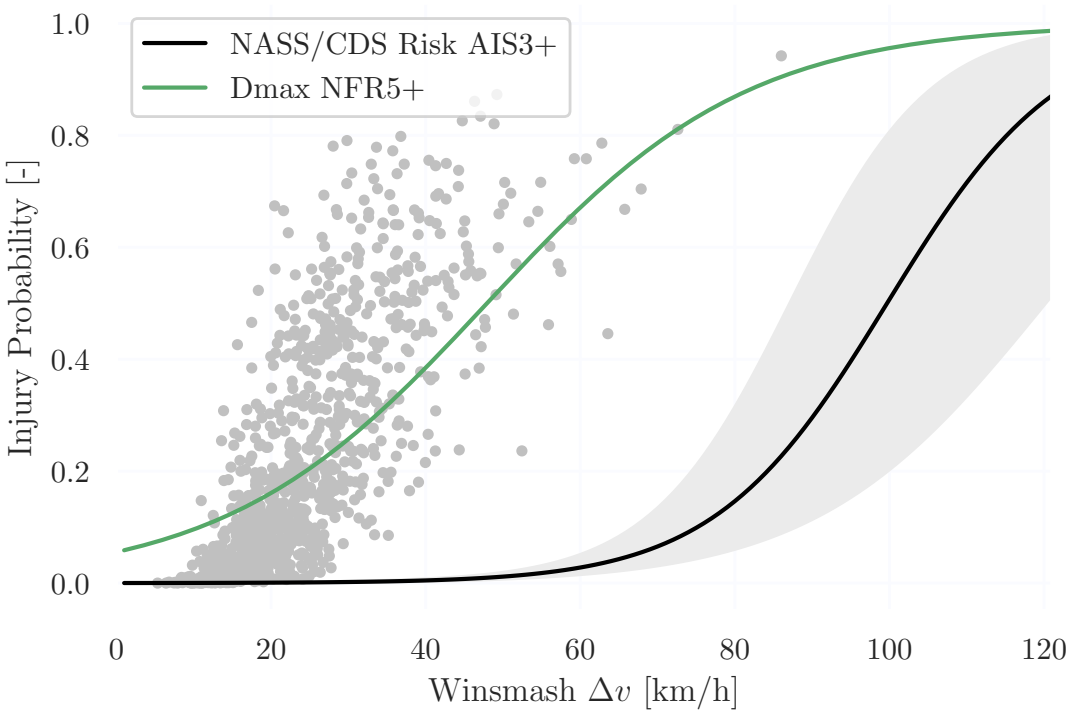

Figure 4.7: Scatter plot and curve fitment for simulation results for D_{max}, as well as the NASS/CDS data. The silver coloured points are the simulation results, i.e., one point corresponds to a risk and a value for the average Winsmash Δv. The 95% confidence interval is marked in grey, around the black NASS/CDS curve.

Leaving the single sensor measures, the criteria considering all of the chest mounted sensors are now presented. $DcTHOR$ shows a better fit to the NASS/CDS data, however still some way off, Figure 4.8. This measure shows a larger cluster of datapoints were collected close to the lower risk, likely due to the threshold in the DcTHOR calculation. Similarly to D_{max}, DcTHOR was computed for NFR5+, instead of AIS3+. As seen for the two previous measures, the risk does not start at zero. The shape of the DcTHOR risk curves corresponds quite decently to the NASS/CDS curve, which makes the comparison easier to make. A Winsmash Δv of 62.9 km/h gives a 50% risk for $DcTHOR$ and an R^2 of 0.271. PCscore shows a more linear increase in risk, compared to the previous, where the simulations in points marked in silver, were collected more closely together, Figure 4.9. The spread among the points was lower. As noted before, the risk curve does not start at zero, and the shape of the PCscore risk curve was a little flatter than the NASS/CDS curve, which makes for a more difficult comparison. Though, this risk curve predicts the same risk of injury for speed around 115 km/h. PCscore was computed according to the AIS3+ injury classification, which makes for a fair comparison between the calculated risk curve and the NASS/CDS risk curve. A Winsmash Δv of 77.6 km/h gives a 50% risk for $PCscore$ and an R^2 of 0.520.

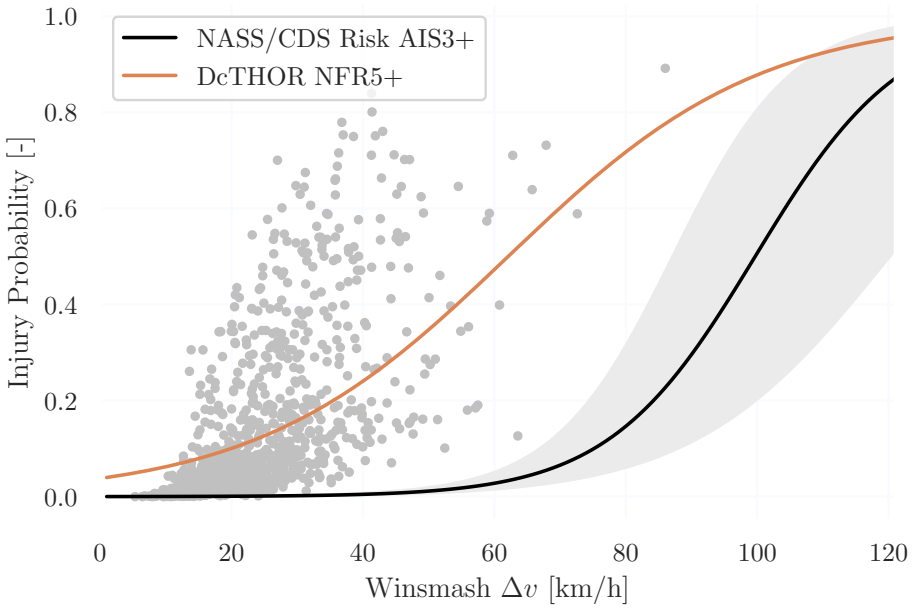

Figure 4.8: Scatter plot and curve fitment for simulation results for *DcTHOR*, as well as the NASS/CDS data, The silver coloured points are the simulation results, i.e., one point corresponds to a risk and a value for the average Winsmash Δv. The 95% confidence interval is marked in grey, around the black NASS/CDS curve.

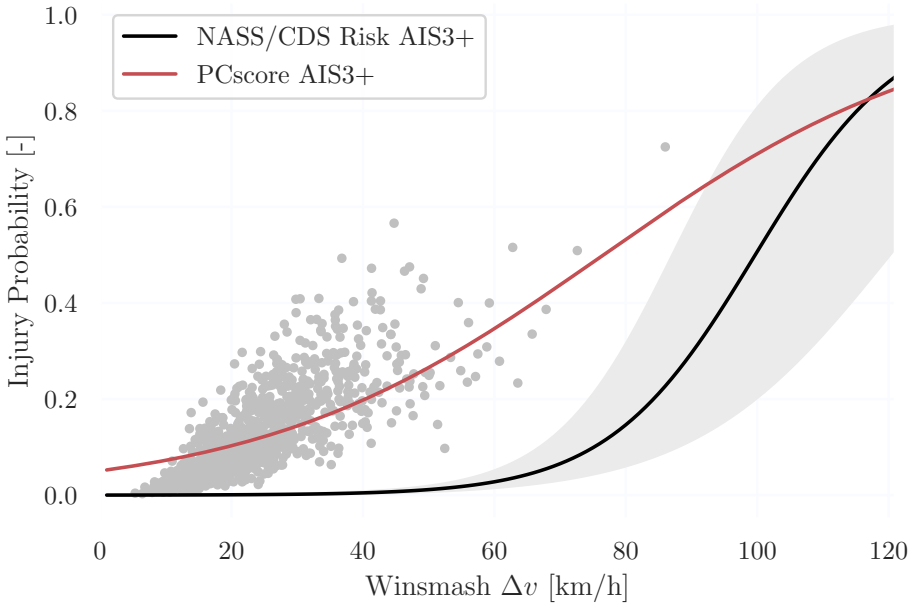

Figure 4.9: Scatter plot and curve fitment for simulation results for *PCscore*, as well as the NASS/CDS data. The silver coloured points are the simulation results, i.e., one point corresponds to a risk and a value for the average Winsmash Δv. The 95% confidence interval is marked in grey, around the black NASS/CDS curve.

TIC_{NFR}, Figure 4.10, shows a similar risk evaluation as $PCscore$, with a Winsmash Δv of 76.9 km/h yielding a 50% risk. TIC_{NFR} was computed using NFR3+ as the injury measure, the same as Troseille et al. (2019) had done, and this makes the direct comparison somewhat difficult. The risk curve does not start at a zero risk. Further, TIC_{NFR} had an R^2 of 0.360. The last measure presented, TIC_{NSFR}, was also the criterion that seems to fit the NASS/CDS data the best, Figure 4.11. TIC_{NSFR} seems to be quite different to the other measures, from the figure it can be noted that the datapoints were generally quite close to the lower risk prediction levels, and it was the only one that started at zero. Generally, it predicts a higher risk than the field data, though a very similar risk towards higher Winsmash Δv. A Winsmash Δv of 95.9 km/h gives a 50% risk for TIC_{NSFR}, and the curve fit had an R^2 of -0.194.

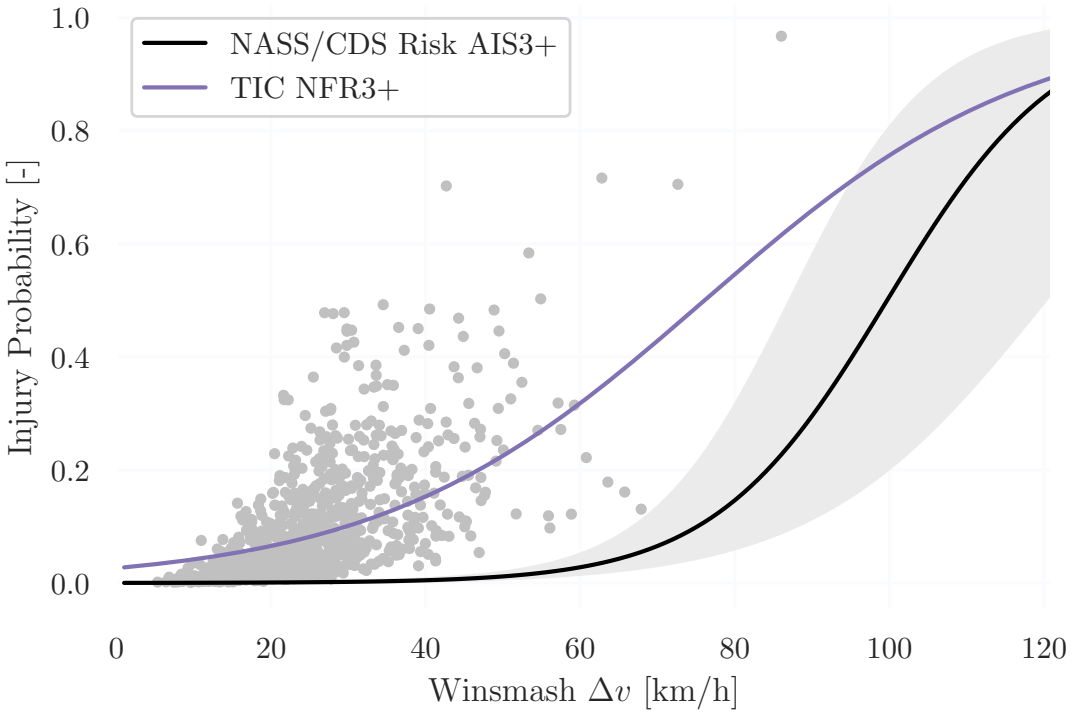

Figure 4.10: Scatter plot and curve fitment for simulation results for TIC_{NFR}, as well as the NASS/CDS data. The silver coloured points are the simulation results, i.e., one point corresponds to a risk and a value for the average Winsmash Δv. The 95% confidence interval is marked in grey, around the black NASS/CDS curve.

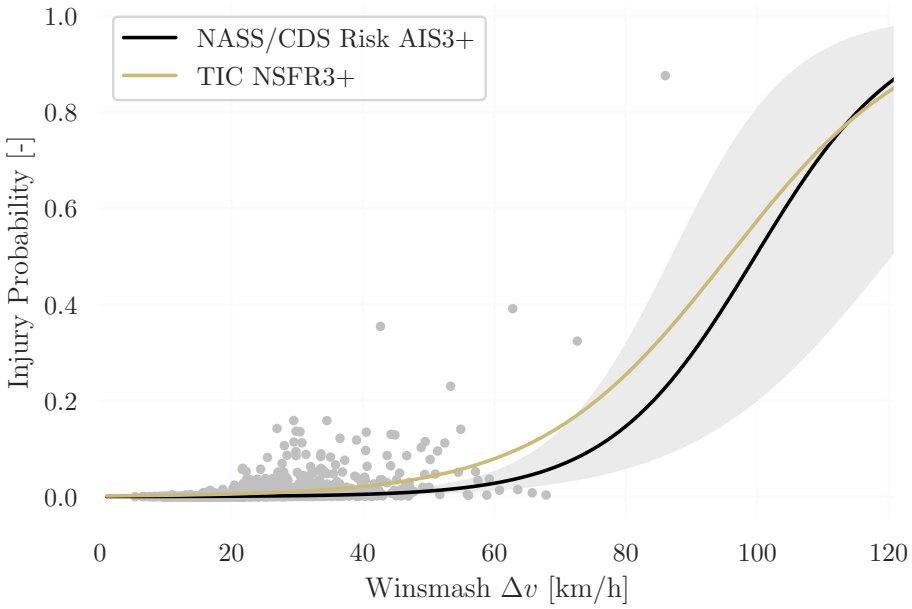

Figure 4.11: Scatter plot and curve fitment for simulation results for TIC_{NSFR}, as well as the NASS/CDS data. The silver coloured points are the simulation results, i.e., one point corresponds to a risk and a value for the average Winsmash Δv. The 95% confidence interval is marked in grey, around the black NASS/CDS curve.

Finally, all fitted risk curves were plotted together in the same figure, with the NASS/CDS curve. The spread among the different criteria was quite large and it can be seen that TIC NSFR fits the field crash data best, Figure 4.12.

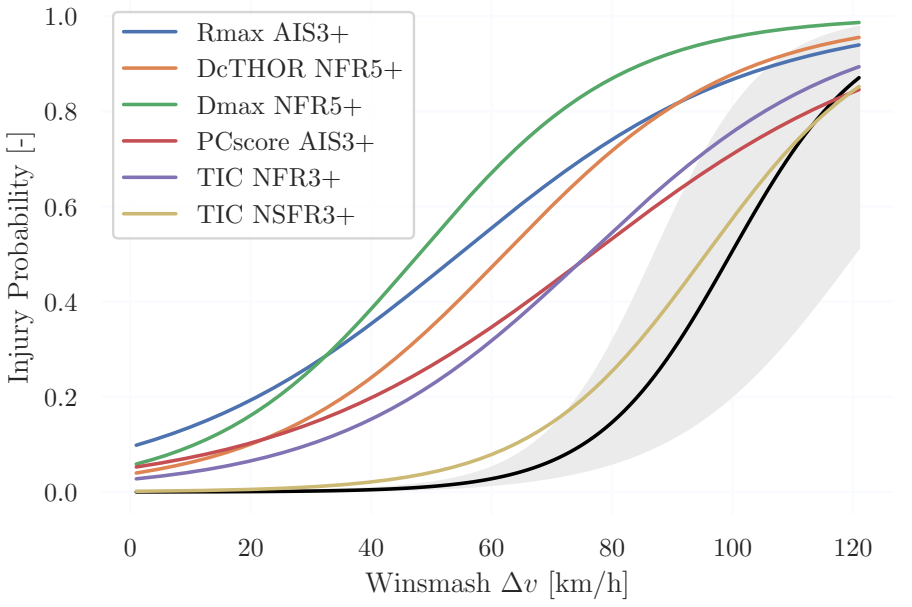

Figure 4.12: All fitted risk curves, as well as the NASS/CDS data

4.3.2 Goodness of Fit

Measurement to find the error in the curve fit was also done. All computed errors are listed in Table 4.2 together with the velocity change for a 50% injury probability and the curve fit parameters.

Table 4.2: All injury criteria and their respective R^2 scores, as well as the Δv at the 50% risk. The curve fit parameters are also included.

	R_{max}	D_{max}	DcTHOR	PCScore	TIC_{NFR}	TIC_{NSFR}	NASS/CDS	Unit
R^2 GLM	0.580	0.378	0.271	0.520	0.360	-0.194	-	-
$Winsmash\Delta v$ 50%	55.5	48.6	62.9	77.6	76.9	95.9	98.8	km/h
Δv 50%	54.6	48.8	62.1	74.6	75.5	101.5	-	km/h
c_{age}	-0.056	-0.071	-0.080	-0.090	-0.091	-0.017	0.089	-
$Intercept$	-0.0014	-0.0018	-0.0020	-0.0018	-0.0023	-0.0041	-12.11	-
$c_{\Delta v}$	0.041	0.059	0.051	0.038	0.048	0.069	0.089	-

One can also note that the Winsmash Δv estimtion did not signigfantly differ from the risk prediction using the real Δv, at the 50%. R^2, the curve fit with respect to the datapoints was the highest for R_{max} and $PCscore$, and the lowest for TIC_{NSFR}. In fact, R^2 for TIC_{NSFR} was negative, meaning a small or maybe even no correlation between the fitted curve and the simulation datapoints.

4.4 Additional Results

In this section some additional results are presented. This includes VPI results with the distribution from the simulations run, a comparison of the calculated risk curves to the SAFER HBM and the change in Δv from the Winsmash correction. A comparison was also be made for a correction of a potentially underpredicted NASS/CDS curve against the calculated risks.

4.4.1 Additional Injury Criteria Evaluation

The additional criteria that was looked at, was also analyzed and checked. After analyzing the abdomen displacements, it was found that none of the simulations showed signs of submarining, Figure 4.13, or other unwanted behavior, as the abdomen deflections were well below the AIS3+ 10% injury probability for abdomen injuries with the THOR ATD (Craig et al.2020).

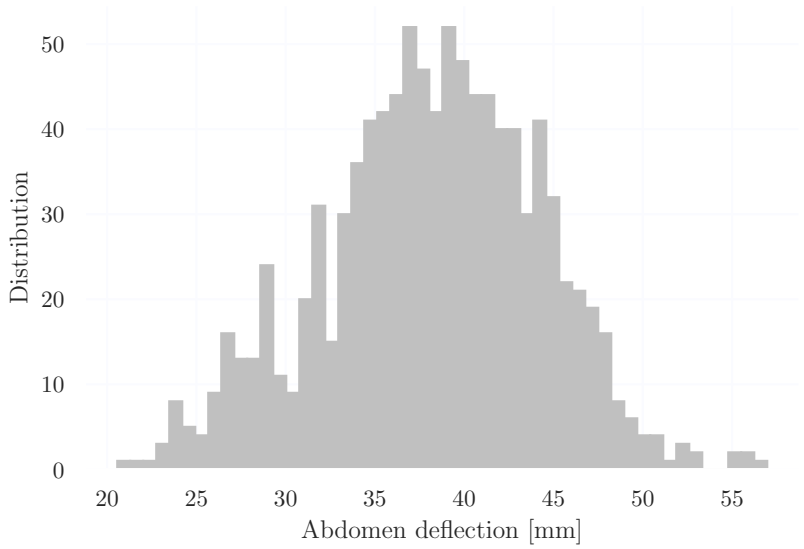

Figure 4.13: Distribution of the peak abdomen displcement for all simulations.

The head itself was considered. As previously mentioned, the head could hit the lining on the roof inside the car, in cases where the crash was on the more severe end. The issue was seen when the HIC values spiked quite heavily as a result of the contact with the roof. The removal of the head-to-roof did fix this issue. When the contact had been removed the HIC values received seemed to be within the expected range and only spiked when hitting hard parts such as the dashboard or windscreen, Figure 4.14.

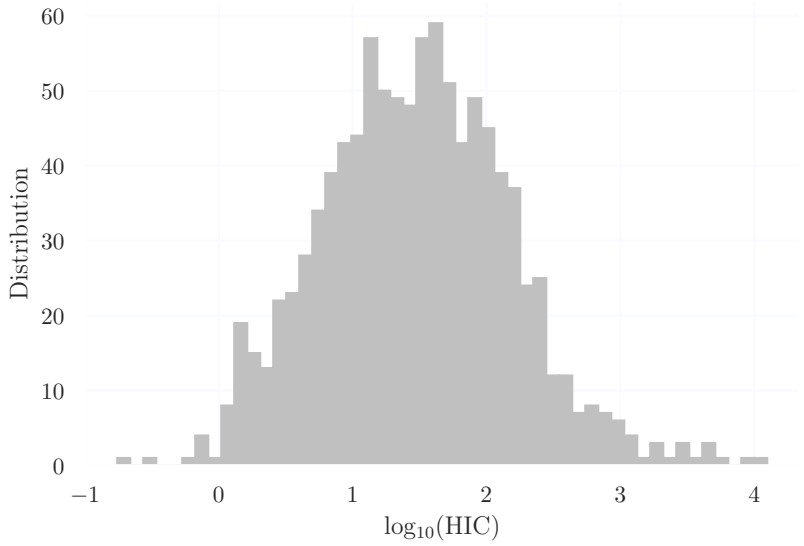

Figure 4.14: Distribution of the peak HIC values from all simulations.

4.4.2 Simulation Analysis with Vehicle Pulse Index

From the distribution figure it can be observed that most of the crashes were subject to a VPI of less than 400 m/s^2, which shows a similar pattern to the one seen before, that there were mostly low severity crashes.

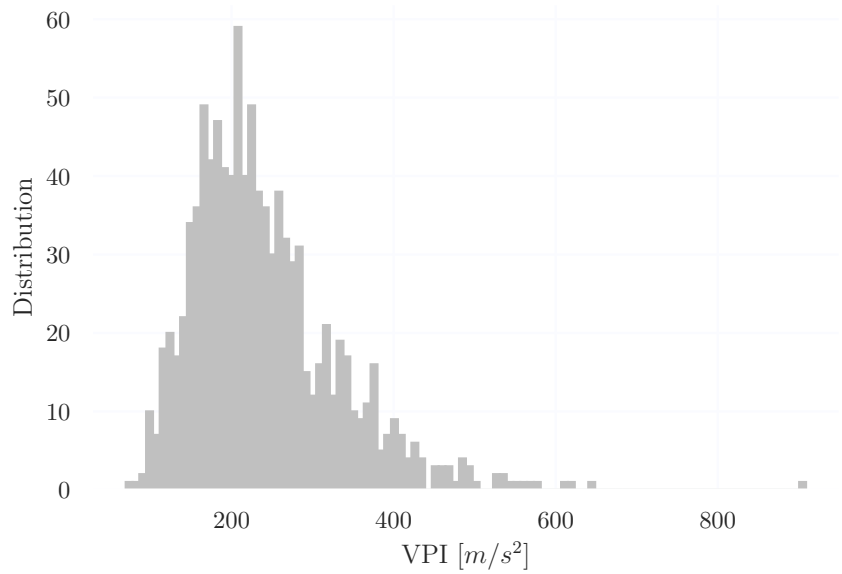

Figure 4.15: Distribution of the Vehicle Pulse Index.

The same regression analysis method was applied for this case, and the resulting risk curves were computed, Figure 4.16. The order among the criteria seem to be more or less the same as then one observed before, with D_{max} seemingly producing the highest risk while TIC NSFR predicts a significantly lower risk than the other. For this analysis, there was no possibility to compare the computed risk functions to the NASS/CDS field data from Iraeus and Lindquist (2016), since one would need the peak acceleration data from a crash. The risk curves all start closer to the zero risk for a VPI of zero.

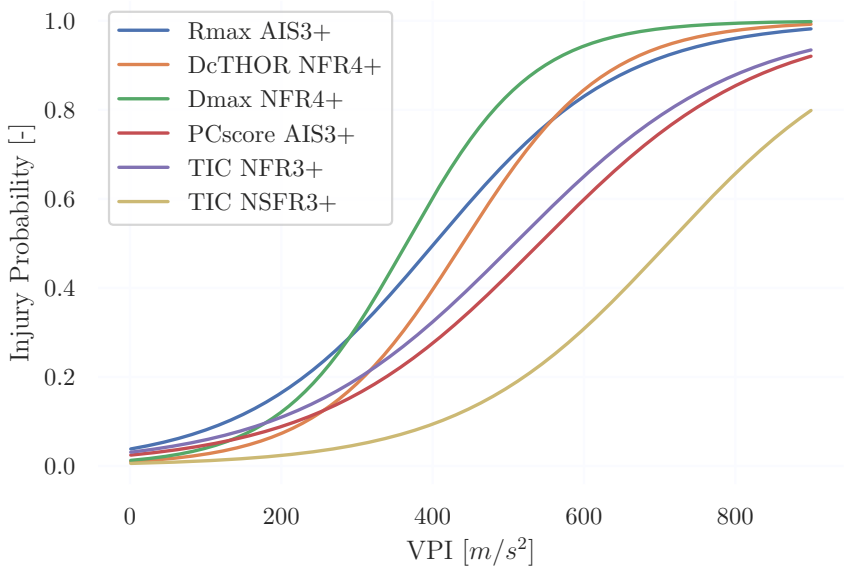

Figure 4.16: Injury risk curves using VPI as the predictor.

4.4.3 HBM comparison

All risk curves were individually compared to the SAFER HBM from Larsson et al. (2021), for Δv. This had to be done for a 30-year-old occupant since the curve were extracted directly from the paper. All the other curves were hence also changed to an occupant of age 30, Figure 4.17.

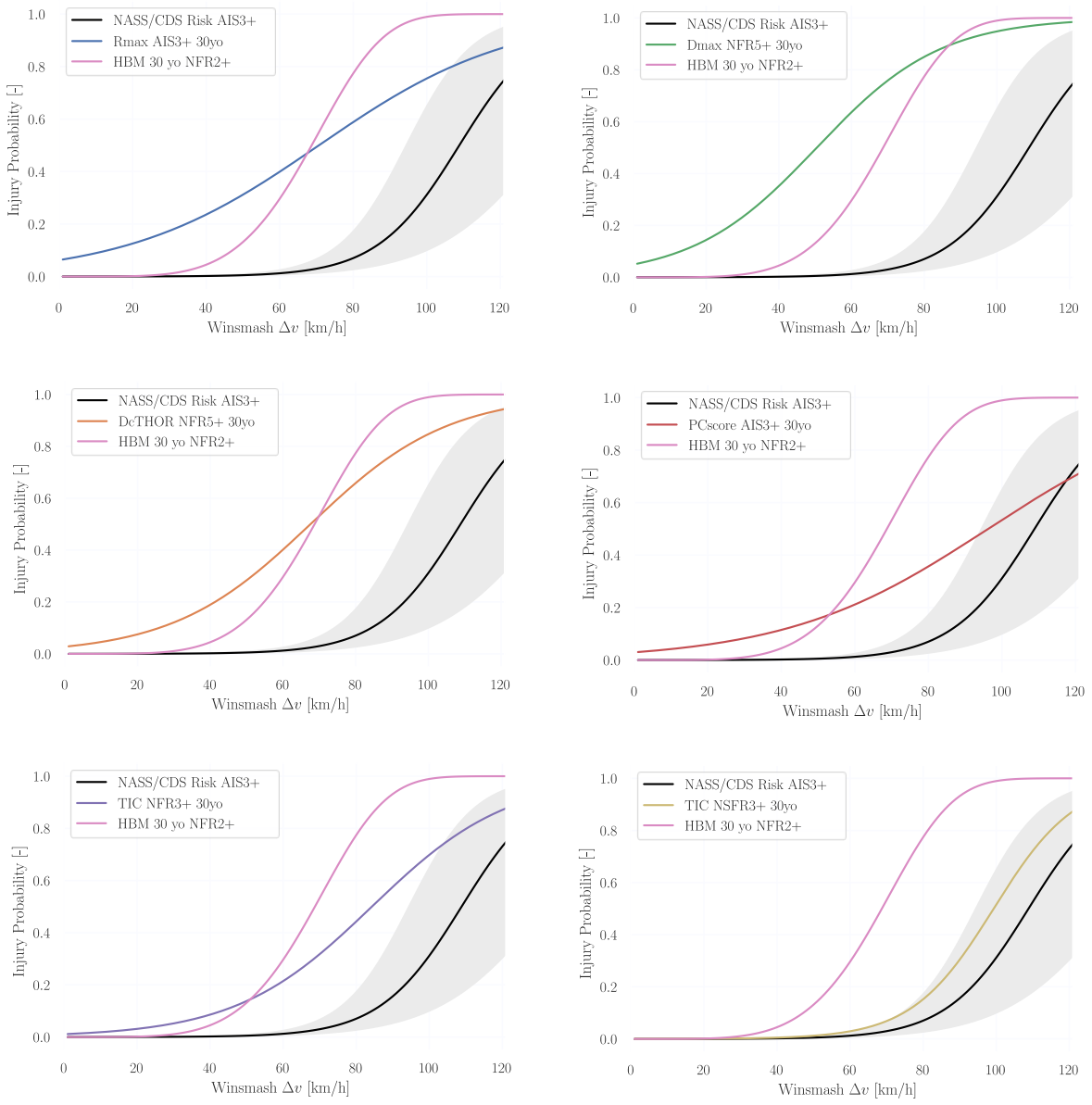

Figure 4.17: Risk curve for the SAFER HBM compared to the calculated injury risks for THOR.

4.4.4 Effects of Underpredicting Rib Fractures in NASS/CDS

The statistical evaluation to regard some uninjured occupants as injured, to explore the effect of underprediction of rib fractures in the field data, meant the NASS/CDS injury probabilities moved to the left, just as found by Iraeus and Lindquist (2016). In figure 4.18 a 70 and 50 % underprediction can be seen. R_{max} predicts more injury compared to all the curves up to a Winsmash Δv of 70 km/h, and D_{max} predicts higher injury for the whole range, Figure 4.18. The shift of the NASS/CDS curve means there was now predicted probability for injuries for speeds above 40 km/h and 20km/h for 50 and 70% underprediction levels, as opposed to the 60km/h limit observed in the unmodified data.

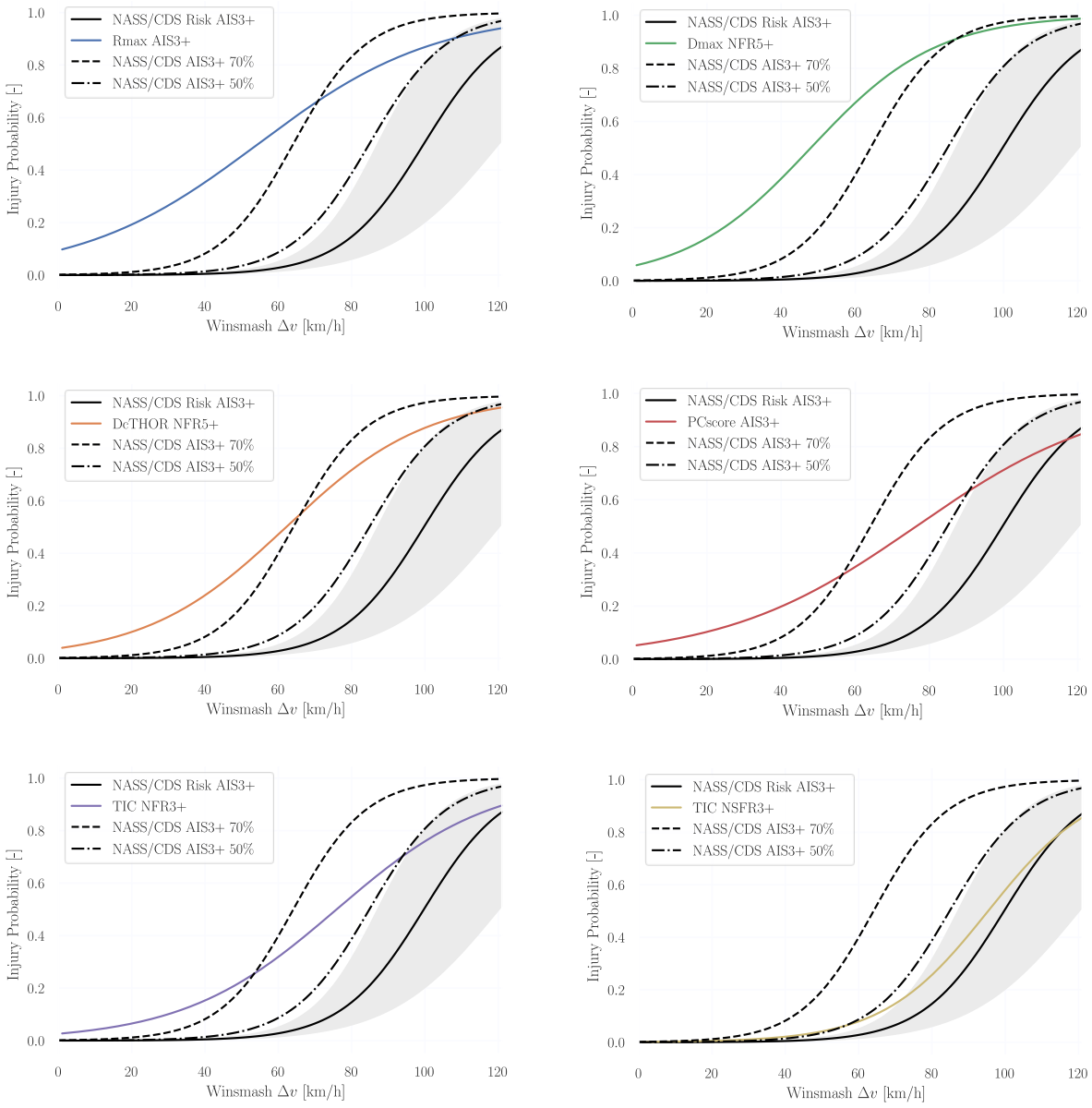

Figure 4.18: Influence of underprediction rib fractures in the NASS/CDS data.

Further it can be noted that for e.g. R_{max}, the calculated injury probability was still higher than what the 70% underprediction level would suggest, for speeds below 70 km/h.

4.4.5 Effects of Adding More Severe Crashes

With the introduction of more crashes of higher severity, the distribution of Δv changes, Figure 4.19. The original distribution was the 1000 previously derived simulations, and crashes were added according to a new uniform distribution of Δv between 60 and 120 km/h. The other parameters were sampled in the same way as before.

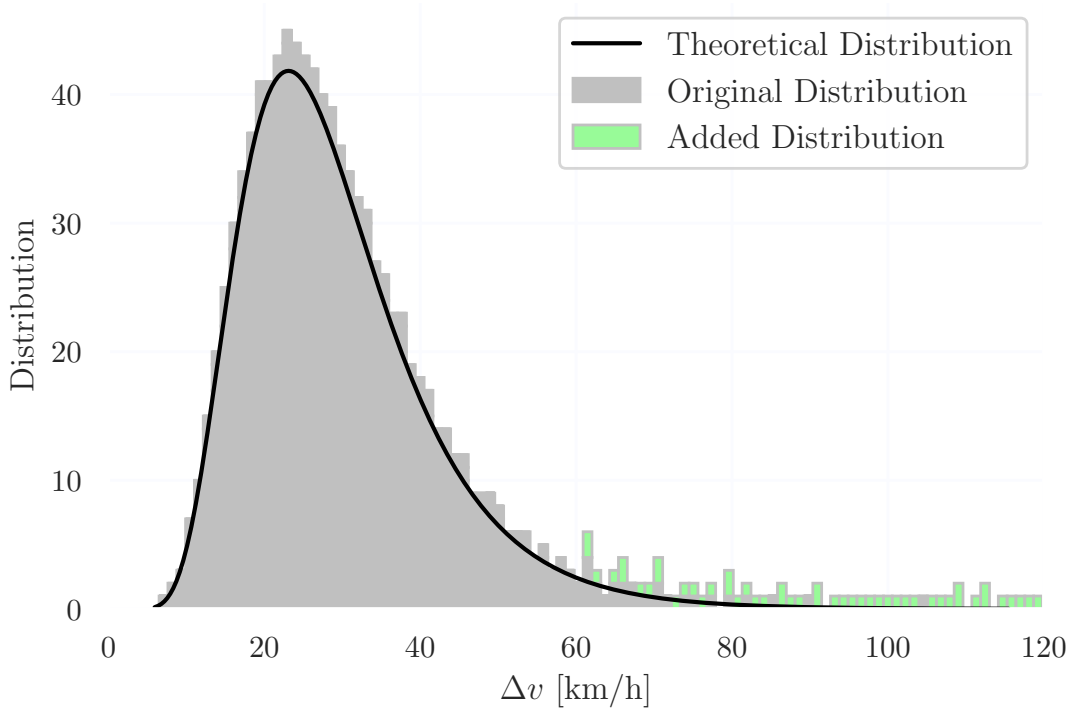

Figure 4.19: The new distribution of Δv after the addition of more severe crashes.

Since the simulations were so violent, all the new simulations were run with the 0.6mm null shell around the chest bushings, to avoid error terminations before the deflection peak. Out of the 50 simulations run 7 of them crashed due to negative volume in an element in the head of the ATD or due to that the belt segment had a free end. 5 of the 7 crashed simulations were discarded since no peak value had been achieved, but 45 of the added simulation was included in a new analysis. The regression was done once more, and the risk curves were computed again for all the 1045 simulations.

The added simulations and their corresponding risk were marked in light green, and it is visible that the new simulation was of higher speeds and generally higher injury probabilities, Figure 4.20. The change between the new and original risk curves were small for all injury criteria and the added simulations generally lie close to the curves.

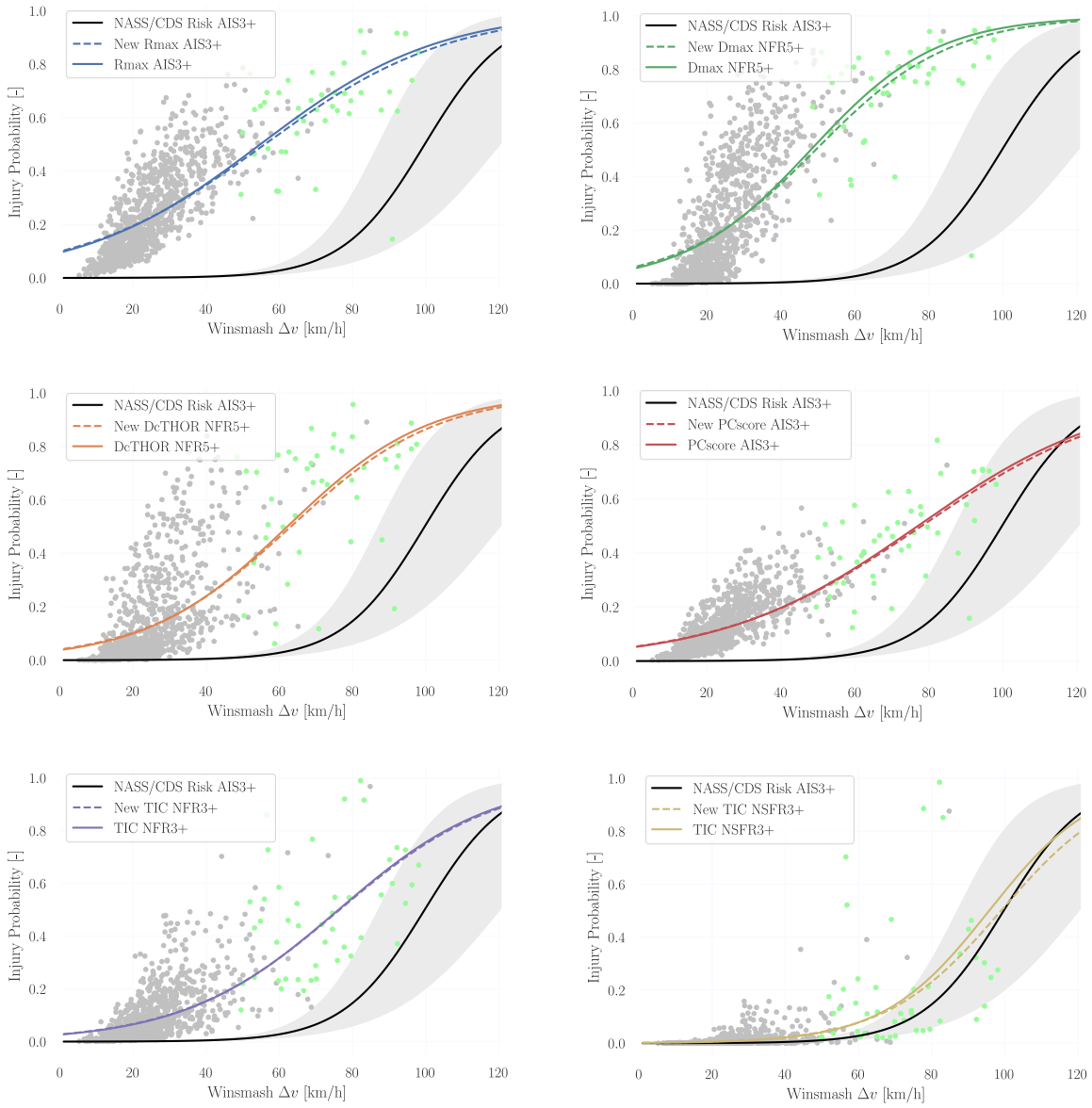

Figure 4.20: The risk curves for the newly added cases, a shift to the right can be seen for all cases.

4.4.6 $R_{max,Adjusted}$

$R_{max,Adjusted}$ had a better fitment against the NASS/CDS data for the 40 year old than the original R_{max} curve, Figure 4.21. The curve was bounded by the 70% and 50% underpredict curves and meets up with the original R_{max} at a Winsmash Δv of 120.

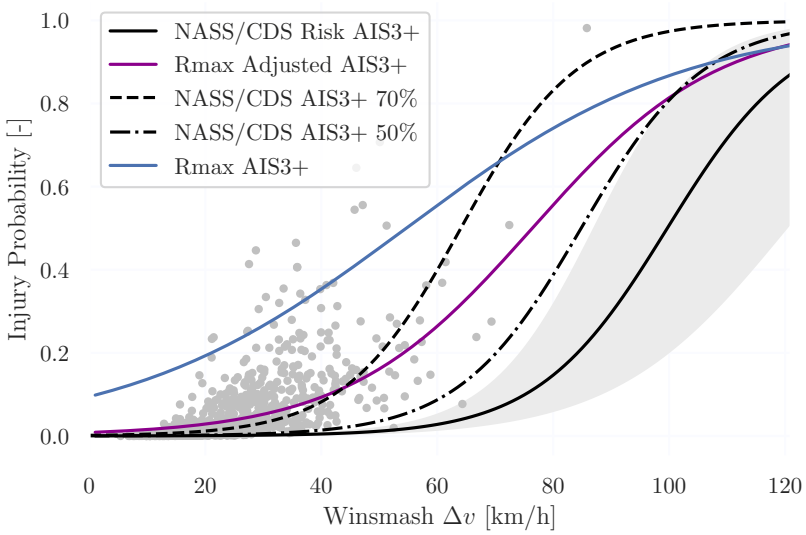

Figure 4.21: Rmax AIS3+ comparison for a 40-year-old between the adjusted and original R_{max} curve. The individual simulations plotted as grey dots for the $R_{max,Adjusted}$.

For the injury probability plotted against R_{max} in mm the difference can be seen between the $R_{max,Adjusted}$ and the R_{max} curves. $R_{max,Adjusted}$ starts the slope much later at around 40 mm but has a steeper incline, Figure 4.22.

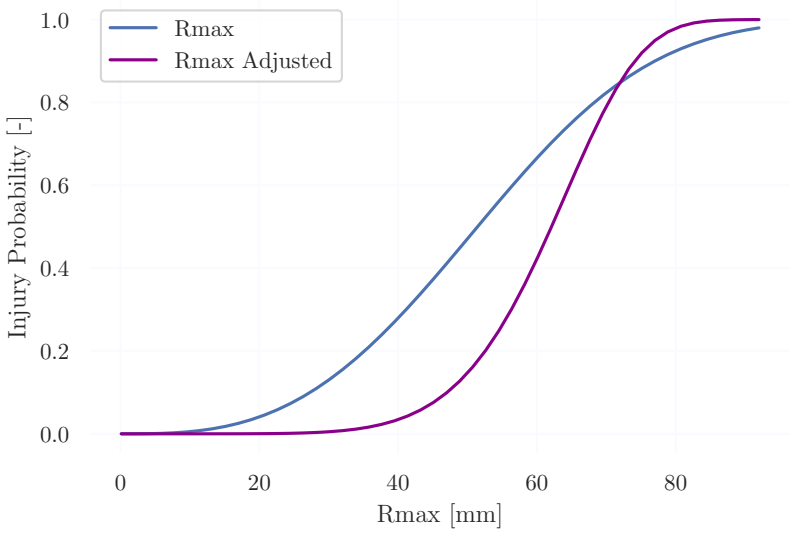

Figure 4.22: Rmax AIS3+ deflection comparison for a 40 year old between the adjusted and original R_{max} curve.

The risk curve can also be seen for the 30-year-old since it was needed to solve for the parameters in the risk function, Figure 4.23. The comparison between the original R_{max} and $R_{max,Adjusted}$ was similar as for the 40-year-old. $R_{max,Adjusted}$ was closer to the NASS/CDS data and was guided by the two underpredicted curves.

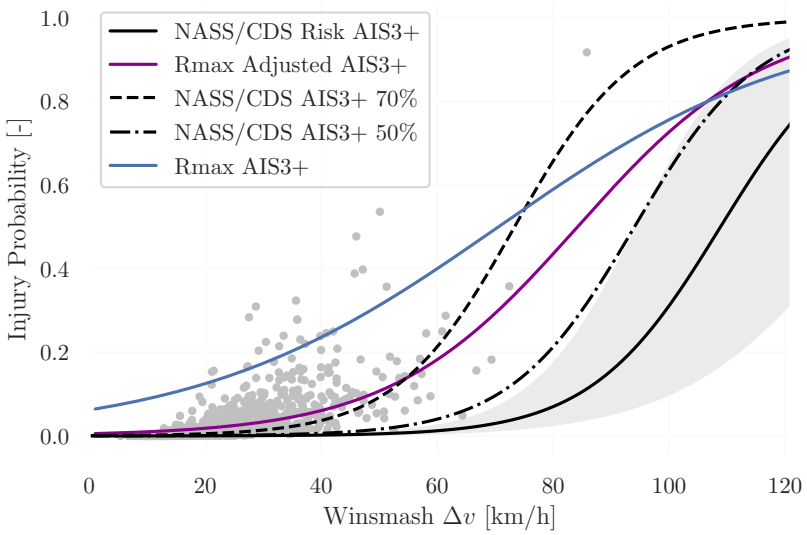

Figure 4.23: Rmax AIS3+ comparison for a 30 year old between the adjusted and original R_{max} curve. The individual simulations plotted as grey dots for the $R_{max,Adjusted}$.

4.4.7 THOR Accuracy

The deflection was recalculated as 30-50% lower than the output from the sensors, Figure 4.24, where the decreased R_{max} curves was closer to the NASS/CDS curve compared to the un-scaled version of R_{max}. The 50% risk now appear for Winsmash Δv of 72 and 87 km/h, recall that the original R_{max} found the 50% for Winsmash Δv of 55 km/h.

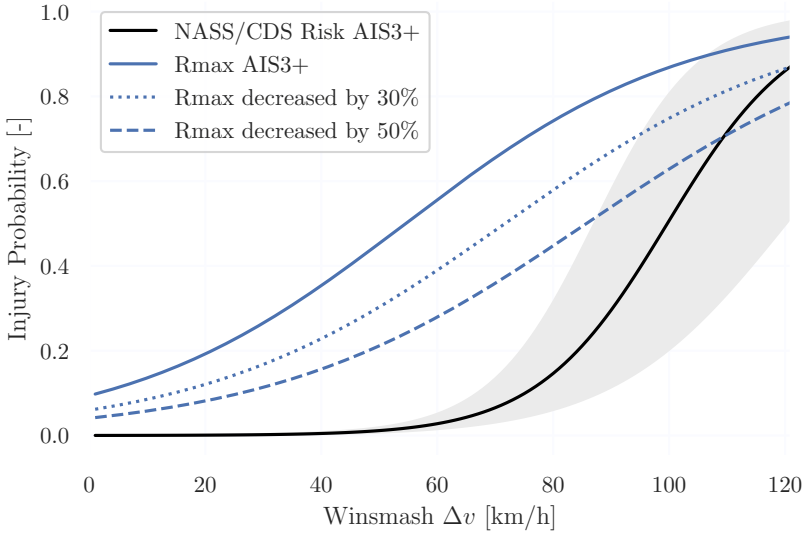

Figure 4.24: R_{max} plotted together with two special cases, the dotted line indicates the cases where the R_{max} value was decreased by 30 %, and the dashed line where the R_{max} value was decreased by 50 %.

4.5 EDR Δv NASS/CDS

The NASS/CDS data from Brumbelow (2019) was plotted for thoracic MAIS3+ injuries, and were compared to the simulation results for true Δv. The simulations results were however computed for AIS3+ for thoracic injuries. In Figure 4.25 the comparison can be seen for the Brumbelown (2019) MAIS3+ thoracic curve for 40-59 years old and the studied injury criteria.

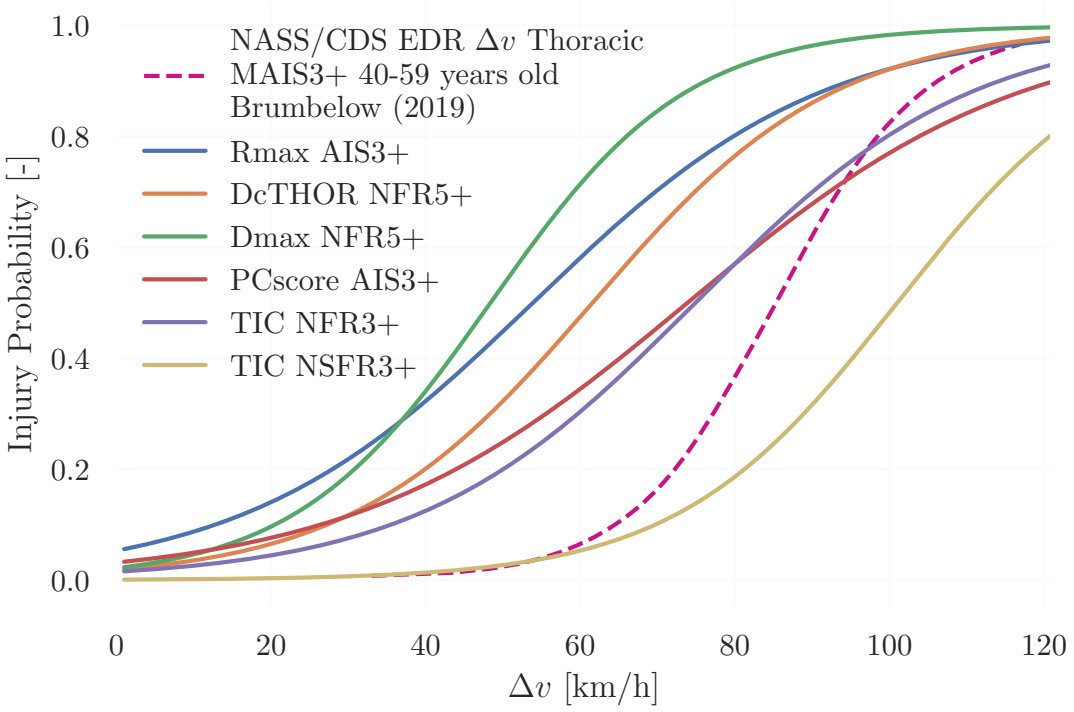

Figure 4.25: All injury criteria for true Δv plotted against Brumbelow (2019) thoracic MAIS3+ curve for 40-59 years old.

$PSscore$ and TIC_{NFR} fits the Brumbelow (2019) curve well but predicts a slightly higher risk for lower Δv while TIC_{NSFR} predicts a lower injury probability above 60 km/h than the Brumbelow (2019) curve.

5 Discussion

The aim of this study was to compare the rib fracture risk predicted by the THOR ATD with the risk of injury in real life crashes from NASS/CDS using the method and generic FE vehicle compartment model developed by Iraeus and Lindquist (2016). The simulations were run with LS-DYNA, and the sampling of the parameters was done in LS-OPT. Several Injury risk functions were evaluated in the post processing in order to find the best prediction of the real-life injury.

5.1 Overpredicting vs Underpredicting Injury Risk

The effects of overpredicting injuries in crash testing could affectthe development of softer safety systems. One could argue that a softer system, which would result from a more sensitive ATD, would be better for the occupants in a crash scenario. This may be the case in less severe crashes, but in the case of higher severity the softer safety system could contribute to more harm than good, since a softer system might bottom out. One argument that strengthens the view is that when the seatbelt pulls with a lower force, the risk of using the full length of the belt increases at a high velocity crash, and hence the restraint system can bottom out. Over predicting risk of injury might lead to other implications as well, and it may make car manufacturers having to adopt softer safety systems into their cars in crash tests. This in turn may led to that the safety systems performs worse in the real world. Lie and Tingvall (2002) studied real life crashes by correlating the injury sustained when crashing with Euro NCAP ranked cars to the star rating of the vehicle. When considering severe and fatal injuries the star rating had a good correlation with real life injury for the years 1996-2000, where higher rated cars were safer. Lie and Tingvall (2002) argues that it is important to monitor the real-life crash outcome to avoid suboptimization, which in turn can lead to worse performance in real-life.

Underpredicting injuries in a crash test may on the other hand contribute to more injuries in the lower velocity cases but could help in high severity crashes. But the rating system for crash test could be skewed, since lower risks would be predicted than the reality. Hence the difference between a bad performing car and a good performing car in a crash test could be harder to spot. This could in the end slow down development since there is small gain in developing safer cars. The best would be to come as close to reality as possible, to avoid safety systems that don't work in the real world.

5.2 Injury Risk Probabilities

From the analysis conducted, it could be seen that TIC_{NSFR} performs best when compared to the real-life outcome in the NASS/CDS data, Figure 4.12. According to the NASS/CDS risk curve, there was close to a 0 % risk of AIS3+ thoacic injuries for Winsmash Δv below 50 km/h. For the same speed, R_{max} predicts a risk of around 45%, and TIC_{NSFR} predicts a risk of approximately 20 %, and the other risk curve lie in between. Considering this, none of the risk curves corresponds very well to the observed field data. The NASS/CDS

curve seems to predict risk of injury for speeds above 50 km/h, though for the simulated cases, there were very few datapoints in this region.

The reason for TIC_{NSFR} seemingly being the best risk function might lie in the nature of the function itself. The measure was computed for NSFR, number of separated fractured ribs, which was the number of fractured ribs that were likely to be diagnosed. On average, one would need 3 NFR to get 1 NSFR (Troseille et al. 2019). In effect, that means that cases where the occupant did indeed suffer an injury, but the injury could not clearly be seen on x-ray, might not have been registered as such. Consequently, this means the overall risk predicted by the function would be lower, as can be seen from Figure 4.11, in which there were few datapoints above the 20% risk level. This might raise the question whether or not the NASS/CDS data is completely accurate. The distribution of simulation datapoints was also studied, Figure 5.1, and this reinforces the idea that the injury risk prediction by TIC_{NSFR} was indeed too insensitive, as almost all risk predictions lie below the 10% risk.

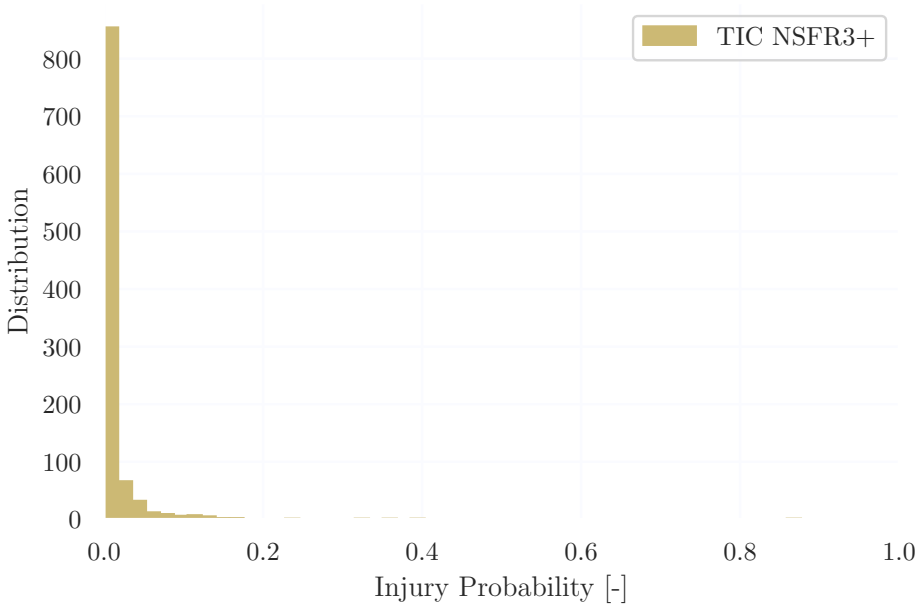

Figure 5.1: Distribution of simulation risk prediction by TIC_{NSFR}.

These arguments means that TIC_{NSFR} could not be stated as the best risk function, but instead $PCscore$ or TIC_{NFR}. These risk functions show decent correlation to the NASS/CDS risk curve, while still being able to capture the different severity levels of a crash. Since $PCscore$ was computed for AIS3+, the same as the NASS/CDS risk curve, it was preferred over TIC_{NFR}. The risk distributions were plotted for $PCscore$ and TIC_{NFR} as well, Figure 5.2, where it can be seen that the spread of risks was greater for $PCscore$ than for TIC_{NFR}. The fact that there seems to be too high risk prediction at the zero level for TIC_{NFR} than for $PCscore$, indicates the same insensitivity tendencies as for TIC_{NSFR}. Therefore, as a results, $PCscore$ would be considered as the best risk function, among the ones that were studied.

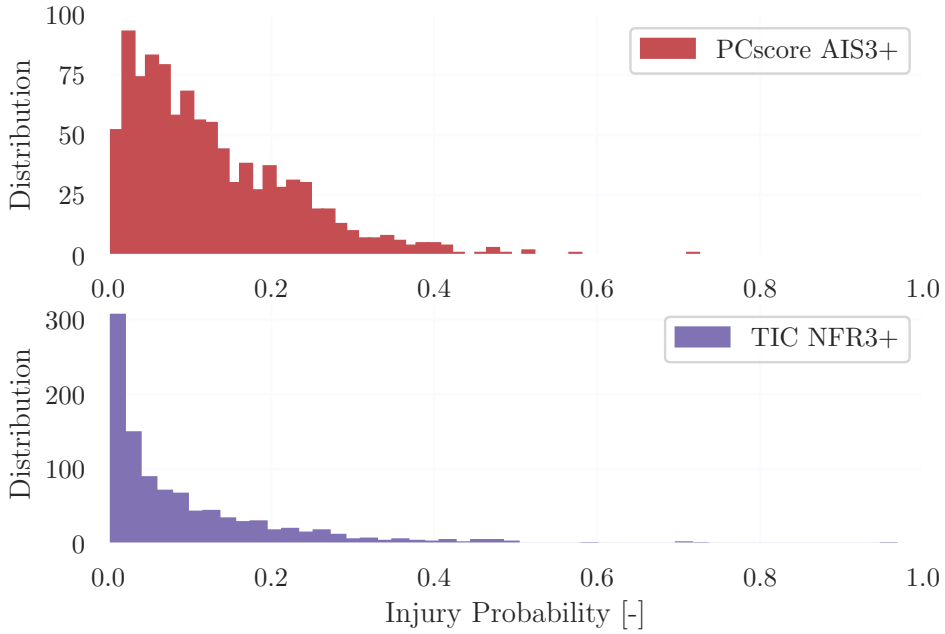

Figure 5.2: Distribution of simulation risk prediction by $PCscore$ and TIC_{NFR}.

On the other hand of the spectrum, one can find R_{max}, D_{max} and $DcTHOR$ seemingly being too sensitive. For the case of R_{max} there really were no possible explanation than to say that it was too sensitive and predicts very high injury risks. However, bearing in mind, that the different risk functions use different injury scales, and might thus not be directly comparable. Though, since the coding for different injury scales were somewhat different a choice was made to use the classifications stated. For instance, D_{max} and $DcTHOR$ are also defined for NFR7+, and a small test was ran to see what influence this had on the injury risk prediction, Figure 5.3.

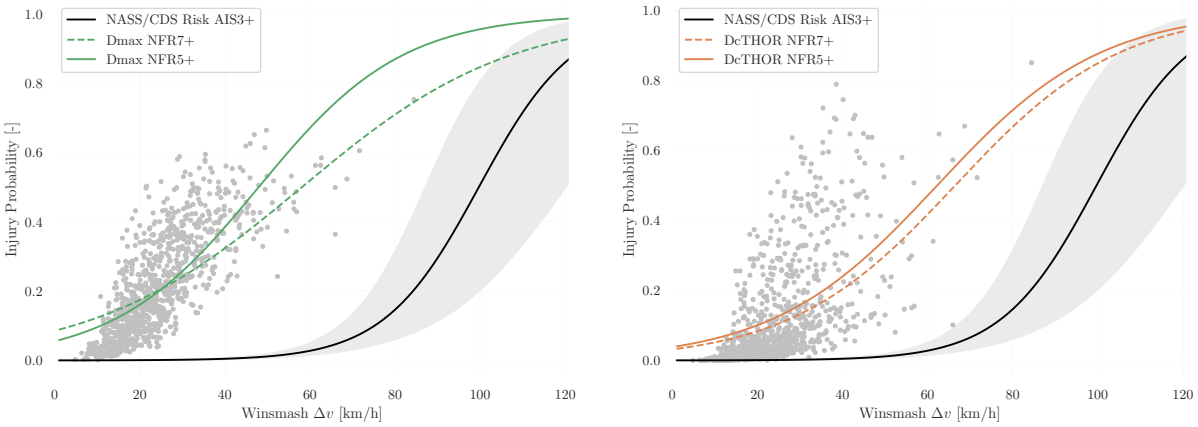

Figure 5.3: Distribution of simulation risk prediction by TIC_{NSFR}.

From Figure 5.3 it can be seen that for $DcTHOR$ there were no major differences in the

injury risk prediction, and this aligns well with the observations from Davidsson et al. (2014). Though, D_{max} differs more when compared to NFR5+, the curve was flatter and predicted a lower risk of injury, especially in the regions above 50 km/h. In fact, D_{max} for NFR7+ was found to be quite close to R_{max}. Even for higher injury classification thresholds for both D_{max} and $DcTHOR$, the risk functions do not provide a better injury risk prediction than neither $PCscore$ nor TIC_{NFR}.

Generally though, for all the injury risk function, there was an apparent pattern, that the risk functions did not predict a zero risk for zero Δv. This was likely due to the logistic regression used to fit the data. This behaviour was however unwanted, since it meant that there would be a risk of injury from just sitting inside a car, which, of course, was not reasonable. The underlying reason for this though, could be due to the measurement for THOR in combination with the associated risk curve, did not have a linear correlation with Δv, Figure 5.4. As can be noted from Figure 5.4, the linear curve does not intersect the points further down the y-axis, thus resulting in a risk curve which does not start at 0.

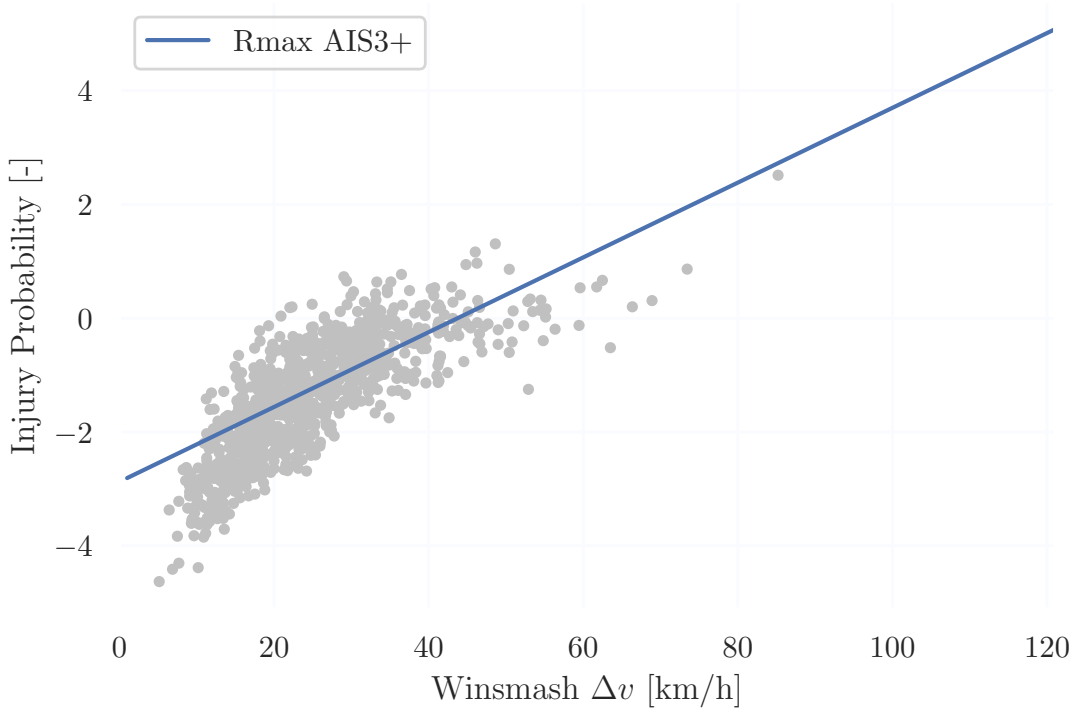

Figure 5.4: Risk curve for R_{max} in log-odds space.

Instead, what could have been done, was to either transform the data in order to get a linear correlation between the risk and Δv or use a non-linear regression model. This might have improved the risk curve, especially at the 0% risk level, where there could have been a closer match to the datapoints.

5.3 Processing of NASS/CDS Data

During the calculation of the injury risk curve for the NASS/CDS data, there seemed to be a lot of uninjured occupants compared to the number of injured ones. This was examined further, Figure 5.5, to get a clearer picture of the distribution. In Figure 5.5, the green markings have been scaled to represent the number of injured occupants encountered for that specific speed. Since the NASS/CDS data contained information about Δv without decimals, many of the markings would be at the exact same location. As can be noted, there were indeed many more uninjured occupants than injured, which is a snapshot of the situation seen in reality.

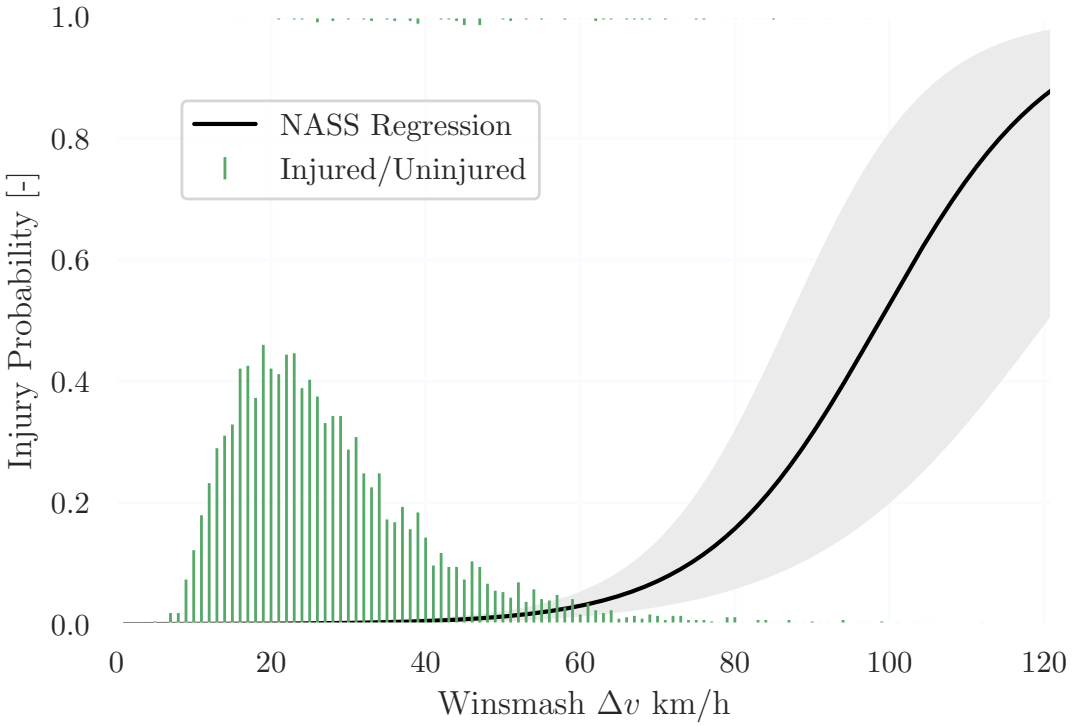

Figure 5.5: The NASS/CDS risk curve, along with the re-scaled markings for injured/uninjured.

5.4 Effects of Under Prediction in NASS/CDS Data

In a study by Crandall et al. (2000), 29 human cadavers were subject to frontal impacts ranging from 25 to 59km/h. One finding in the study was that only 40% of the total fractures were seen on x-ray. A similar study by Schulze et al. (2013), where 51 subjects were assessed with both CT-scan and autopsy, showed that 15% of the total fractures were missed in the postmortem CT-scan compared to the autopsy. Another study by Lederer et al. (2004), studied the aftermath of Cardiopulmonary Resuscitation (CPR) on adults. The conclusion was that 6 out of the 19 studied were diagnosed with a rib fracture

when run through a chest x-ray and 17 were diagnosed with rib fractures when subject to an autopsy. This would lead to about a 70% underprediction rate. When studying Figure 4.18, which shows the injury criteria calculated, plotted against the NASS/CDS data for an underprediction rate of 0, 50 and 70%, R_{max} in particular predicts a higher risk for lower Winsmash Δv for all curves up to 70km/h. R_{max} was directly comparable to the curves since it was, as for the NASS/CDS data, calculated for the AIS3+ injury classification. The same direct comparison could be done for PCscore, which was closer to the NASS/CDS data and hence was performing better. When moving an occupant from uninjured to injured, the assumption was that for high and low Δv, the underprediction was the smallest. For higher Δv, the autopsy as a source was more common, though for lower Δv the false rate could in practice be higher than 70%. Although there is generally less injuries for lower impact velocities.

5.5 Comparison to Human Body Model

Larsson et al. (2021) conducted a study with the SAFER HBM and studied rib fracture risk for a 30- and 70-year-old driver. The curves seen in Figure 4.17 is plotted for the 30-year-old case, and the risk estimate for the HBM was the risk of a NFR2+ rib fracture. This was not directly comparable to any of the calculated risk functions in this study, but the risk to sustain an NFR2+ injury should in practice be higher for the same Δv than the risk for both NFR3+ and AIS3+. When comparing the calculated injury criteria in this study to the HBM curve, the HBM predicted a lower risk than eg. D_{max} for the same Winsmash Δv. This should in practice not be possible but was most likely due to the overprediction of injury in D_{max}.

5.6 Vehicle Pulse Index

VPI was computed as a representation of the acceleration on the occupant inside the car, instead of just purely the acceleration on the car itself. This means that the occupant will have to endure a slightly higher acceleration than the car, as a result of slack in the system. This slack comes from the occupant's interaction with the seatbelt.

When using VPI as the predictor for injury risk it was found the injury criteria ranked more or less the same as when using Δv, Figures 4.16 and 4.12 respectively. However, there was no acceleration data available in the NASS/CDS data, a comparison to real life outcome could not be made. It could though, be argued that VPI would be an alternative to Δv, since it does not only consider the velocity during a crash event, but the duration as well. E.g. a crash with a low Δv can be very severe if the stop is very sudden, i.e. a short crash duration, yielding a very high acceleration.

A small study was made, to find out whether the two measurements correlate, with a linear regression and computing the coefficient of determination, also known as R^2. From this analysis it was seen that the two correlate quite well, with $R^2 = 0.77$, and showing a clear trend towards an increasing Δv also giving an increased VPI, Figure 5.6

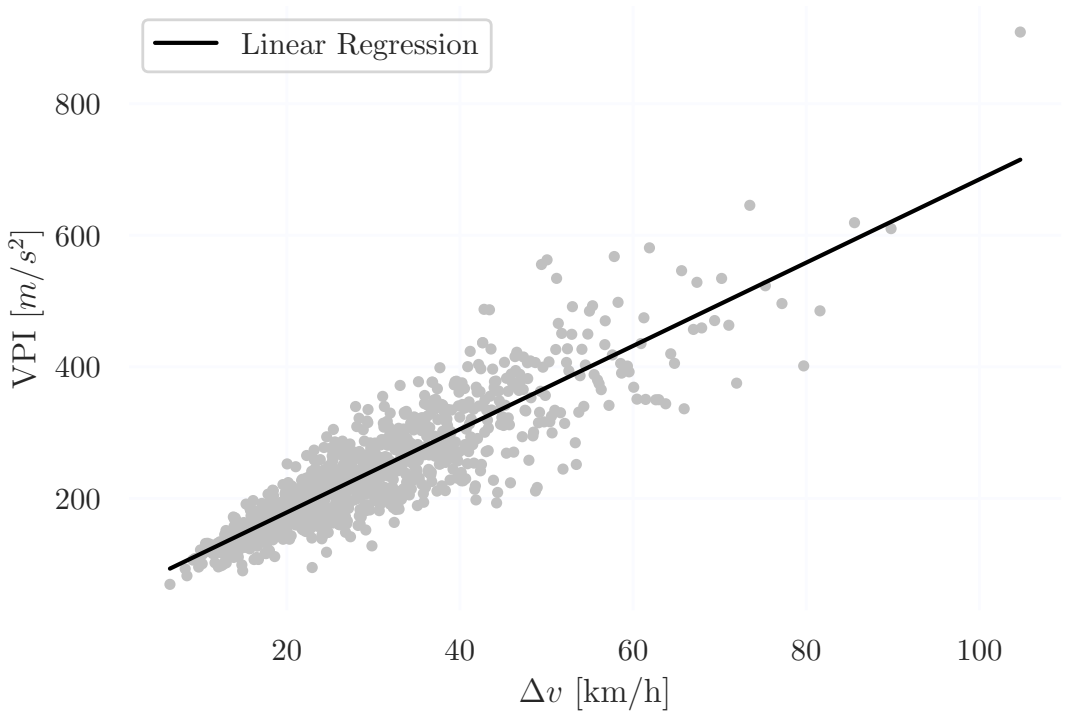

Figure 5.6: The Vehicle Pulse Index as a function of Δv, with the linear regression line in black.

To be able to use VPI as a predictor for injuries in car crashes, acceleration data must be saved by the car in such an event. The Winsmash Δv velocity is an estimation that can be made after the crash. Estimating the crash acceleration would however be a more difficult task. Consequently, it would require data to be recorded by each car. If such equipment would be in place, storing the peak acceleration during a crash might be a good way of doing it. Thus, the peak acceleration may then be used to calculate VPI. Possible solutions for this can be an Event Data Recorder (EDR), with is a device installed in cars to record technical vehicle information. In addition, smartphones of today may be able to record such information. With this, however, comes the question of privacy and the handling of personal information, which may hinder this development.

Tsoi and Gabler (2015) did a study very similar to this study, where they had access to EDR data and could quite accurately compute VPI, among other measures to predict the injury risk. Tsoi and Gabler (2015) found that VPI was a significantly better predictor of injury risk than e.g., Δv. The risk curve from Tsoi and Gabler (2015) was recreated and added for comparison, Figure 5.7. Though, this risk curve was computed for the MAIS3+,

for injury to the 3+ level for the spine, thorax or abdomen. Thus, if considering AIS3+ injury to the thorax instead, the Tsoi and Gabler (2015) curve should be shifted to the right since less areas of the body to sustain an injury on would be included in the data.

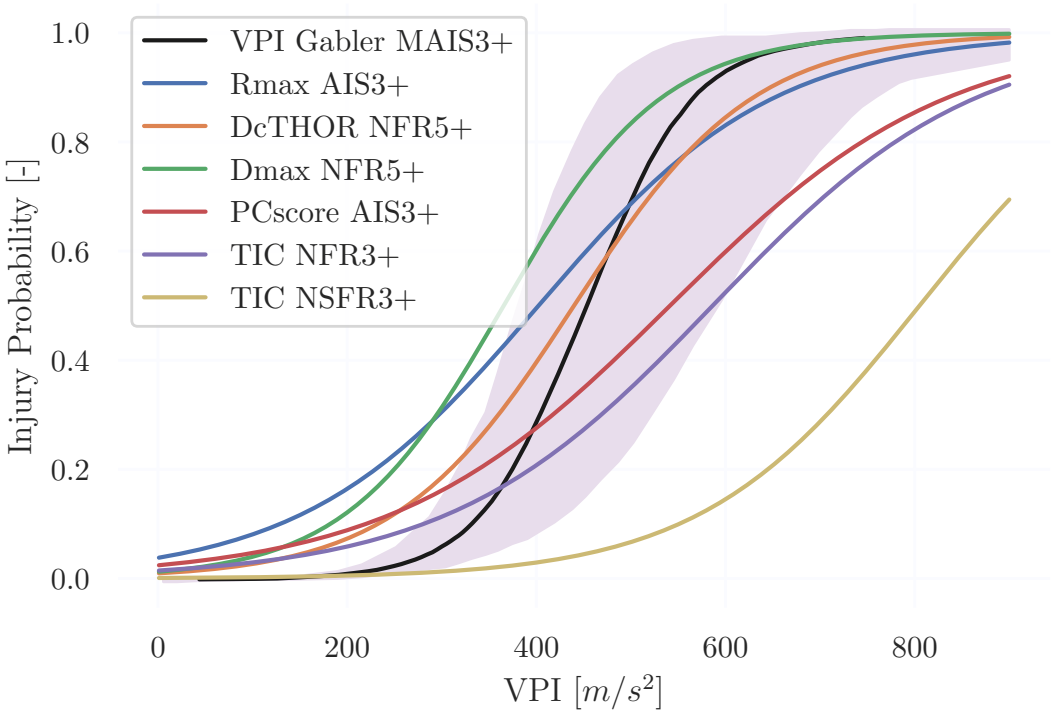

Figure 5.7: The risk curves for all injury criteria and compared to the VPI risk curve from Tsoi and Gabler (2015). Note that this risk was computed using the MAIS3+ injury scale.

5.7 Validation of the Generic Sled

The generic car model used in this study was the same as used and developed by Iraeus and Lindquist (2016). The parameters for the model were tuned by replicating frontal oblique tests with complete vehicles, that had been run with a Hybrid III. For the validation of the sled used in the study, a comparison to real-life crashes was made, on a population level. From this validation test, the Objective Rating Method (ORM) peak and peak time rating varied between 83% and 94%, Iraeus (2015). These results can be compared to the guidelines by Eriksson et al. (2009), which states that good correlation show ORM values of 90% or above and Iraeus (2015) states that all ORM values correspond well to these guidelines.

5.8 THOR Validation

The THOR ATD is a frontal impact test device, however there were no clear indications as to what this really meant. Thus, several papers were surveyed, with the intension of investigating the valid PDOF range for THOR. In addition, an examination of THORs performance with respect to real world crashes was made, to find out if there was something in the construction of the ATD that might explain the observed softness.

5.8.1 Crash Angles Valid for THOR

Biofidelity evaluations of the THOR ATD in oblique loading have previously been studied by Parent et al. (2017). Parent tested the lower ribcage in an oblique impact by impacting the eight rib with a pendulum of the mass 23.4 kg. Overall, the THOR ATD got a higher biofidelity score than the Hybrid III, when compared to PMHS corridors (Parent et al. 2017). The test was run by rotating the ATDs 15° and hence impacting to the side of the thorax.

5.8.2 Correlation Between FE-THOR and Physical THOR

Umale et al. (2018) studied the differences between FE ATDs and the physical ATDs. Among the tested FE ATDs were the THOR, Worldwide Harmonized Side Impact Dummy (World SID) and the Hybrid III. The tests conducted were oblique 60° sled tests and pure lateral sled test with PDOF 90°. The tests were also run for PMHS for a biofidelic comparison. All the tested FE-models showed good correlation to the physical ATDs according to Umale et al.(2018). The author also states that the THOR and Worlds SID ATDs showed more biofidelic responses than the Hybrid III when compared to the PMHS tests.

This study was run with a PDOF ranging from -45 to 10°. Although there is studies to support that the THOR ATD can handle the load cases studied, there is one example of where the deflection output was smaller than initially expected. The outlier is marked in Figure 5.8 where a velocity of 112km/h, corrected to Winsmash Δv to 92km/h and PDOF approaching -45°, THOR predicted a small injury probability. When studying this simulation an almost pure lateral loading of the thorax could be seen since the ATD completely misses the airbag and the longitudinal forces acted on the head and the arm. This is the same plot for R_{max} as seen in Figure 4.20.

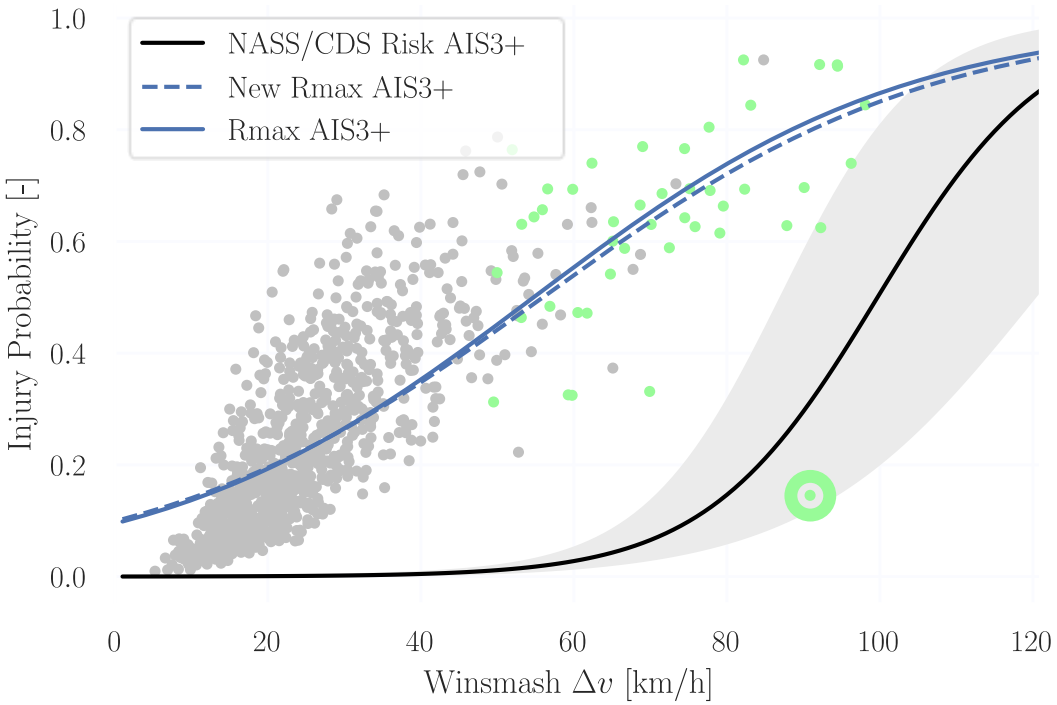

Figure 5.8: The risk curve for R_{max}, with the special case marked with a green circle.

5.9 Winsmash Δv Effects on Risk Prediction

The effect of the Winsmash estimation was investigated. As previously mentioned, the Winsmash estimation contains a bias and an uncertainty. With respect to the risk curves, these must natrually change when the speed estimator changes. What could be seen from the analysis was that the Winsmash estimation made the risk curve flatter, Figure 5.9. This was the result of the curve fitting property, which depends on the variance in x and y, though with the Winsmash estimation the variance in x was changed, but not in y, thus yielding a flatter curve.

When determining Δv using the Winsmash estimation method, somewhat accurate approximation of speed changes could be made by the use of simple linear relationships between the impact speed change, and the residual crush of the vehicle. Such assumptions do of course contain over-simplifications of complex crash structures, though the estimation was found to be a reasonably sufficient estimation of the speed change in a crash. It was although obvious that the usage of this speed estimation was not ideal and constitutes to an unwanted uncertainty. In addition, Winsmash Δv systematically underestimates Δv, Figure 4.5, and Niehof and Gabler (2006) found that Winsmash Δv underestimates Δv by 23%, on average.

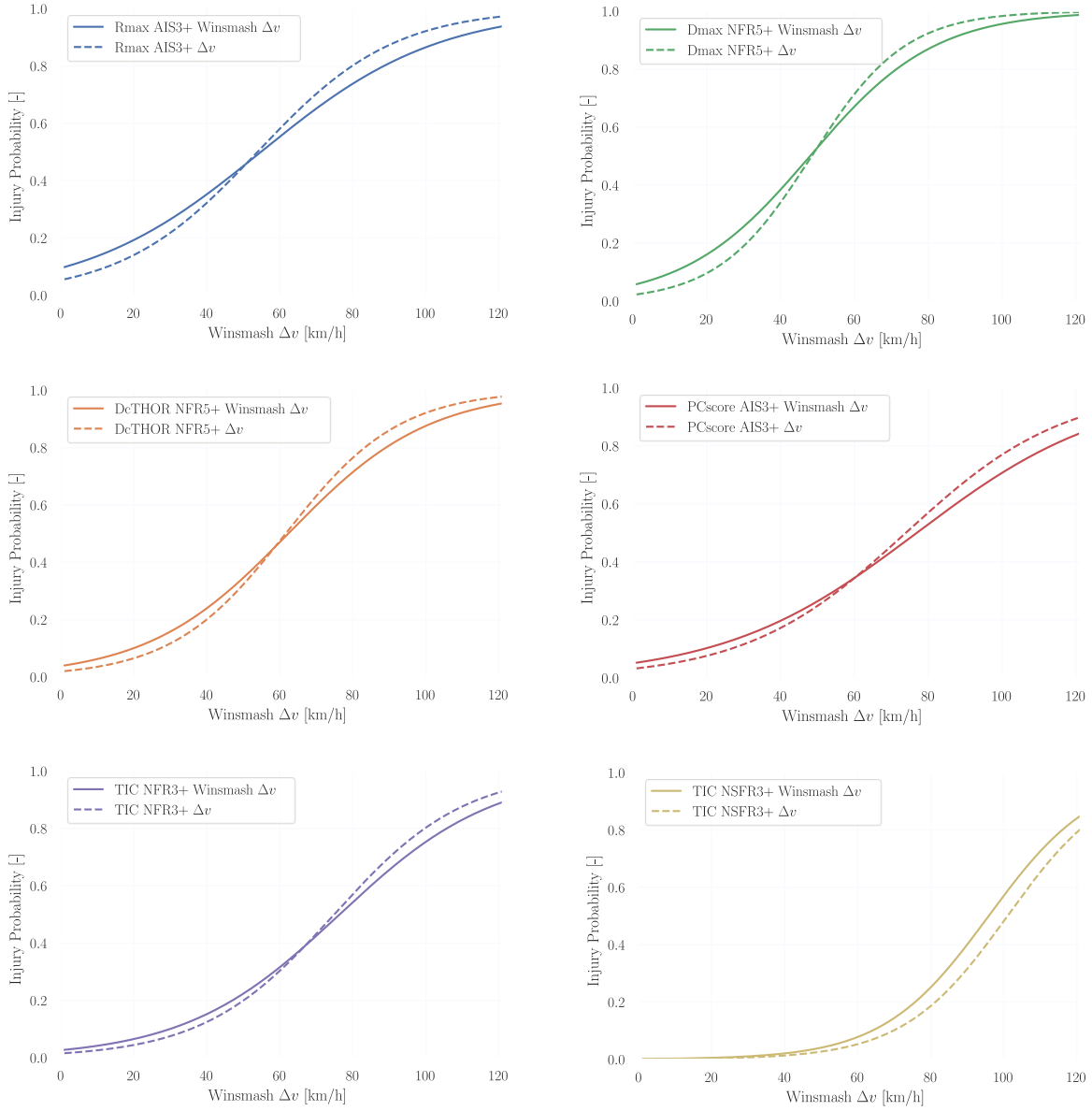

Figure 5.9: The effect of changing Δv according to the Winsmash estimation. The dashed line represents the risk curve for the Δv used in the simulations, while the solid line was the Winsmash Δv

The Winsmash estimation of Δv does make the curves flatter, 5.9. The reason for that lies in the regression model used. The regression model computes the linear function y_{glm} as in Equation 5.1.

$$y_{glm} = kx + m \tag{5.1}$$

The slope k depends on the variance in both x and y

$$k \approx cor(x, y)\frac{var(y)}{var(x)} \tag{5.2}$$

x and y does in this case represent Δv and injury risk, respectively. $cor(x, y)$ is the correlation between x and y. Thus, if the Winsmash estimation move the datapoints in the x-axis only, the variance will increase only for x, thus yielding a higher value in the denominator, which in turn gives a lower value, for the slope k, i.e. a flatter curve.

All risk curves were computed for true Δv, Figure 5.10 this meant that a direct comparison to the NASS/CDS data cannot be made. From Figure 5.10 it can be observed that there were no major differences in the injury risk prediction, and the risk curves are, as discussed, somewhat steeper. It can also be noted that the risk curves start closer to a 0% risk for a Δv of 0. However, the order among the curves remains approximately the same as observed before, and the 50% risk lie not far from that of the Winsmash estimation, Table 4.2.

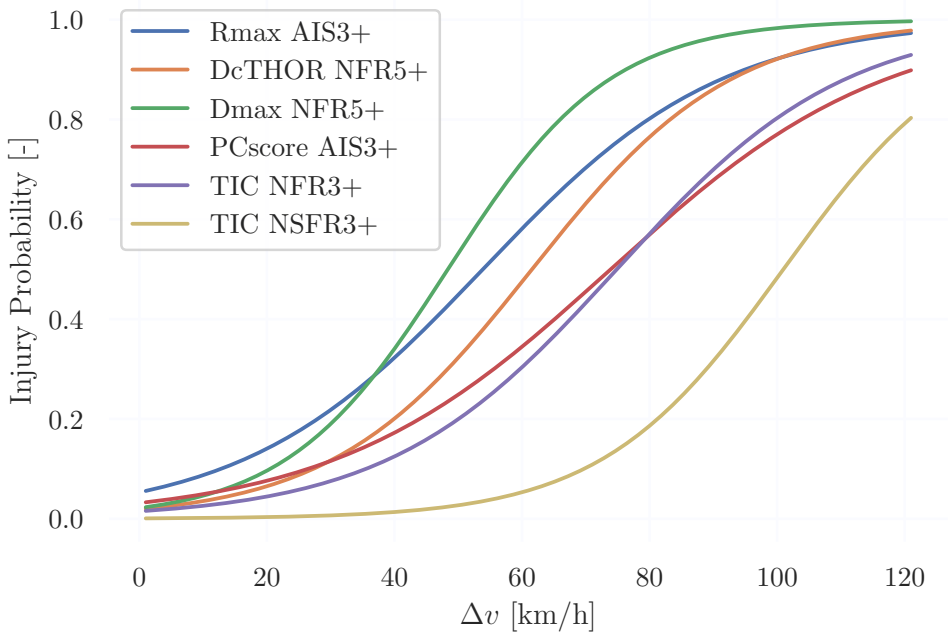

Figure 5.10: The risk curves computed and plotted for true Δv.

5.10 THOR Accuracy

Although the biofidelity of THOR is good (Parent et al. 2017), THOR may seem to be too soft, when compared to a real human. It would hence be more time and cost effective to adjust the injury criteria rather than adjusting the ATD itself. A higher deflection of an ATD does not necessarily mean a skewed result. Rather one could argue that the ATD should not be seen as a perfect human, the most important is that the results extracted can represent a human after re-calculations of the outputs and data. As seen from Figure 4.24 a stiffer THOR response would indeed lower the risk prediction quite significantly, however, as mentioned a reconstruction of the ATD might not be the best solution.

5.11 Adjusted R_{max}

An adjusted verion of R_{max} was developed by changing the parameters in the original risk function. This led to that the $R_{max,Adjusted}$ came closer to the NASS/CDS risk curve. As seen in Figure 4.22 the incline of $R_{max,Adjusted}$ started after 40mm of deflection, which is not optimal since all deflection less than 40mm mean a 0% risk of AIS3+ injury to the thorax. The simulation data was also potted for a 70-year-old occupant, Figure 5.11. It can be spotted here that the original R_{max} curve starts at 0.3 injury probability, while the simulation points, here plotted in blue for the original, were showing a step curve characteristic. The overall curve fitment against the points was poor but the individual simulation data shows an overpredictment compared to all curves in the figure. $R_{max,Adjusted}$ simulation points were plotted in grey.

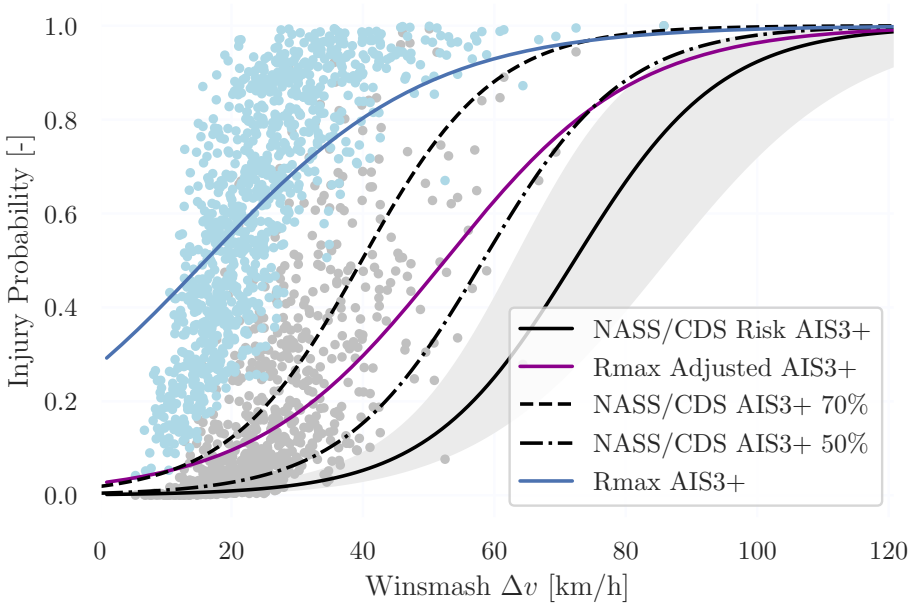

Figure 5.11: Rmax AIS3+ comparison for a 70-year-old between the adjusted and original R_{max} curve. The individual simulations plotted as grey dots for the Adjusted R_{max} and plotted in light blue for the original R_{max}.

Even though there were signs that R_{max} overpredicts injury, $R_{max,Adjusted}$ may not be the best representation of reality. Since the approach of choosing the underpredicted curves was taken, the discussion about the correctness of the underpredicted curves itself arises. The assumption was that the underpredict was the smallest at high Δv. At high Δv the crash data from the NASS/CDS data was more commonly consisting of autopsy than at lower speeds. This may contribute to that the data was in fact closer to reality at higher speeds. The assumption was the same for low speeds, and here there may be more uncertainty than assumed in the study for the development of the underpredict curves. The $R_{max,Adjusted}$ should hence be seen as a test to investigate the possibility of an adjusted risk function rather than the solution. It could be deemed that R_{max} has the possibility of predicting a risk closer to real-life with an adjustment of the risk function.

5.12 EDR Δv NASS/CDS

An additional dataset to compare with the risks calculated in the simulations was extracted from Brumbelow (2019) and a recalculation of Iraeus and Lindquist (2016) NASS/CDS curve was made for thoracic MAIS3+ injuries. When comparing the curves in Figure 3.17, the recalculated curve Iraeus and Lindquist (2016) fits between the curves from Brumbelow (2019). The curve was flatter than the EDR Δv curves, most likely due to the Winsmash Δv approximation. This was in line with the findings from Section 5.9 where the Winsmash corrected curves were flatter. Winsmash Δv may hence be sufficiently good way of estimating the velocities, but EDR data is preferred due to the better accuracy of the data.

Since MAIS3+ includes additional injuries than rib fracture risk, the MAIS3+ curve will in theory predict higher risk of injury compared to AIS3+. The MAIS3+ curve, Figure 4.25 from Brumbelow (2019) includes older ages ranging from 40-59, which would mean it is further overestimating injuries compared to a 40-year-old. As the MAIS3+ thoracic injury risk from Iraeus and Lindquist (2016) matches the thoracic MAIS3+ injury risk from another study, that of Brumbelow (2019) it supports that the rib fracture AIS3+ curve from Iraeus and Lindquist (2016) was a good representation of real-life injury risk. Though, the underprediction in the NASS/CDS data may be biased in both the data sources studied, as already discussed.

Another comparison could be made with regards to the usage of true Δv. Tsoi and Gabler (2015) had access to EDR-data from car crashes, and could thus extract a more accurate value for Δv. The risk curve for Δv in Tsoi and Gabler (2015) was digitized and plotted versus the computed risks for the simulations, Figure 5.12, where it could be seen that the Tsoi and Gabler (2015) risk curve was shifted quite significantly to the left, compared to the risk curve derived by Iraeus and Lindquist (2016), seen in Figure 3.13. The age for which the risk curve was computed was unknown, which might explain why it shifted to the left by such extent. Mainly General Motors (GM) vehicles were included in the study since these vehicles are more often equipped with an EDR recorder. With 83% GM vehicles, the data may still represent the whole vehicle fleet, but there was some uncertainty. This may be a contributing factor to the risk curve moving to the left compared to the other data sources studied.

Another difference between real-life crashes and PMHS tests is muscle activity, which may also affect the kinematics in a crash scenario. Ejima et al. (2009) conducted sled tests with a deceleration of 0.8G on human volunteers and found that the motion of the upper torso was affected by muscle tension in the pre-impact phase. Since PMHS does not have any muscle activity, the injury criteria based on PMHS data may predict a higher risk than real-life due to the difference in body kinematics.

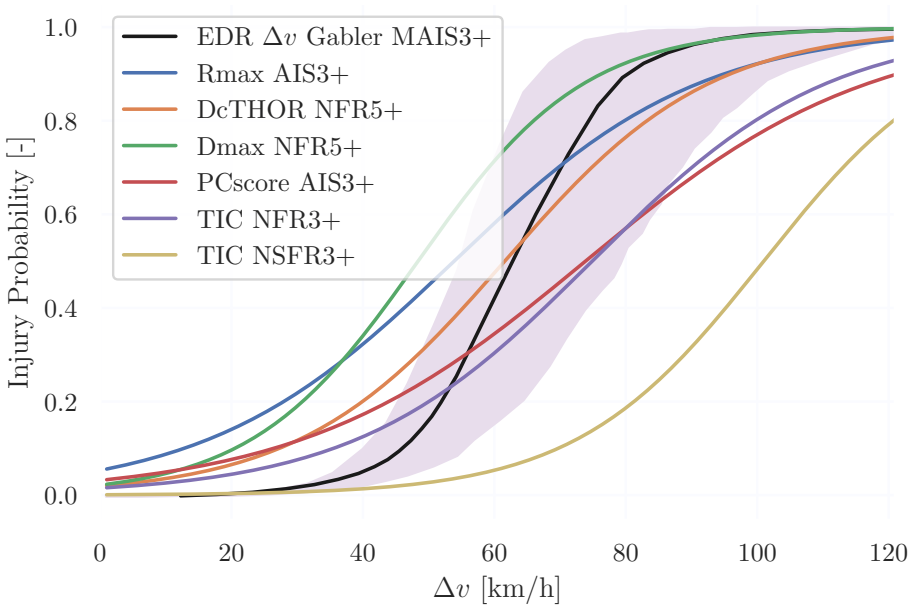

Figure 5.12: The risk curves computed and plotted for true Δv, and compared to the risk curve derived using EDR Δv from Tsoi and Gabler (2015).

The Tsoi and Gabler (2015) risk curve was however computed for MAIS3+ for the whole body, rather than AIS3+ thorax injuries. Tsoi and Gabler (2015) considered thorax, spine and abdomen injuries as whole-body injuries. All THOR rib fracture AIS3+/NFR5+/NFR3+ risk curves still predicted a higher risk of injury at 40 km/h, except TIC_{NSFR}. For instance, the risk of AIS3+ rib fracture according to R_{max} was 45% at 40 km/h, while the MAIS3+ injury risk from Tsoi and Gabler (2015), which includes more types of injuries and ought to be higher, was just 5%, indicating that the R_{max} rib fracture risk for THOR was overestimated. Hence with a risk curve consisting of real data that underpredicts in the given scenario, R_{max} still outputs a higher risk than the comparison. Tsoi and Gabler (2015) may have developed a good risk curve for real crash data, but it was hard to compare with the calculated risks from the simulations in this study.

5.13 Post Mortem Human Subjects and Real Life Crashes

All the rib fracture criteria for the THOR ATD included in this study (Craig et al. (2020), Davidsson et al. (2014), Troseille et al. (2019) and Poplin et al. (2017)) were based on comparison of THOR chest responses to those of PMHS test data. This means that the humanlike response was ensured, however there may be a difference in e.g. bone strength between a live human and a PMHS. This does of course influence the results and parameters for each criterion. For the most part PMHS used in tests might often be older and thus more vulnerable than the average person being involved in a crash. Eppinger et al. (1999) describes how the thoracic injury risk curve may change when accounting for

this over-reporting of rib fractures. This may then lead to a criterion that would be too soft, i.e. the deflection measure indicates a higher value than what would actually be the case for a live human. Thus, higher deflection values from THOR may be the expected results, which, in turn, gives a higher risk prediction for THOR, Craig et al. (2020).

5.14 Limitations

This study, as with most studies, has, of course, limitations. Firstly, as discussed in Iraeus and Lindquist (2016) the sampling of the parameters, were based on data samples and might not represent the NASS/CDS data entirely. For instance, the vehicle parameters were based on 14 vehicles (Table 3.1). Some of the distributions were based on data from EDR, which mainly consists of GM vehicles. Other limitations was that the effects of sex, seating posture and morphology were not studied.

The analysis of the simulation includes the statistical determination of Winsmash Δv, which affects the prediction of rib injuries. This method was most likely implemented correctly, however the effect of the rib fracture predictions were based on the assumption about how the risk of misclassifications depends on the regression variables.

Finally, the results depend heavily on the gather data in NASS/CDS, and the comparison was done thereafter. As already discussed, there was evidence for a clear under prediction of rib fractures when considering x-ray footage. Therefore, it may be said that the comparative dataset was not the most accurate, and that improved accuracy could be obtained using EDR data for Δv, while an accurate representation of rib fracture risk from the field data is harder to obtain.

5.15 Future Work

For similar studies in the future, some recommendations can be made as to what changes to the method might improve the study, similar observations as Iraeus and Lindquist (2016) have already made. Firstly, the Latin Hypercube sampling scheme is a superior alternative to regular Monte Carlo sampling, it is still quite inefficient for this application. This, since most sample points will represent low severity crashes, i.e. in situations where the probability of injury is low. However, this is natural since the distributions were based on distributions from real life crashes. Consequently, this will lead to very few crashes of higher severity being sampled.

With a more efficient sampling strategy, the study could be re-done, including the missing age effects. Furthermore, given the status of the generic model, it would in practice be easy to incorporate validation for other body parts.

In addition, one could also re-do the study for the currently most used ATD, the Hybrid III. This, to get a comparison between THOR and Hybrid III different characteristics and different results may appear.

6 Conclusion

The rib fracture risk predicted by the THOR ATD was compared with a selection of data from NASS/CDS, using a generic vehicle compartment model. Six different injury risk functions were considered. The rib fracture risk functions using R_{max}, D_{max} and DcTHOR were too sensitive and overpredicted the risk of rib fracture. For example, the risk functions for R_{max} and D_{max} displayed a 50% rib fracture risk at 56 and 49 km/h, respectively, while the NASS/CDS risk curve predicted that the 50% risk would lay at 99 km/h.

The TIC_{NSFR} criteria was shown to be the best correlated injury risk function with respect to the risk curve from the selection of NASS/CDS data. However, TIC_{NSFR} cannot be said to be the best risk function, since it was too insensitive. Of all simulations, only five cases predicted over 20% risk, and only one over 50% risk of rib fracture.

The criteria TIC_{NFR} and $PCscore$ were the best for predicting rib fractures, since they showed both a good correlation with the selected NASS/CDS data, as well as capturing differences between crash severity levels. Both risk functions predicted a 50% for approximately 77 km/h. $PCscore$ would be the preferred injury risk function, as it was defined for AIS3+, which the NASS/CDS risk curve was as well. In addition, the curve fit for $PCscore$ had an R^2 of 0.520 compared to 0.360 for TIC_{NFR}, which indicates a better curve fit for $PCscore$.

By predicting the risk of injury in the most accurate way possible, the development of car safety can be aided, thus leading to fewer car crash fatalities. From the population based stochastic study done here to compare the rib fracture risk predictions of the THOR ATD with that real-life data from NASS/CDS, $PCscore$ is recommended as the criterion to be used for evaluating thorax injuries in car crash testing with THOR.

References

Belytschko, T., Liu, W.K., Moran, B., Elkhodary, K.I., (2014): *Nonlinear Finite Elements for Continua and Structures, Second Edition*

Craig, M., Parent, D., Lee. E., Rudd. R., Takhounts. E., Hasija. V. (2020): *Injury Criteria for the THOR 50th Male ATD*

Crandall. J., Kent, R., Patrie, J., Fertile, J., Martin, P., (2000): *Rib Fracture Patterns and Radiologic Detection – A Restraint-Based Comparison*

Davidsson, J., Carroll, J., Hynd, D., Lecuyer, E., Song, E., Trosseille, X., Eggers, A., Sunnevang, C., Praxl, N., Martinez, L., Lemmen, P., Been, B. (2014): *Development of injury risk functions for use with the THORAX Demonstrator; an updated THOR*

Ejima, S., Zama, Y., Ono, K., Kaneoka, K., Shiina, I., Asada, H. (2009): *PREDICTION OF PRE-IMPACT OCCUPANT KINEMATIC BEHAVIOR BASED ON THE MUSCLE ACTIVITY DURING FRONTAL COLLISION*

Eppinger, R., Sun, E., Bandak, F., Haffner, M., Khaewpong, N., Maltese, M., Kuppa, S., Nguyen, T., Takhounts, E., Tannous, R., Zhang, A., Saul, R., (1999): *Development of improved injury criteria for the assessment of advanced automotive restraint systems–II.*

Eriksson L, Zellmer H, Fograscher K, Drexl B., (2009): *Using the Objective Rating Method (ORM) as a quality assessment tool for physical tests, test methods, and mathematical models.*

Foster, J. K., Kortge. J. O., Wolanin. M. J. (1977): *Hybrid III - A Biomechanically Based Crash Test Dummy*

Funk, J. R., Cormier, J. M., Gabler, H.C. (2008) *Effect of delta-V errors in NASS on frontal crash risk calculations*

Gennarelli, T. A. & Wodzin, E. (2005): *ABBREVIATED INJURY SCALE*

Glantz, S.A., Slinker, B.K., Neilands, T.B., (2017) *Applied Regression & Analysis of Variance, Third Edition*

Gray, H. (1918) *Anatomy of the Human Body* 20$^{\text{th}}$ edition (1924)

Hallman, J. J., Yoganandan, N., Pintar, F. A. (2011): *Injury Differences Between Small and Large Overlap Frontal Crashes*

Humanetics (2020) *THOR-50M - Looking Ahead to the Future Availabe at: https://humanetics.humaneticsgroup.com/perspectives/thor-50m-looking-ahead-to-the-future (Accessed: 2022-05-11)*

Humanetics Innovative Solutions Inc. (2016): *USER MANUAL: 3D IR-TRACC THOR-50M*

Insurance Institute for Highway safety. (2019): *Fatality Facts*

Iraeus, J. (2015): *Stochastic Finite Element Simulations of Real Life Frontal Crashes*

Iraeus, J. & Lindquist, M. (2015): *Pulse shape analysis and data reduction of real-life frontal crashes with modern passenger cars*

Iraeus, J. & Lindquist, M. (2016): *Development and validation of a generic finite element vehicle buck model for the analysis of driver rib fractures in real life nearside oblique frontal crashes*

Kuppa, S., Eppinger, R. (1998): *Development of an improved thoracic injury criterion.*

Larsson. K., Blennow. A., Iraeus. J., Pipkorn. B., Lubbe. N. (2021): *Rib Cortical Bone Fracture Risk as a Function of Age and Rib Strain: Updated Injury Prediction Using Finite Element Human Body Models*

Lederer, W., Mair, D., Rabl, W., Baubin, M. (2004): *Frequency of rib and sternum fractures associated with out-of-hospital cardiopulmonary resuscitation is underestimated by conventional chest X-ray*

Lie, A., Tingvall, C. (2002): *How Do EURO NCAP Results Correlate with Real-life Injury Risks? A Paired Comparison Study of Car-to-Car Crashes*

McCartt, A.T. & Wells J.K., (2010) *Consumer Survey about Vehicle Choice*

Morgan, R.M., Eppinger, R.H., Haffner, M.P., Yoganandan, N., Pintar, F.A., Sances, A., Crandall, J.R., Pilkey, W.D., Klopp, G.S., Kallieris, D., Miltner, E., Mattern, R., Kuppa, S.M., and Sharpless, C.L., (1994): *Thoracic trauma assessment formulations for restrained drivers in simulated frontal impacts.*

Niehoff, P. & Gabler, H.C, (2006) *The Accuracy of Winsmash Delta-V Estimates: The Influence of Vehicle Type, Stiffness, and Impact Mode*

Parent P. D., Craig M., Moorhouse. K. (2017): *Biofidelity Evaluation of the THOR and Hybrid III 50th Percentile Male Frontal Impact Anthropomorphic Test Devices*

Pipkorn. B., Iraeus. J., Björklund. M., Bunketorp. O., Jakobsson. L. (2019): *Multi-Scale Validation of a Rib Fracture Prediction Method for Human Body Models*

Poplin, G. S., McMurry, T. L., Forman, J. L., Ash, J., Parent, D. P., Craig, M. J., Song, E., Kent, R., Shaw, G., Crandall, J. (2017): *Development of thoracic injury risk functions for the THOR ATD*

Schmitt, K., Niederer, P. F., Cronin, D. S., Morrison III, B, Muser, M. H, Walz, F. (2019): *Trauma Biomechanics: An Introduction to Injury Biomechanics*

Schulze, C., Hoppe, H., Schweitzer, W., Schwendener, N., Grabherr, S., Jackowski, C. (2013): *Rib fractures at postmortem computed tomography (PMCT) validated against the autopsy*

Sherwood, C. P., . Nolan, J. M. & . Zuby, D. S. (2009): *Characteristics of small overlap crashes*

Shimamura, M., Ohhashi, H., Yamazaki, M., (2003): *The effects of occupant age on patterns of rib fractures to belt-restrained drivers and front passengers in frontal crashes in Japan.*

Society of Automotive Engineers International. (2003): *SURFACE VEHICLE RECOMMENDED PRACTICE (SAE J211-1 Revised DEC2003)*

Swedish Standards Institute. (2016): *Road vehicles – Traffic accident analysis – Part 3: Guidelines for the interpretation of recorded crash pulse data to determine impact severity (ISO/TR 12353-3:2013, IDT)*

Trosseille, X., & Baudrit P. (2019): *UPDATED CHEST INJURY CRITERION FOR THE THOR DUMMY*

Tsoi. A. H. & Gabler. H. C. (2015): *Evaluation of Vehicle-Based Crash Severity Metrics*

Umale. S., Arun. M. W. J., Hauschild. H., Humm. J. R., Pintar. F. A., Yoganandan. N. (2018): *Quantitative Evaluation of THOR, World SID and Hybrid III under Far-Side Impacts: A Finite Element Study*

World Health Organization. (2018): *Global status report on road safety*

Yoganandan, N., Pintar, F., Rinaldi, J., (2009): *Evaluation of the Rib Eye deflection measurement system in the 50th percentile Hybrid III dummy.*

DEPARTMENT OF MECHANICS AND
MARITIME SCIENCES CHALMERS
UNIVERSITY OF TECHNOLOGY
Gothenburg, Sweden 2022
www.chalmers.se

CHALMERS
UNIVERSITY OF TECHNOLOGY